2017

Silica Nanoparticles for the Delivery of DNA and RNAi in Cancer Treatment

Michael Aaron Vrolijk
University of Vermont

SILICA NANOPARTICLES FOR THE DELIVERY OF DNA AND RNAI IN CANCER TREATMENT

A Thesis Presented

by

Michael Aaron Vrolijk

to

The Faculty of the Graduate College

of

The University of Vermont

In Partial Fulfillment of the Requirements
for the Degree of Master of Science
Specializing in Chemistry

October, 2017

Defense Date: May 22, 2017
Thesis Examination Committee:

Christopher C. Landry, Ph.D., Advisor
Christopher Steward Francklyn, Ph.D., Chairperson
José Madalengoitia, Ph.D.
Matthew D. Liptak, Ph.D.
Cynthia J. Forehand, Ph.D., Dean of the Graduate College

ABSTRACT

DNA and interfering RNA (RNAi) – short interfering RNA (siRNA) and micro RNA (miRNA) – are promising new cancer therapies, especially for drug resistant lines. However, they require a delivery system in vivo to prevent degradation and off target effects. Silica based nanoparticles, both solid and mesoporous, are a promising option due to their biocompatibility, ease of preparation and morphology control, reproducibility, and facile addition of functional groups including targeting ligands.

After a brief introduction to cancer treatment and review of the current nanoparticle treatments undergoing clinical trials, this thesis details the many methods explored over the past ten years to fine-tune particle preparation, pore size, functionalization, and delivery strategies. The majority of both solid and mesoporous silica nanoparticles are synthesized using the sol-gel method and then various functionalization techniques are employed to load and protect the oligonucleotides. Externally loaded systems generally use a combination of polyethylenimine (PEI) and polyethylene glycol (PEG). Mesoporous silica nanoparticles internally load the DNA or RNAi, resulting in the added variable of pore size. Several groups have investigated how pore size alters loading and release kinetics to perfect this variable. Many groups have also tested ligands targeting for over expressed proteins on the intended cancer, triggered release techniques, cell-penetrating peptides in order to create a viable in vivo delivery system.

By compiling the techniques employed by researchers over the past ten years, this thesis will elucidate which approaches are most promising for future research. Furthermore, overall strategies within the field are suggested to more easily compare studies and evaluate methods.

ACKNOWLEDGEMENTS

There are a number of people who helped me finish this thesis and the M.S. in Chemistry. First and foremost, I could not have finished this project without the help of Christopher Landry and my groupmates. Beyond all the helpful feedback and support by everyone in the Landry group, I am grateful for the extra help from Jenna Taft.

I was also fortunate to have an excellent and helpful committee. Other professors, Willem Leenstra, Rory Waterman, and Eyal Amiel, also provided invaluable guidance that helped me finish this project. I am indebted to Mona Sharafi for her help throughout my process of writing and developing my presentation. Finally, I could not have finished this project without the support of my family, friends, and Neda.

TABLE OF CONTENTS

Page

LIST OF TABLES

Table Page

LIST OF FIGURES

Figure Page

1. Kruk, M. Access to Ultralarge-Pore Ordered Mesoporous Materials through Selection of Surfactant/Swelling-Agent Micellar Templates. *Acc. Chem. Res.* **2012,** *45*, 1678-1687.
2. Kim, S.; Na, H. K.; Won, C.; Min, D. H. In-Depth Study on the Gene Silencing Capability of Silica Nanoparticles with Different Pore Sizes: Degree and Duration of RNA Interference. *RSC Adv.* **2016,** *6*, 27143-27150.
3. Lin, D. S.; Cheng, Q.; Jiang, Q.; Huang, Y. Y.; Yang, Z.; Han, S. C.; Zhao, Y. N.; Guo, S. T.; Liang, Z. C.; Dong, A. J. Intracellular Cleavable Poly(2-Dimethylaminoethyl Methacrylate) Functionalized Mesoporous Silica Nanoparticles for Efficient siRNA Delivery In Vitro and In Vivo. *Nanoscale* **2013,** *5*, 4291-4301.
4. Choi, M.; Kleitz, F.; Liu, D.; Lee, H. Y.; Ahn, W.-S.; Ryoo, R. Controlled Polymerization in Mesoporous Silica Toward the Design of Organic− Inorganic Composite Nanoporous Materials. *J. Am. Chem. Soc.* **2005,** *127*, 1924-1932.

CHAPTER 1: INTRODUCTION TO SILICA BASED DELIVERY SYSTEMS FOR RNAI AND DNA IN CANCER TREATMENT

1.1 The need for new cancer treatments

Cancer is a costly disorder that results in much personal suffering even when treated. Improvements in early detection and treatment have increased cancer survival rates overall (**Figure 1.1.**) but not for some specific cancers.[1] Death rates are rising for cancers of the oropharynx, anus, liver, pancreas, and soft tissue.[2] For men there is an increase in tonsil cancer and melanoma deaths; for women there is an increase in uterine cancer deaths.[2] Furthermore, cancer is now the second leading cause of death (23% of deaths in 2011 in the United States) after heart disease and is suspected to overtake heart disease as the leading cause of death within the next several years.[2]

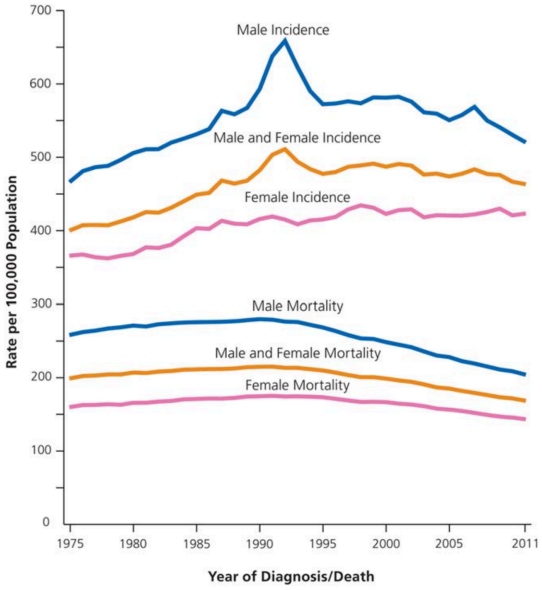

Figure 1.1. Cancer incidence and death rates from 1975 – 2011 adjusted to the 2000 US standard population. Figure modified from reference 2.

In addition to limited effectiveness in many cases, current treatments can result in debilitating side-effects and long-term effects depending on treatment and type of cancer. Common side-effects during chemotherapy and radiation treatment include anemia, digestive problems (constipation, appetite loss, etc.), cognitive problems, edema, fatigue, hair loss, infection, mouth ulcers, nausea and vomiting, among others.[3] Long-term effects vary based on therapy and type of cancer. For example, 25-60% of women develop chronic, though usually not severe, pain following breast cancer treatment.[4] Chemotherapy regiments containing oxaliplatin used to treat colon and rectum cancer often result in neuropathy.[4] Consequently, new therapies are needed to improve cancer survival and better mitigate short and long-term side effects. One possible and promising solution to these problems is gene therapy.

1.2 Brief history of gene therapy via nanoparticle delivery for treating cancer

Gene therapy is a promising treatment for cancer that can treat cellular abnormalities by counteracting or correcting the malfunctioning gene within a cancerous cell.[5] This treatment utilizes DNA or interfering RNA (RNAi) such as short interfering RNA (siRNA) or microRNA (miRNA). The delivered oligonucleotide either counteracts harmful protein production or corrects the aberrant gene. Both processes can result in cell death. However, delivery remains a significant obstacle. In the blood stream unmodified oligonucleotides are degraded by enzymes (RNases and DNases), are not taken up by target tissue, and can cause cellular immune response.[6] Consequently, a delivery system is necessary for clinical translation of DNA and RNAi therapies.

The first therapy employing gene transfer was approved for clinical use in 2003 by the Chinese State Food and Drug Administration. The gene delivery system Gendicine, a modified adenovirus, treats head and neck cancers by delivering the p53 gene that, once expressed, promotes apoptosis of the targeted cell.[7-8] However, a definitive report of phase IV safety and efficacy has not been published and Genedicine has not been approved by the US FDA.[9] In fact, currently no gene therapies have gained FDA approval, although many organic and inorganic formulas are undergoing Phase I or II testing.[10]

While gene therapy is promising, delivery of a therapeutic gene to cancer cells has proven to be the largest obstacle. Viral vectors, such as Gendicine, face several limitations such as safety concerns, effectiveness, and unintended immune response.[11] A promising alternative is lipid, polymer, and silica nanoparticles that can have a diameter anywhere between 20-1,000 nm.[12-14] These nanoparticle systems have higher loading and less safety concerns than viral vectors. Lipid nanoparticles form liposomes, phospholipid structures that assemble in water to form hydrophobic and hydrophilic compartments.[15] Neutrally charged liposomes are most often used, since negatively and positively charged liposomes can induce immune response in vivo.[15] Polymer nanoparticles can be synthesized a number of ways (emulsion, interfacial polymerization, precipitation polymerization, etc.) and utilize different polymers depending on the intended cargo.[16] The final polymer nanoparticle can form a micelle or complex that traps the cargo in a matrix.[17] One promising strategy uses polyethylene glycol (PEG) decorated block copolymers that self-assemble into polymer micelle nanoparticles and load hydrophobic cargo in the interior (such as CALAA-01, described in section 1.3).[16] Silica nanoparticles

provide an easily tunable and modifiable platform to load cargo either on the exterior and/or within pores, depending on the morphology of the nanoparticle.[18]

Nanoparticle formulas, both organic and inorganic, must overcome many challenges to be able to effectively deliver an oligonucleotide therapy. The majority are delivered systemically and, consequently, must contain peptides targeting overexpressed receptors on the specific cancer cell line to avoid damage to healthy cells. The nanoparticles must also encapsulate the gene to avoid its degradation and possible immune response.[15, 19] They must avoid the reticuloendothelial system (RES), uptake by macrophages, long enough to find their target.[20-21] Evading macrophage uptake can be achieved by reducing the particle's diameter to below 250 nm and including exterior functionalization such as PEG.[17] Larger particles are recognized by macrophages as foreign and are thus removed from the system and degraded.[17]

In vivo efficacy is also determined by how the nanoparticle interacts with proteins and other components in blood, since studies have shown that the protein corona that occurs in serum can influence the nanoparticle's uptake and behavior.[22] The nanoparticle's size, charge, and exterior functionalization with a ligand such a PEG alter the corona formed and, consequently, the fate of the delivery system.[23] Most nanoparticle delivery systems are designed to penetrate the cell through the endocytosis pathway, either by specifically recognizing proteins on the nanoparticle's exterior or independent of specific ligands.[17] The endocytosis pathway results in the nanoparticle entering the cell in an endosome that is routed to a lysosome for degradation.[24] The nanoparticle must escape the endosome to deliver its' cargo in the cytosol, so the DNA or RNAi can successfully reach the nucleus or inhibit mRNA protein production.[17] The particles

discussed in this thesis target endosomal uptake by limiting diameter to under 500 nm and including targeting functional groups. However, larger particles, such as microparticles, can be internalized via a phagocytosis route due to non-specific interactions between the particle and cell[25-26] or via an actin-mediated process.[27] Finally, nanoparticle systems must also be non-toxic and biodegradable.

To date there are two dominant strategies for targeting delivery: passive and active. Passive targeting refers to systems that use the enhanced permeability and retention effect (EPR) to reach tumors. EPR occurs when a solid tumor grows large enough that normal vasculature is unable to provide enough oxygen and new blood vessels are built to support the cancer cells' rapid growth.[28] Once this happens, leaky vasculature develops in solid tumors, termed the EPR effect, that results in the accumulation of nanoparticles with a diameter less than 200 nm.[29] However, formulations less than 50 nm in diameter usually are not retained in tumors for long, because they often undergo extravasation, leakage from the blood vessel to the tissue around it.[29] Active targeting employs a ligand on the exterior of the particle that binds to a protein overexpressed on the intended cancer cell line. The promise of active targeting is to reduce off-target effects as much as possible by specific delivery. These two strategies are often used together. By utilizing both active and passive targeting, the nanoparticle reaches close enough proximity for the targeting ligand to bind to its substrate on the cancer cell's exterior.

1.3 Active targeting nanoparticles currently in clinical trials

There are currently numerous organic and inorganic targeted nanoparticle treatments undergoing clinical trials for imaging and delivery of drugs, DNA, siRNA, cytokines, antigens, and monoclonal antibody delivery. These systems demonstrate the promise of precisely delivering a therapy while minimizing or eliminating harming healthy cells. Both organic and inorganic nanoparticles have an average diameter ranging from 5 – 200 nm and undergo both passive and active targeting.

Most organic nanoparticles are liposomes with PEG conjugated to the exterior to increase circulation time and reduce clearance by immune cells.[30-35] These nanoparticles encapsulate medications that would be degraded in the blood stream (such as DNA and RNAi) or cause serious side effects. For example, MM-302 loads doxorubicin[30] that can cause severe chemotherapy-induced nausea and vomiting;[36] SGT-53 loads genes, such as p53 cDNA[37]; and TKM-080301 encapsulates siRNA.[38] Unlike the other nanoparticles delivering therapies directly to the tumor, Lipovaxin-MM is a liposomal immunotherapy/vaccine for malignant melanoma that targets dendritic cells to elicit an immune response against the targeted cancer cells.[39]

Polymer nanoparticles are core-shell structure with the payload encapsulated.[40-41] CALAA-01 was the first targeted delivery system for siRNA tested in humans. It is a cyclodextrin-containing polymer with PEG for steric stabilization and a human transferrin protein-targeting agent.[41] In clinical use it is prepared by mixing two components to produce the siRNA encapsulated polymer nanoparticle for intravenous injection.[41] Another example is BIND-014 that uses hydrophobic polylactic acid polymeric core to encapsulate docetaxel.[42] BIND-014 also uses a PEG coating in addition

Table 1.1.: Nanoparticles using active targeting in clinical trials for treating cancer

Type of Nanoparticle	Cargo/Use	Size (Average Diameter)	Product Name	Clinical Trial
Organic				
Lipid Based[30, 32, 34-35, 37, 39, 43-45]	Doxorubicin	100-200 nm	Anti-EGFR Immuno-liposomes	NCT01702129★ NCT02833766
	Trastuzumab and Chemotherapy	100 nm	MM-302	NCT01304797 NCT02213744 NCT02735798
	p53 pDNA	210 nm	SGT-53	NCT02340156 NCT02354547 NCT00470613 NCT02340117
	RB94 pDNA	166 nm	SGT-94	NCT01517464
	Oxaliplatin	185 nm	MBP-426	NCT00355888★ NCT00964080
	Melanoma antigens and IFNγ	Not published	Lipovaxin-MM	NCT01052142★
	Doxorubicin	Not published	2B3-101	NCT01386580★ NCT01818713
	PLK1 siRNA	80 nm	TKM 080301	NCT01262235★ NCT02191878★ NCT01437007★
Polymers				
Polymeric Micelle[40-42, 45-47]	Docetaxel	95 nm	BIND-014	NCT02283320★ NCT01812746★ NCT01300533★ NCT01792479★ NCT02479178*
	RRM2 siRNA	75 nm	CALAA-01	NCT00689065*

Inorganic				
Iron Oxide[48]	Imaging	100 nm		NCT01411904*
Silica[49]	Imaging	6-7 nm	C dots	NCT02106598

* terminated
⁒ recruitment status unknown
★ completed

to prostate-specific membrane antigen (PSMA) targeting ligands.[42] Other preclinical studies include targeted core-crosslinked polymeric micelles where the drug, doxorubicin, is covalently trapped.[50]

Whereas liposomes and polymer nanoparticles deliver a therapy directly to the tumor or, in the case of Lipovaxin-MM, to dendritic cells for immunotherapy, targeted inorganic nanoparticles are currently in clinical trials for biopsy and imaging. The superparamagnetic nanoparticles made of iron oxide (SPIONs) target CD34 surface receptors on leukemia cells in order to preferentially collect them during bone marrow sampling procedures.[48] This technique has also been investigated in vivo for the detection of breast cancer by conjugating the single-core iron oxide nanoparticles to a Her2 monoclonal antibody.[51] Similarly, targeted PEGylated gold nanoparticles have undergone in vivo studies for imaging but are yet to begin clinical trials.[52]

C dots, dye labeled core-shell silica nanoparticles, were developed for sentinel lymph node (SLN) mapping in the diagnosis and treatment of melanoma. For this application, the particle was modified with peptide ligands (cyclic arginine-glycine-aspartic acid-tyrosine (cRGDY)) that is attached to methoxy-terminated PEG bound to the particle.[49] Although C dots are currently only being investigated for SLN, they can

easily be modified with a different targeting ligand for an alternate tumor target. Thus, C dots and other silica based particles can be thought of as platforms. While C dots are the only silica based nanoparticle in clinical trials, silica based delivery systems are advantageous due to their biocompatibility, facile interior and exterior modification, high loading capacity, and ease of scaling up production.[18] Silica nanoparticles can be synthesized to have mesoporous that can be optimized. Once this is achieved, internal and external modifications can be altered to produce controlled, targeted delivery to a variety of cancer cells.

1.4 Advantageous of using silica nanoparticles for DNA and RNAi delivery

Silica nanoparticles' surface can easily be modified with alkoxysilanes and are biocompatible, making both solid and mesoporous silica based systems an attractive solution to deliver DNA and RNAi.[53] Solid nanoparticles, like C Dots, can have polymers conjugated to their surface that load and protect nucleic acids.[54] In addition to protecting the DNA or RNAi on the surface, a targeting ligand can be added for specific delivery.[55]

For systems that internalize their cargo, mesoporous silica nanoparticles (MSN) are a promising platform due to their biocompatibility, high loading capacity, facile preparation and control of physical properties, large surface area, and ease of modifying both the pores and external surface. Particle size and pore size are tailored by altering synthesis conditions, both of which allow batch-to-batch reproducibility.[54] The surface and pores can then be modified with different functional groups by using alkoxysilanes. The ease of altering the silica surface has resulted in triggerable drug release systems. This is usually achieved by covalently linking the drug to the nanoparticle with cleavable

bonds or functionalization of the outer surface of the MSN with a coating that will release the payload upon an environmental change, such as pH or temperature.[56] Controlled release will likely be ready for clinical application in the near future, as numerous capping mechanisms are being explored in biomedical application for MSNs[57] and have been shown to increase efficacy and efficiency.[58]

Mesoporous silica nanoparticles (MSNs) have been shown to be biocompatible and excreted through urine and sometimes feces, depending on the particle's size, surface area, and charge. Unlike other inorganic particles such as gold or iron oxide, silica nanoparticles can be biodegraded and excreted through the urine.[59-60] In general MSNs are found to accumulate in the liver, spleen, and lungs, likely due to phagocytosis by macrophages.[59] However, uptake by macrophages does not decrease their ability to function and ingest apoptotic or antibody-opsonized target cells.[61] PEGylation reduces the biodistribution in these organs.[59-60] Size also influences biodistribution. He and colleagues compared different particle sizes (80, 120, 200, and 360 nm) to investigate how size affected particle fate. They found the smaller particle sizes could avoid capture by the liver and spleen more easily and were consequently more slowly biodegraded.[60] Numerous studies have reported no pathological abnormalities of the mice injected with MSNs.[60, 62-63]

The ease of pore modification allows efficient loading and controlled delivery to be achieved. In the case of siRNA and DNA, larger pores (8-23 nm) with positively charged modifications have been found to best load siRNA and DNA internally as opposed to smaller pores where the siRNA was unable to fully enter the pore.[64-66] For example, 23 nm pores were found to adsorb more siRNA internally as compared to 2 nm

pores.[64] While larger pores load more siRNA, release can be compromised. One study found that while multilayer adsorption could occur in 15 nm pores, 8 nm pores resulted in optimal loading and maximized release.[67] The same study additionally found the degree of pore functionalization resulted in changes in loading capacity and subsequent release of siRNA for pores 8 nm or larger.[67] Once pore size and functionalization is fine-tuned, this system could be used for a variety of nucleic acids of similar size.

1.5 General synthesis of solid and mesoporous silica nanoparticles

Both mesoporous and solid silica nanoparticles are usually synthesized using the sol-gel method where a silica precursor hydrolyzes and then condenses to create spherical particles (**Figure 1.2.**). Tetraethyl orthosilicate (TEOS) is usually used as the silica precursor, since it allows a high degree of control based on varying synthesis conditions such as pH.[68]

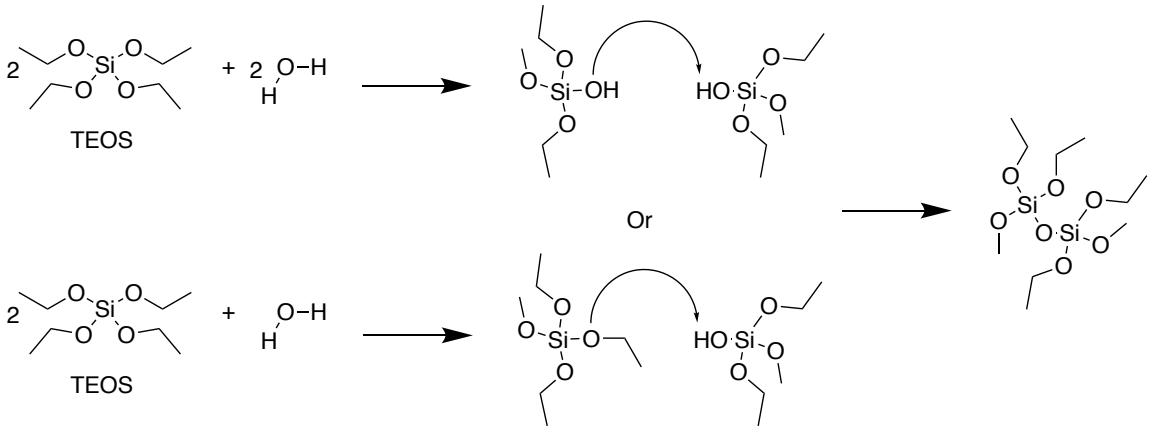

Figure 1.2. Initial hydrolysis and subsequent condensation of TEOS.

An acid or base catalysis is usually used to increase hydrolysis and condensation of the silicon alkoxide. An acid catalyst reversibly pronates the negatively charged alkoxide ligand and forms a better leaving group for hydrolysis. Basic catalysts create better OH^- groups for hydrolysis and deprotonated the silanol groups for faster condensation. Thus, hydrolysis is faster in acidic conditions, while condensation is faster in basic conditions.[68] A surfactant is used to synthesize mesoporous silica nanoparticles. Surfactants have a long, hydrophobic tail and a hydrophilic head. The silica precursor self-assembles around the surfactant forming pores mesoporous nanoparticles (**Figure 1.3.**).

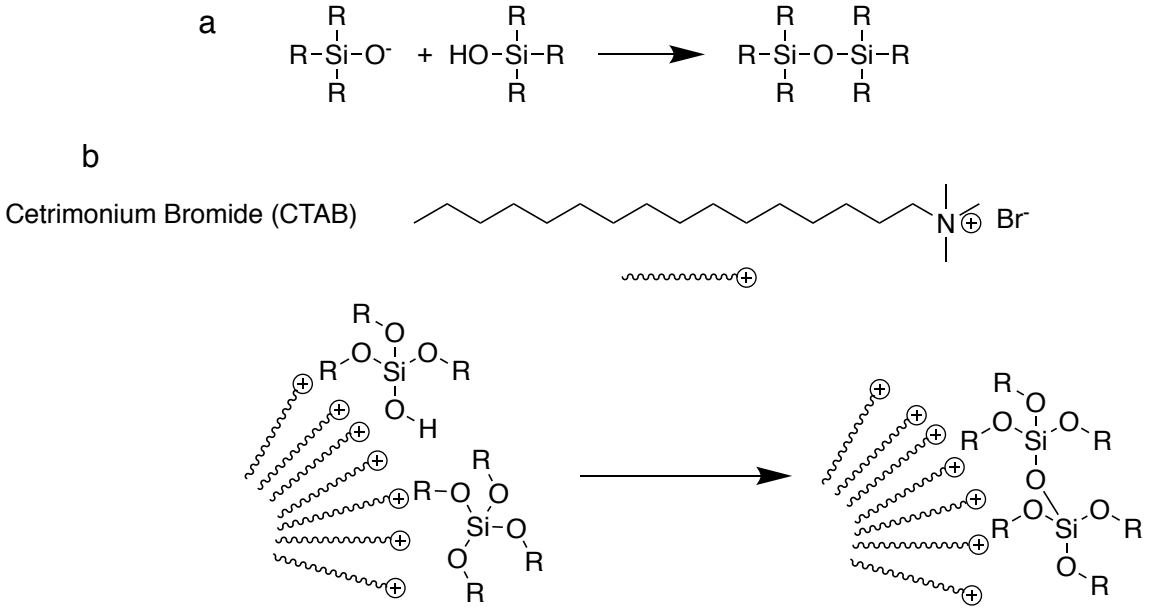

Figure 1.3. A) The silica condensation reaction. B) The silica precursor electrostatically assembles around the cationic surfactant micelles. The silica then condenses around the surfactant, creating porous silica. The surfactant, CTAB, is represented as a squiggly line for the long, hydrophobic tail and a positively charged head.

1.6 Characterization techniques

Several characterizing techniques are employed to determine instrumental features of solid and mesoporous silica nanoparticles. From nitrogen physisorption (porosimetry) a particle's surface area, pore volume, and pore diameter can be determined. Diameter can be found either using transmission electron microscope (TEM), or the hydrodynamic diameter can be obtained using dynamic light scattering (DLS). External morphology is often ascertained using a scanning electron microscope (SEM). Finally, the particle's charge can be estimated based on zeta potential that measures the charge at the boundary of strongly held charges and the bulk solution.

1.6.1. Nitrogen physisorption (porosimetry)

Nitrogen physisorption is used to characterize a porous material's surface area, pore volume, and pore diameter. In this technique, the sample is first degassed in order to remove all physisorbed species.[69] In isothermal conditions, nitrogen is then introduced at a slow enough rate that a quasi-equilibrium is reached between each increase in order to properly determine adsorption.[70] Once adsorption is complete, desorption is measured. The graphed data, an isotherm, contains the amount adsorbed against the equilibrium relative pressure (P/P_o), where P_o is the saturation pressure of the adsorptive at the temperature of the measurement against P, the pressure when the temperature is above the critical temperature of the adsorptive.[69]

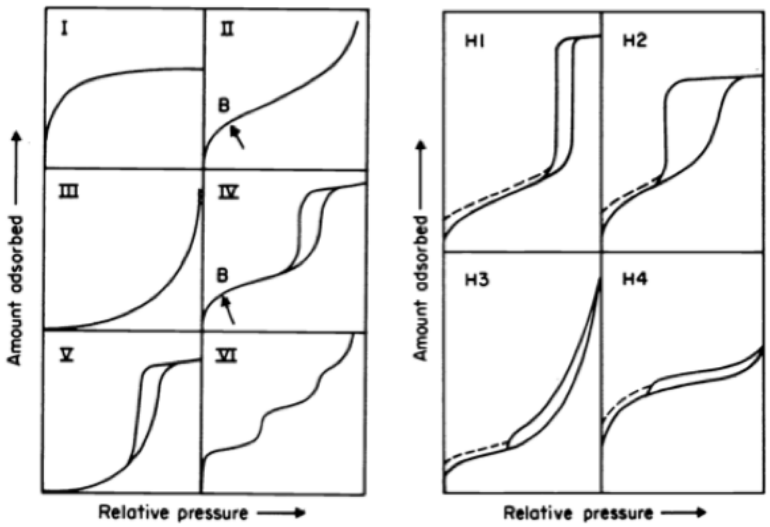

Figure 1.4. The left image is six characteristic isotherms. The right image is four common hysteresis loops. Image modified from reference 71.

Most isotherms can be grouped into six categories, as seen in **Figure 1.4.** (left). For the purposes of the current project, isotherm IV is most applicable due to being characteristic of mesoporous materials.[71] The initial section of the isotherm is due to monolayer adsorption where the nitrogen gas is adsorbed onto the silica surface.[69] The end of monolayer adsorption and beginning of multilayer adsorption is indicated by the arrow on Type II and IV. The change in slope is due to the shift from adsorbent-adsorptive interactions to interactions between the gas molecules in their condensed state.[72] The gas molecules in multilayer filling interact with the already adsorbed nitrogen gas and are thus assumed to have liquid-like properties.[70] The hysteresis loop, or the loop between the adsorption and desorption, is a result of the capillary condensation occurring in mesopores.[69] This occurs at a high P/P_o for mesoporous materials, since capillary condensation is secondary to multilayer adsorption.[70] The desorption branch is a result of delayed condensation due to the metastability of the adsorbed multilayer.[72]

Hysteresis loop can be further characterized, as seen in **Figure 1.4.** (right). The differences between these four examples have been correlated with various pore structures. [69] Type H1 is often associated with approximately uniform pores in a fairly regular array with narrow pore distribution; H2 is not well defined but is usually due to porous adsorbents (e.g. porous glass); H3 is attributed to plate-like particles with slit-shaped pores; H4 is associated with narrow slit-like pores or microporosity. [69]

Porosimetry also allows the surface area to be derived using the Brunauer-Emmett-Teller (BET) gas adsorption method. This method relies upon the amount of gas adsorbed at the relative pressure P/P_o and the monolayer capacity.[69] Pore volume and diameter are derived using the Barrett-Joyner-Halenda (BJH) method.

1.6.2. Dynamic light scattering (DLS)

DLS uses a laser (usually 675 nm) and photodetector to determine a small particle's geometric structure by measuring its Brownian motion or the random movement of microscopic particles in a fluid due to the bombardment from other molecules in the medium.[73-74] The photodetector is 90° from the laser in order to capture light scattered by the suspended particles. The particles size and shape can be determined based on the frequency shifts, angular distribution, polarization, and intensity of the scattered light.[74]

1.6.3. Zeta potential

Zeta potential is the potential difference between the slipping plane, where the nanoparticle and ions act as a single entity and move together under an applied electric

field, and the bulk solution.[75] The charge difference is determined by measuring the frequency shift of scattered light of a nanoparticle moving under an applied field, which indicates its electrophoretic mobility and can be used to calculate its zeta potential.[75] Zeta potential indicates the surface charge but is not a direct measurement. Since it also uses light scattering, zeta potential is measured in the same instrument as DLS.

1.6.4. Scanning and transmission electron microscopy

In scanning electron microscopy (SEM) an electron probe between 0.5-10 nm in diameter scans over the specimen.[76] An image is then produced by different signals from secondary electrons (exit energies around 2-5 eV) and backscattered electron (around 50 eV) that alter the cathode-ray tube's beam intensity.[76] The cathode-ray tube produces the image based on the altered signal due to electron-specimen interactions.[76]

Transmission electron microscopy (TEM) differs from SEM in that the electron beam penetrates a thin specimen. TEM has higher accelerating voltages and a broad, static beam.[77] The electrons pass through a thin specimen and interact strongly via elastic and inelastic scattering.[77] The scattered electrons are collected and focused to project an image.

1.7 Thesis goals

Since silica based delivery systems are uniquely poised solve the obstacles facing DNA and RNAi delivery, this thesis will investigate the strategies published in the last ten years to develop a silica based gene delivery system. Two main strategies, solid silica nanoparticles and mesoporous silica nanoparticles, will be discussed. While strategies

will be compared in some cases, the variation between each study (preparation method, particle functionalization, evaluation techniques) presents significant difficulty in appropriately contrasting specific technical components.[78] Thus the goal of this thesis is to both highlight the areas where creating a benchmark would further the field of research[78] and identify the most promising techniques being pursued toward developing a silica based delivery system.

1.8 References

1. DeSantis, C. E.; Lin, C. C.; Mariotto, A. B.; Siegel, R. L.; Stein, K. D.; Kramer, J. L.; Alteri, R.; Robbins, A. S.; Jemal, A. Cancer Treatment and Survivorship Statistics, 2014. *CA. Cancer J. Clin.* **2014,** *64*, 252-271.
2. Siegel, R. L.; Miller, K. D.; Jemal, A. Cancer Statistics, 2015. *CA. Cancer J. Clin.* **2015,** *65*, 5-29.
3. Side Effects - National Cancer Institute. https://www.cancer.gov/about-cancer/treatment/side-effects (accessed 3/10/2017).
4. Miller, K. D.; Siegel, R. L.; Lin, C. C.; Mariotto, A. B.; Kramer, J. L.; Rowland, J. H.; Stein, K. D.; Alteri, R.; Jemal, A. Cancer Treatment and Survivorship Statistics, 2016. *CA. Cancer J. Clin.* **2016,** *66*, 271-289.
5. Naldini, L. Gene Therapy Returns to Centre Stage. *Nature* **2015,** *526*, 351-360.
6. Barnaby, S. N.; Sita, T. L.; Petrosko, S. H.; Stegh, A. H.; Mirkin, C. A., Therapeutic Applications of Spherical Nucleic Acids. In *Nanotechnology-Based Precision Tools for the Detection and Treatment of Cancer*, Springer: New York, 2015; pp 23-50.
7. Cross, D.; Burmester, J. K. Gene Therapy for Cancer Treatment: Past, Present and Future. *Clin. Med. Res.* **2006,** *4*, 218-227.
8. Li, Y.; He, W.; Wang, R.; Yang, L.; Zhou, C.; Zhang, B. Antitumor Effects of Recombinant Human Adenovirus‐p53 Against Human Cutaneous Squamous Cell Carcinoma in Mice. *Exp. Ther. Med.* **2016,** *12*, 4159-4167.
9. Cheok, C. F.; Verma, C. S.; Baselga, J.; Lane, D. P. Translating p53 Into the Clinic. *Nat. Rev. Clin. Oncol.* **2011,** *8*, 25-37.
10. Shi, J.; Kantoff, P. W.; Wooster, R.; Farokhzad, O. C. Cancer Nanomedicine: Progress, Challenges and Opportunities. *Nat. Rev. Cancerr* **2017,** *17*, 20-37.
11. Chaudhry, A. T.; Akhtar, D. Gene Therapy and Modification as a Therapeutic Strategy for Cancer. *University of Ottawa Journal of Medicine* **2016,** *6*, 44-48.
12. Kanasty, R.; Dorkin, J. R.; Vegas, A.; Anderson, D. Delivery Materials for siRNA Therapeutics. *Nat. Mater.* **2013,** *12*, 967-977.

13. Mekaru, H.; Lu, J.; Tamanoi, F. Development of Mesoporous Silica-Based Nanoparticles with Controlled Release Capability for Cancer Therapy. *Adv. Drug Delivery Rev.* **2015,** *95*, 40-49.
14. Yang, Y.; Yu, C. Advances in Silica Based Nanoparticles for Targeted Cancer Therapy. *Nanomed.* **2016,** *12*, 317-332.
15. Pecot, C. V.; Calin, G. A.; Coleman, R. L.; Lopez-Berestein, G.; Sood, A. K. RNA Interference in the Clinic: Challenges and Future Directions. *Nat. Rev. Cancer* **2011,** *11*, 59-67.
16. Kamaly, N.; Yameen, B.; Wu, J.; Farokhzad, O. C. Degradable Controlled-Release Polymers and Polymeric Nanoparticles: Mechanisms of Controlling Drug Release. *Chem. Rev.* **2016,** *116*, 2602-2663.
17. Resnier, P.; Montier, T.; Mathieu, V.; Benoit, J. P.; Passirani, C. A Review of the Current Status of siRNA Nanomedicines in the Treatment of Cancer. *Biomaterials* **2013,** *34*, 6429-6443.
18. Mamaeva, V.; Rosenholm, J. M.; Bate-Eya, L. T.; Bergman, L.; Peuhu, E.; Duchanoy, A.; Fortelius, L. E.; Landor, S.; Toivola, D. M.; Lindén, M. Mesoporous Silica Nanoparticles as Drug Delivery Systems for Targeted Inhibition of Notch Signaling in Cancer. *Mol. Ther.* **2011,** *19*, 1538-1546.
19. Gandhi, N. S.; Tekade, R. K.; Chougule, M. B. Nanocarrier Mediated Delivery of siRNA/miRNA in Combination with Chemotherapeutic Agents for Cancer Therapy: Current Progress and Advances. *J. Controlled Release* **2014,** *0*, 238-256.
20. Gabizon, A.; Shmeeda, H.; Barenholz, Y. Pharmacokinetics of PEGylated Liposomal Doxorubicin. *Clin. Pharmacokinet.* **2003,** *42*, 419-436.
21. Wang, M.; Thanou, M. Targeting Nanoparticles to Cancer. *Pharmacol. Res.* **2010,** *62*, 90-99.
22. Braeckmans, K.; Buyens, K.; Bouquet, W.; Vervaet, C.; Joye, P.; Vos, F. D.; Plawinski, L.; Doeuvre, L.; Angles-Cano, E.; Sanders, N. N. Sizing Nanomatter in Biological Fluids by Fluorescence Single Particle Tracking. *Nano Lett.* **2010,** *10*, 4435-4442.
23. Lundqvist, M.; Stigler, J.; Elia, G.; Lynch, I.; Cedervall, T.; Dawson, K. A. Nanoparticle Size and Surface Properties Determine the Protein Corona with Possible Implications for Biological Impacts. *Proc. Natl. Acad. Sci.* **2008,** *105*, 14265-14270.
24. Grant, B. D.; Donaldson, J. G. Pathways and Mechanisms of Endocytic Recycling. *Nat. Rev. Mol. Cell Biol.* **2009,** *10*, 597-608.
25. Hu, L.; Mao, Z.; Gao, C. Colloidal Particles for Cellular Uptake and Delivery. *J. Mater. Chem.* **2009,** *19*, 3108-3115.
26. Nel, A. E.; Mädler, L.; Velegol, D.; Xia, T.; Hoek, E. M.; Somasundaran, P.; Klaessig, F.; Castranova, V.; Thompson, M. Understanding Biophysicochemical Interactions at the Nano–Bio Interface. *Nat. Mater.* **2009,** *8*, 543-557.
27. Blumen, S. R.; Cheng, K.; Ramos-Nino, M. E.; Taatjes, D. J.; Weiss, D. J.; Landry, C. C.; Mossman, B. T. Unique Uptake of Acid-Prepared Mesoporous Spheres by Lung Epithelial and Mesothelioma Cells. *Am. J. Respir. Cell Mol. Biol.* **2007,** *36*, 333-342.

28. Bertrand, N.; Wu, J.; Xu, X.; Kamaly, N.; Farokhzad, O. C. Cancer Nanotechnology: The Impact of Passive and Active Targeting in the Era of Modern Cancer Biology. *Adv. Drug Delivery Rev.* **2014,** *66*, 2-25.
29. Babu, A.; Templeton, A. K.; Munshi, A.; Ramesh, R. Nanoparticle-Based Drug Delivery for Therapy of Lung Cancer: Progress and Challenges. *J. Nanomater.* **2013,** *2013*, 14.
30. Espelin, C. W.; Leonard, S. C.; Geretti, E.; Wickham, T. J.; Hendriks, B. S. Dual HER2 Targeting with Trastuzumab and Liposomal-Encapsulated Doxorubicin (MM-302) Demonstrates Synergistic Antitumor Activity in Breast and Gastric Cancer. *Cancer Res.* **2016,** *76*, 1517-1527.
31. Chen, Y.; Wu, J. J.; Huang, L. Nanoparticles Targeted with NGR Motif Deliver C-MYC siRNA and Doxorubicin for Anticancer Therapy. *Mol. Ther.* **2010,** *18*, 828-834.
32. Wicki, A.; Ritschard, R.; Loesch, U.; Deuster, S.; Rochlitz, C.; Mamot, C. Large-Scale Manufacturing of GMP-Compliant Anti-EGFR Targeted Nanocarriers: Production of Doxorubicin-Loaded Anti-EGFR-Immunoliposomes for a First-In-Man Clinical Trial. *Int. J. Pharm.* **2015,** *484*, 8-15.
33. Anselmo, A. C.; Mitragotri, S. Nanoparticles in the Clinic. *Bioengineering & Translational Medicine* **2016**.
34. Mamot, C.; Drummond, D. C.; Noble, C. O.; Kallab, V.; Guo, Z.; Hong, K.; Kirpotin, D. B.; Park, J. W. Epidermal Growth Factor Receptor–Targeted Immunoliposomes Significantly Enhance the Efficacy of Multiple Anticancer Drugs In Vivo. *Cancer Res.* **2005,** *65*, 11631-11638.
35. Eriguchi, M.; Yanagie, H.; Maruyama, K.; Fujisawa, T., Liposome Preparations Containing Oxaliplatin. US20040022842 A1: Feb 5, 2004.
36. Sun, C. C.; Bodurka, D. C.; Weaver, C. B.; Rasu, R.; Wolf, J. K.; Bevers, M. W.; Smith, J. A.; Wharton, J. T.; Rubenstein, E. B. Rankings and Symptom Assessments of Side Effects from Chemotherapy: Insights from Experienced Patients with Ovarian Cancer. *Support. Care Cancer* **2005,** *13*, 219-227.
37. Senzer, N.; Nemunaitis, J.; Nemunaitis, D.; Bedell, C.; Edelman, G.; Barve, M.; Nunan, R.; Pirollo, K. F.; Rait, A.; Chang, E. H. Phase I Study of a Systemically Delivered p53 Nanoparticle in Advanced Solid Tumors. *Mol. Ther.* **2013,** *21*, 1096-1103.
38. Northfelt, D. W.; Hamburg, S. I.; Borad, M. J.; Seetharam, M.; Curtis, K. K.; Lee, P.; Crowell, B.; Vocila, L.; Fredlund, P.; Gilbert, M. J. In *A Phase I Dose-Escalation Study of TKM-080301, a RNAi Therapeutic Directed Against Polo-Like Kinase 1 (PLK1), in Patients with Advanced Solid Tumors: Expansion Cohort Evaluation of Biopsy Samples for Evidence of Pharmacodynamic Effects of PLK1 Inhibition*, ASCO Annual Meeting Proceedings, 2013.
39. Altin, J.; Atmosukarto, I.; De Wildt, R. M.; Parish, C.; Price, J., Composition for Targeting Dendritic Cells. US8779107 B2: July 15, 2014.
40. Hrkach, J.; Von Hoff, D.; Ali, M. M.; Andrianova, E.; Auer, J.; Campbell, T.; De Witt, D.; Figa, M.; Figueiredo, M.; Horhota, A. Preclinical Development and Clinical

Translation of a PSMA-Targeted Docetaxel Nanoparticle with a Differentiated Pharmacological Profile. *Sci. Transl. Med.* **2012,** *4*, 128ra39.

41. Davis, M. E. The First Targeted Delivery of siRNA in Humans Via a Self-Assembling, Cyclodextrin Polymer-Based Nanoparticle: From Concept to Clinic. *Mol. Pharmaceutics* **2009,** *6*, 659-668.
42. Von Hoff, D. D.; Mita, M. M.; Ramanathan, R. K.; Weiss, G. J.; Mita, A. C.; LoRusso, P. M.; Burris, H. A.; Hart, L. L.; Low, S. C.; Parsons, D. M.; Zale, S. E.; Summa, J. M.; Youssoufian, H.; Sachdev, J. C. Phase I Study of PSMA-Targeted Docetaxel-Containing Nanoparticle BIND-014 in Patients with Advanced Solid Tumors. *Clin. Cancer Res.* **2016,** *22*, 3157-3163.
43. LoRusso, P.; Krop, I.; Miller, K.; Ma, C.; Siegel, B. A.; Shields, A. F.; Molnar, I.; Wickham, T.; Reynolds, J.; Campbell, K. Abstract CT234: A phase I Study of MM-302, a HER2-targeted PEGylated Liposomal Doxorubicin, in Patients with HER2+ Metastatic Breast Cancer. *Cancer Res.* **2015,** *75*, CT234-CT234.
44. Pirollo, K. F.; Rait, A.; Zhou, Q.; Zhang, X. Q.; Zhou, J.; Kim, C.-S.; Benedict, W. F.; Chang, E. H. Tumor-Targeting Nanocomplex Delivery of Tumor Suppressor RB94 Chemosensitizes Bladder Carcinoma Cells In Vitro and In Vivo. *Clin. Cancer Res.* **2008,** *14*, 2190-2198.
45. van der Meel, R.; Vehmeijer, L. J. C.; Kok, R. J.; Storm, G.; van Gaal, E. V. B. Ligand-Targeted Particulate Nanomedicines Undergoing Clinical Evaluation: Current Status. *Adv. Drug Delivery Rev.* **2013,** *65*, 1284-1298.
46. Davis, M. E.; Zuckerman, J. E.; Choi, C. H. J.; Seligson, D.; Tolcher, A.; Alabi, C. A.; Yen, Y.; Heidel, J. D.; Ribas, A. Evidence of RNAi in Humans from Systemically Administered siRNA Via Targeted Nanoparticles. *Nature* **2010,** *464*, 1067-1070.
47. Zuckerman, J. E.; Gritli, I.; Tolcher, A.; Heidel, J. D.; Lim, D.; Morgan, R.; Chmielowski, B.; Ribas, A.; Davis, M. E.; Yen, Y. Correlating Animal and Human Phase Ia/Ib Clinical Data with CALAA-01, a Targeted, Polymer-Based Nanoparticle Containing siRNA. *Proc. Natl. Acad. Sci.* **2014,** *111*, 11449-11454.
48. Jaetao, J. E.; Butler, K. S.; Adolphi, N. L.; Lovato, D. M.; Bryant, H. C.; Rabinowitz, I.; Winter, S. S.; Tessier, T. E.; Hathaway, H. J.; Bergemann, C.; Flynn, E. R.; Larson, R. S. Enhanced Leukemia Cell Detection Using a Novel Magnetic Needle and Nanoparticles. *Cancer Res.* **2009,** *69*, 8310-8316.
49. Bradbury, M. S.; Phillips, E.; Montero, P. H.; Cheal, S. M.; Stambuk, H.; Durack, J. C.; Sofocleous, C. T.; Meester, R. J.; Wiesner, U.; Patel, S. Clinically-Translated Silica Nanoparticles as Dual-Modality Cancer-Targeted Probes for Image-Guided Surgery and Interventions. *Integr. Biol.* **2013,** *5*, 74-86.
50. Talelli, M.; Oliveira, S.; Rijcken, C. J.; Pieters, E. H.; Etrych, T.; Ulbrich, K.; van Nostrum, R. C.; Storm, G.; Hennink, W. E.; Lammers, T. Intrinsically Active Nanobody-Modified Polymeric Micelles for Tumor-Targeted Combination Therapy. *Biomaterials* **2013,** *34*, 1255-1260.
51. Adolphi, N. L.; Butler, K. S.; Lovato, D. M.; Tessier, T. E.; Trujillo, J. E.; Hathaway, H. J.; Fegan, D. L.; Monson, T. C.; Stevens, T. E.; Huber, D. L.; Ramu, J.; Milne, M. L.;

Altobelli, S. A.; Bryant, H. C.; Larson, R. S.; Flynn, E. R. Imaging of Her2-Targeted Magnetic Nanoparticles for Breast Cancer Detection: Comparison of SQUID-Detected Magnetic Relaxometry and MRI. *Contrast Media Mol. Imaging* **2012,** *7*.

52. Popovtzer, R.; Agrawal, A.; Kotov, N. A.; Popovtzer, A.; Balter, J.; Carey, T. E.; Kopelman, R. Targeted Gold Nanoparticles Enable Molecular CT Imaging of Cancer. *Nano Lett.* **2008,** *8*, 4593-4596.
53. Liberman, A.; Mendez, N.; Trogler, W. C.; Kummel, A. C. Synthesis and Surface Functionalization of Silica Nanoparticles for Nanomedicine. *Surf. Sci. Rep.* **2014,** *69*, 132-158.
54. Ngamcherdtrakul, W.; Morry, J.; Gu, S.; Castro, D. J.; Goodyear, S. M.; Sangvanich, T.; Reda, M. M.; Lee, R.; Mihelic, S. A.; Beckman, B. L. Cationic Polymer Modified Mesoporous Silica Nanoparticles for Targeted siRNA Delivery to HER2+ Breast Cancer. *Adv. Drug Delivery Rev.* **2015,** *25*, 2646-2659.
55. Knežević, N. Ž.; Durand, J. O. Targeted Treatment of Cancer with Nanotherapeutics Based on Mesoporous Silica Nanoparticles. *ChemPlusChem* **2015,** *80*, 26-36.
56. Mamaeva, V.; Sahlgren, C.; Lindén, M. Mesoporous Silica Nanoparticles in Medicine—Recent Advances. *Adv. Drug Delivery Rev.* **2013,** *65*, 689-702.
57. Li, Z.; Barnes, J. C.; Bosoy, A.; Stoddart, J. F.; Zink, J. I. Mesoporous Silica Nanoparticles in Biomedical Applications. *Chem. Soc. Rev.* **2012,** *41*, 2590-2605.
58. Lee, B. Y.; Li, Z.; Clemens, D. L.; Dillon, B. J.; Hwang, A. A.; Zink, J. I.; Horwitz, M. A. Redox-Triggered Release of Moxifloxacin from Mesoporous Silica Nanoparticles Functionalized with Disulfide Snap-Tops Enhances Efficacy Against Pneumonic Tularemia in Mice. *Small* **2016,** *12*, 3690–3702.
59. Rosenholm, J. M.; Mamaeva, V.; Sahlgren, C.; Lindén, M. Nanoparticles in targeted cancer therapy: mesoporous silica nanoparticles entering preclinical development stage. *Nanomedicine* **2012,** *7*, 111-120.
60. He, Q.; Zhang, Z.; Gao, F.; Li, Y.; Shi, J. In vivo biodistribution and urinary excretion of mesoporous silica nanoparticles: effects of particle size and PEGylation. *Small* **2011,** *7*, 271-280.
61. Witasp, E.; Kupferschmidt, N.; Bengtsson, L.; Hultenby, K.; Smedman, C.; Paulie, S.; Garcia-Bennett, A. E.; Fadeel, B. Efficient Internalization of Mesoporous Silica Particles of Different Sizes by Primary Human Macrophages Without Impairment of Macrophage Clearance of Apoptotic or Antibody-Opsonized Target Cells. *Toxicol. Appl. Pharmacol.* **2009,** *239*, 306-319.
62. Steinbacher, J. L.; Lathrop, S. A.; Cheng, K.; Hillegass, J. M.; Butnor, K. J.; Kauppinen, R. A.; Mossman, B. T.; Landry, C. C. Gd-Labeled Microparticles in MRI: In vivo Imaging of Microparticles After Intraperitoneal Injection. *Small* **2010,** *6*, 2678-2682.
63. Lu, J.; Li, Z.; Zink, J. I.; Tamanoi, F. In Vivo Tumor Suppression Efficacy of Mesoporous Silica Nanoparticles-Based Drug-Delivery System: Enhanced Efficacy by Folate Modification. *Nanomed.* **2012,** *8*, 212-220.

64. Na, H. K.; Kim, M. H.; Park, K.; Ryoo, S. R.; Lee, K. E.; Jeon, H.; Ryoo, R.; Hyeon, C.; Min, D. H. Efficient Functional Delivery of siRNA Using Mesoporous Silica Nanoparticles with Ultralarge Pores. *Small* **2012,** *8*, 1752-1761.
65. Hartono, S. B.; Gu, W.; Kleitz, F.; Liu, J.; He, L.; Middelberg, A. P.; Yu, C.; Lu, G. Q.; Qiao, S. Z. Poly-L-lysine Functionalized Large Pore Cubic Mesostructured Silica Nanoparticles as Biocompatible Carriers for Gene Delivery. *ACS Nano* **2012,** *6*, 2104-2117.
66. Kim, M. H.; Na, H. K.; Kim, Y. K.; Ryoo, S. R.; Cho, H. S.; Lee, K. E.; Jeon, H.; Ryoo, R.; Min, D. H. Facile Synthesis of Monodispersed Mesoporous Silica Nanoparticles with Ultralarge Pores and Their Application in Gene Delivery. *ACS Nano* **2011,** *5*, 3568-3576.
67. Steinbacher, J. L.; Landry, C. C. Adsorption and Release of siRNA from Porous Silica. *Langmuir* **2014,** *30*, 4396-4405.
68. Owens, G. J.; Singh, R. K.; Foroutan, F.; Alqaysi, M.; Han, C.-M.; Mahapatra, C.; Kim, H. W.; Knowles, J. C. Sol–Gel Based Materials for Biomedical Applications. *Prog. Mater. Sci.* **2016,** *77*, 1-79.
69. Sing, K. S. W.; Everett, D. H.; Haul, R. A. W.; Moscou, L.; Pierotti, R. A.; Rouquerol, J.; Siemieniewska, T., Reporting Physisorption Data for Gas/Solid Systems. In *Handbook of Heterogeneous Catalysis*, Wiley-VCH: Weinheim, 2008.
70. Sing, K. The Use of Nitrogen Adsorption for the Characterisation of Porous Materials. *Colloids Surf., A* **2001,** *187*, 3-9.
71. Branton, P. J.; Hall, P. G.; Sing, K. S.; Reichert, H.; Schüth, F.; Unger, K. K. Physisorption of Argon, Nitrogen and Oxygen by MCM-41, a Model Mesoporous Adsorbent. *J. Chem. Soc., Faraday Trans.* **1994,** *90*, 2965-2967.
72. Thommes, M.; Kaneko, K.; Neimark, A. V.; Olivier, J. P.; Rodriguez-Reinoso, F.; Rouquerol, J.; Sing, K. S. Physisorption of Gases, with Special Reference to the Evaluation of Surface Area and Pore Size Distribution (IUPAC Technical Report). *Pure Appl. Chem.* **2015,** *87*, 1051-1069.
73. Goldburg, W. Dynamic Light Scattering. *Am. J. Phys.* **1999,** *67*, 1152-1160.
74. Sartor, M. Dynamic Light Scattering. *University of California, San Diego* **2003**, 2-21.
75. Vauthier, C.; Ponchel, G., *Polymer Nanoparticles for Nanomedicines: A Guide for their Design, Preparation and Development*. Springer: New York, 2017.
76. Reimer, L., *Transmission Electron Microscopy: Physics of Image Formation and Microanalysis*. Springer: New York, 2013; Vol. 36.
77. Kohl, H.; Reimer, L., *Transmission Electron Microscopy*. Springer: New York, 2008.
78. Bligaard, T.; Bullock, R. M.; Campbell, C. T.; Chen, J. G.; Gates, B. C.; Gorte, R. J.; Jones, C. W.; Jones, W. D.; Kitchin, J. R.; Scott, S. L. Toward Benchmarking in Catalysis Science: Best Practices, Challenges, and Opportunities. *ACS Catal.* **2016,** *6*, 2590-2602.

CHAPTER 2: EXTERNAL CONJUGATION DELIVERY SYSTEMS

2.1 Preparation methods

There are two main silica systems using conjugation of DNA or RNAi to the exterior of the silica for gene therapy: solid and mesoporous with very small pores. Most of the systems are synthesized using the sol-gel method where a colloidal solution or sol is created and then assembled upon through condensation. The mesoporous system uses surfactant that produces pores through self-assembly by the silica precursor around the surfactant. However, in some cases the pores are too small after surface functionalization to allow for loading DNA and RNAi in the pores, so external conjugation is used.

Variations in preparation method alter the particle size and morphology as well as determining how easily production could be scaled up for clinical use. The silica core's size and morphology alters the outcome of the particle in vivo.[1] Thus, a primary goal is to produce a base particle that is biocompatible and successfully delivers its' therapy in vivo upon which targeting and oligonucleotide specific functionalization can be altered based on the cargo and target.

2.1.1. Solid silica systems

Several preparation methods have been used to synthesize the solid silica core for DNA and RNAi delivery. The most common strategy is the sol-gel method that involves hydrolysis and then condensation. Xiao and colleagues[2] and Buchman and colleagues[3] both prepared their solid silica particles via this method. Their method involved using ammonium as the base catalyst, absolute ethanol, and TEOS. Buchman's group produced

nanoparticles with an average diameter of 31.5 ± 5.2 nm based on TEM measurements and a zeta potential of -26.5 mV determined by a Zetasizer Nano.[3] Xiao and colleagues added thionyl chloride and benzene in order to produce chlorinated silica for their functionalization. This mixture was stirred for 50 hours. Both zeta potential and size were measured after the chlorinated SNPs were functionalized with amino groups. The final product was nearly spherical in shape, had a diameter of 20-30 nm based on DLS, and a zeta potential of +11.3 mV.[2]

Ye et al. modified the sol-gel method to produce cross-linked hybrid organosilica NPs from gelatin/3-glycidoxypropyl-trimethoxysilane (GPSM) and (3-aminopropyl)trimethoxysilane (APTMS) (**Figure 2.1.**). This method was developed to simplify preparation and avoid environmentally harmful solvents.[4] In acidic conditions GPSM's epoxy group was protonated and thus activated to undergo a nucleophilic attack from the NH_2 side chain on gelatin.[5] The sol was formed by the GPSM/gelatin molecule, since the methoxy silane groups (Si-OCH_3) of GPSM was hydrolyzed to produce Si-OH.[5] The hydrophilic portion where gelatin attached to GPSM forms the inner section on the sol.[4] Once APTMS is added, the pH is changed to 8-9. This basic solution caused the hydrolyzed GPSM and APTMS molecules to co-condense and form a siloxane network.[5] The amine group from APTMS is mainly on the exterior of the nanoparticles, because the GSNPs form organized micelles where the hydrophilic portion is on the interior and the hydrophobic portion containing the amine is on the exterior.[4] This was confirmed by silicon-29 cross-polarization magic angle spinning nuclear magnetic resonance spectrum (^{29}SiCP/MAS NMR) that found condensation of Si-OH groups were 93.6% complete.[4] The final GSNP ranged in size from 140-160 nm.[4]

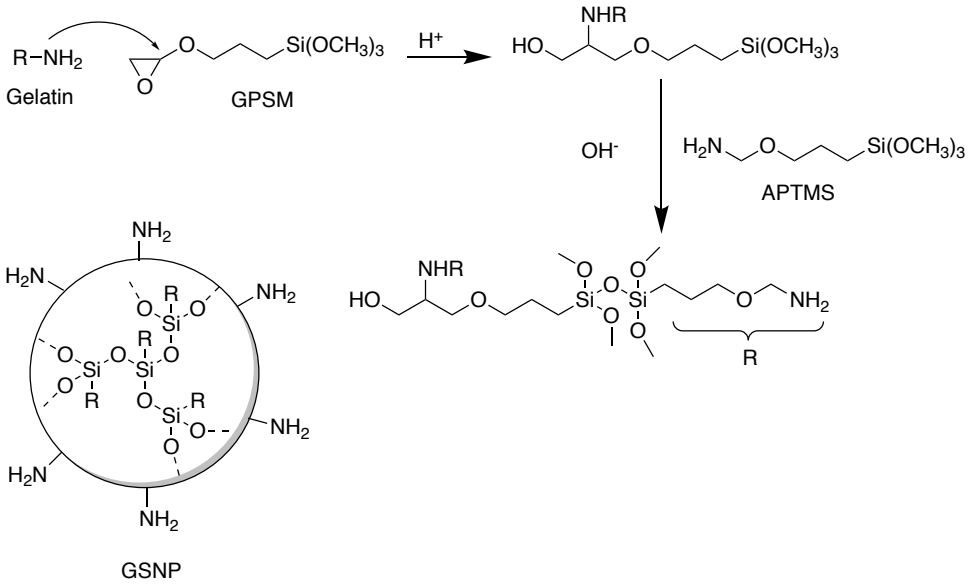

Figure 2.1. Synthesis of GSNPs. Image adapted from reference 4.

Another method was used by Rejeeth and colleagues by forming non-polar cores in a micellar medium made from the surfactant (Aerosol OT (AOT)), co-surfactant (*n*-butanol (BuOH)), and water.[6] Dimethyl sulfoxide (DMSO) creates the nonpolar core around which AOT, BuOH and water micelles form. Vinyltriethoxysilane (VTES) and 3-aminopropyltriethoxysilane (APTES) are hydrolyzed together to form a hybrid amino-functionalized nanoparticle.[6] The resulting silica nanoparticles were separated from AOT and BuOH by dialysis and re-suspended in water.[6-7] The final nanoparticle had a mean diameter of 54 nm (determined with transmission electron microscopy (TEM)) and a zeta potential of approximately 8 mV due to the positively charged amine groups in APTES. The benefit of this synthesis method include avoiding additional purification steps due

to grafting amines post particle formation and the addition of organic groups is thought to add some degree of flexibility to the rigid silica matrix.[6]

2.1.2. Mesoporous systems for exterior loading

The sol-gel method is also the most common strategy to synthesize mesoporous silica nanoparticles for external loading. Ngamcherdtrakul and colleagues prepared 47-nm mesoporous silica core with the base catalyzed sol-gel method using cetyltrimethylammonium chloride (CTAC) as the surfactant to form the pores, triethylamine (TEA), and TEOS as the silica precursor.[8] TEA, a base, and CTAC are first mixed in water before TEOS is added. The particles are formed first by TEOS being hydrolyzed. The silica precursor then condenses and forms the seeds from which the particles are built.[9] TEA, a base, acts to keep these seeds apart during the condensation process by retarding hydrolysis of TEOS' alkoxides.[10] The CTAC's ammonium anions act as a structure directing agent due to their positively charged NH_4^+ head around which the silica precursor self-assembles during the co-condensation process by forming the pores.[10] The surfactant was removed by being refluxed in methanol and hydrochloric acid overnight.[8] The silica nanoparticle's diameter used in the study was 47-nm based on TEM measurements.[8]

2.2 External functionalization

Delivery systems where the oligonucleotide is loaded on the nanoparticle's exterior use cationic functional groups to electrostatically attach and protect the negatively charged DNA or siRNA. External functionalization, such as PEG, also acts to

protect the gene or RNAi from degradation by enzymes like DNase 1 by repelling proteins in the bloodstream.[6] External cationic functionalization has the added benefit of binding with high affinity to the lipid groups of a cell due to their negative charge resulting in endocytosis,[11] although positively charged nanoparticles are taken up by the immune system in vivo.[12] Thus, PEG is often used to reduce immune system uptake.

Decorating the exterior with a polymer such as polyethylenimine (PEI) results in endosomal swelling and eventual rupture leading to endosome escape, which is necessary for successful transfection.[12] PEI accomplishes endosomal escape, because its' unsaturated amino groups bind with free protons in the endosome.[11] This causes the proton pumps (v-ATPase) to continue pumping protons into the endosome to replenish the protons bound to the PEI. For each proton pumped into the endosome, one free chloride and water to enter the vesicle.[11] The extra water molecules cause swelling and the eventual rupture that allows the nanoparticle to escape to the cytoplasm.[11]

2.2.1. Amino groups for gene and siRNA loading

Several groups used an amino group exterior to load and protect siRNA. For example, Rejeeth and colleagues loaded p53 onto their particles by first functionalizing the exterior with a synchronous hydrolysis of vinyltriethoxysilane (VTES) and 3-aminopropyltriethoxysilane (APTES).[6] DNA electrostatically attached to the positively charged amino groups on the particle's surface. Once loaded, the particle diameter increased to an average of 59 nm to 113 nm based on TEM measurements.[6] Zeta potential on the loaded particles was reported to be more positive than preloaded NPs, 8 mV and 13 mV respectively based on analysis by electrophoretic light scattering

spectrophotomer.[6] This result is counter to the other studies in this review where loading negatively charged plasmid DNA (pDNA) reduces a system's zeta potential. Unfortunately, the authors do not address this abnormal reading.

Successful loading and delivery of the pDNA was demonstrated with an in vitro growth assay using MCF-7 cells (**Figure 2.2.**). The cells were transfected with either the unloaded nanoparticles (control), p53 alone, p53 loaded onto their nanoparticles (ORMOSILNs), or p53 loaded in Lipofectin®. After transfection, the number of viable cells was determined. Cell growth was significantly inhibited by the p53/ORMOSILNs treated group compared to the control and free p53 treated groups. Their system also out performed p53 loaded Lipofectin.

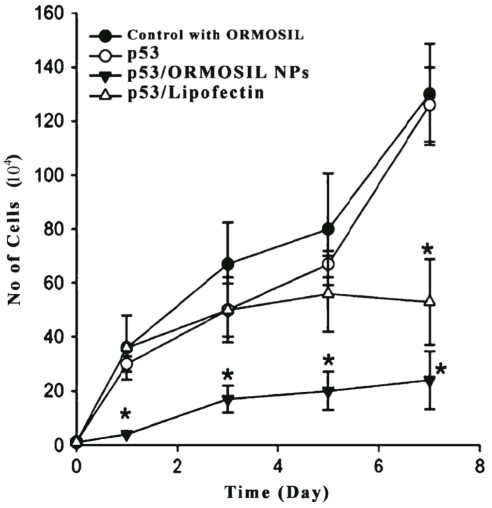

Figure 2.2. In vitro growth inhibition of MCF-7 cells after transfection with unloaded nanoparticles (control), free p53, ORMOSILNs loaded with p53, and Lipofectin loaded with p53. *$p < 0.05$ compared with the in vitro growth inhibition of the control. Image modified from reference 6.

Like Rejeeth's group, Xiao and colleagues used amino groups to electrostatically attach the p53 gene.[2] They functionalized their NPs' surface by first chlorinating the silica by including thionyl chloride with benzene in their particle preparation (**Figure 2.3.**). This produces a surface of Si-Cl bonds that will react with an alcohol or amine to form Si-O or Si-N linkages.[13] The advantage of this method is that it eliminates competition between intermolecular reactions and surface attachment.[13] In order to ensure alcohol attachment to the surface and external amino functionalization, Xiao and colleagues used 3-(Fmoc-amino)-1-propanol. The Fmoc group was then removed in piperidine in DMF. The average diameter of the modified particles (AMSNs) was 20-30 nm as determined by DLS and the zeta potential was 11.3 mV.[2]

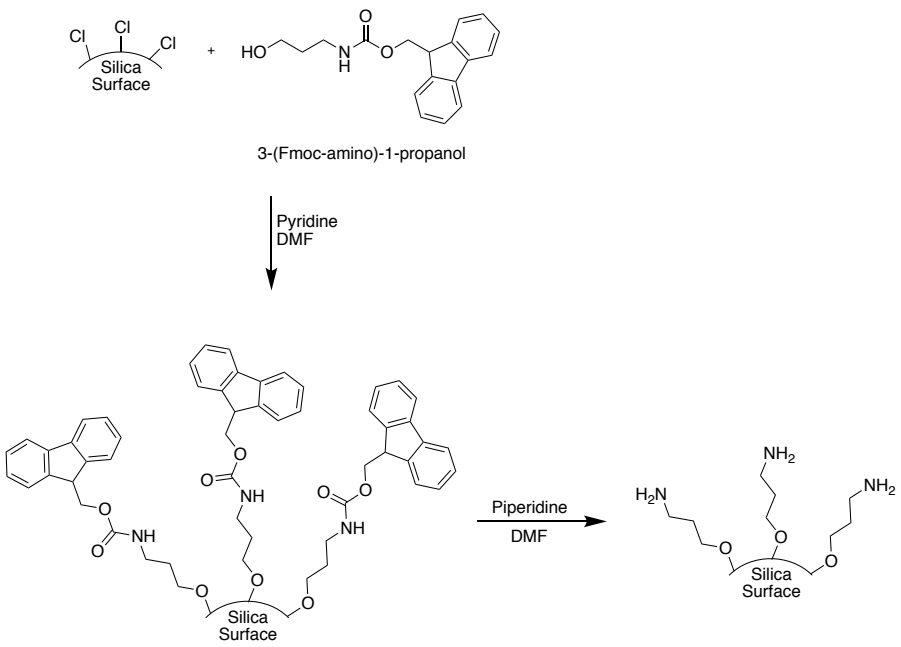

Figure 2.3. Xiao et al. functionalization method.

DNA was electrostatically attached to the amino modified nanoparticles by incubation. To determine whether the DNA bound to the functionalized particles, the group used agarose gel electrophoresis (**Figure 2.4.**). Once DNA was bound to the nanoparticles, the entire complex would weigh too much to travel on the gel. The mobility of DNA was retarded after a weight ratio of 30 nanoparticles to 1 DNA.[2] The high ratio of nanoparticles to DNA implies the positive charge of multiple nanoparticles is necessary to electrostatically bind the negatively charged DNA. This suggests the external modification employed would not be adequate for in vivo delivery.

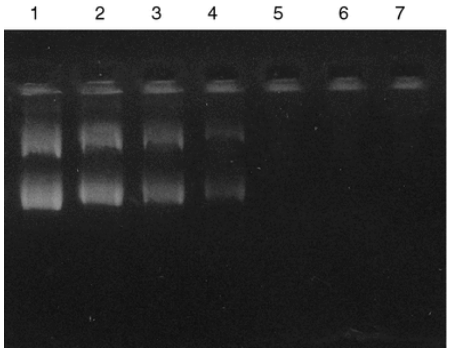

Figure 2.4. Examining the binding capacity of AMSNs with agarose gel electrophoresis. DNA mobility was retarded once complexed with the AMSNs. Lane 1: control plasmid DNA. Lane 2-7 NPs to DNA ratios (w/w) of 1:1, 5:1, 30:1, 50:1, 100:1. Image modified from reference 2.

Transfection efficiency was found to be approximately 48% when measured by fluorescence microscopy (**Figure 2.5.**). Xiao's group used the reporter plasmid p53 enhanced green fluorescent protein (pp53-EGFP) to measure transfection in HepG2 cells. When comparing transfection efficiency between their system (60 μg) and Lipofectin (8 μg), the two were comparable when compared with Western blot analysis (**Figure 2.6.**).

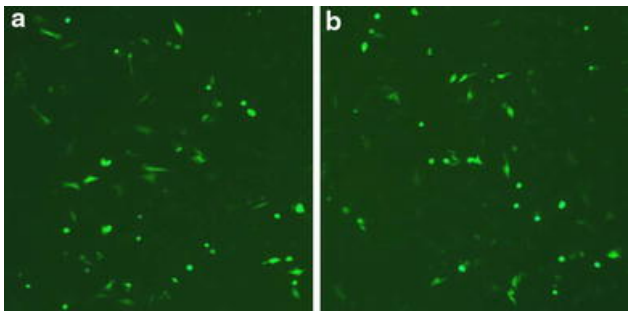

Figure 2.5. Fluorescence microscopy analysis of pp53-EGFP transfected HepG2 cells. A) Amino functionalized nanoparticles B) Lipofectin. Image modified from reference 2.

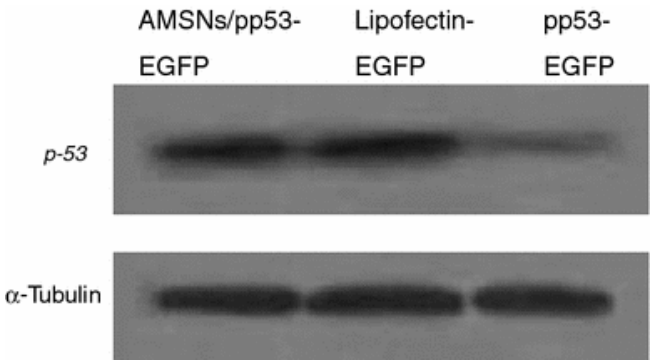

Figure 2.6. Western blot analysis of p53 protein expression in pp53-EGFP transfected cells. Free DNA (pp53-EGFP) resulted in very little protein expression, while AMSN and Lipofectin loaded nanoparticles resulted in similar expression. α-tubulin was consistent across treated groups. Image modified from reference 2.

Ye and colleagues also tested external amino groups to externally load oligonucleotides. They conjugated the amino groups to solid gelatin-silica nanohybrids (GSNPs) as well as three fusion peptides: Tat, R8, HA2.[4] The Tat peptide, originally discovered on HIV-1, has been found to cause cell uptake of a wide variety of molecules.[14] The N-terminal domain of influenza virus hemagglutinin-2 (HA2) may cause membrane lysis at low pH thus mediating endosomal escape.[4] Octaarginine (R8)

has been shown to enhance cellular uptake and endosomal escape of liposomes.[15] In all they tested six different surface chemistries: plain GSNPs (GS), Tat (GS-Tat), HA2 (GS-HA2), R8 (GS-R8), Tat/HA2 (GS-TH), and Tat/R8 (GS-TR) modified GSNPs. To conjugate the fusion peptides to the particles' surfaces, thiol groups were introduced using succinimidyl 3-(2-pyridyldithio)propionate (SPDP) reagent (**Figure 2.7.**). This allowed sulfhydrl-containing peptides to easily be conjugated to the nanoparticle's surface using disulfide bonds. The ratio of peptides to gelatin-silica for all six groups was approximately 1.58 μmol/mg.[4] DNA loading was then performed by incubating the DNA with the final particles at 100 μg/mL.[4] The final particles with complexed DNA had a mean diameter of 190-230 nm determined with DLS and a positive zeta potential of +20-22 mV based on Zetasizer Nano measurements.[4]

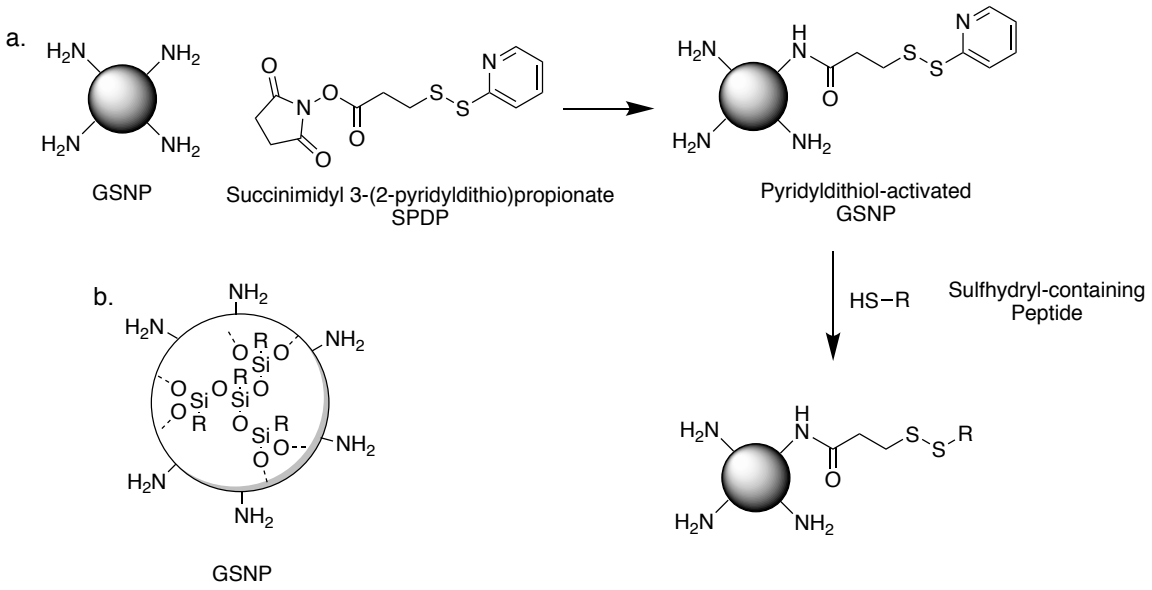

Figure 2.7. A) Conjugation of the three sulfhydryl-containing peptides to GSNPs. B) Internal particle structure of GSNPs. Image modified from reference 4.

In vitro studies and intratumor injection in vivo both demonstrated that the GSNP-Tat/HA2 (or GSNP-TH) nanoparticles transfected the most genetic material (**Figure 2.8.**).[4] However, intravenous injection of the plain GSNP and three fusion peptide decorated GSNPs resulted in the majority of luciferase gene expression in the liver and spleen with low levels of gene expression in the tumor.[4] This is likely due to immune system uptake into the reticuloendothelial system (RES). In future research the group will likely explore using PEG in addition to the cell penetrating peptides in order to escape the RES and improve circulation time.[4] Extended circulation time will improve the likelihood of the nanoparticle system arriving close enough to its' intended target for the uptake moiety to work. The in vivo group also did not demonstrate significant differences between peptides. Further studies are needed to determine whether the in vitro findings translate to intravenous administration.

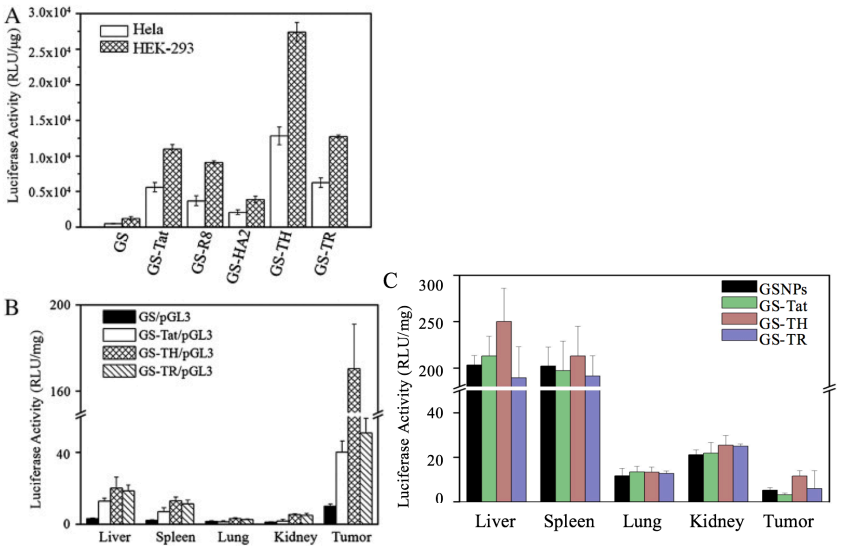

Figure 2.8. The above graphs used luciferase quantification via an FB12 luminometer. A) In vitro transfection of the luciferase gene (pGL3) into HeLa or HEK-293 cells with the

six different external modifications. B) In vivo expression of the luciferase gene in the liver, spleen, lung, kidney and tumor via intratumoral injection. C) In vivo expression of the luciferase gene in the liver, spleen, lung, kidney, and tumor via intravenous injection. Image modified from reference 4.

2.2.2. Polymers for DNA and siRNA loading

Polymers are often used to functionalize the exterior of nanoparticles due to their ability to compact and deliver RNAi and DNA. PEI and PEG are most commonly used. PEI aids in transfection by increasing the influx of hydrated protons due to its unprotonated secondary and tertiary amines.[8] PEG prevents corona formation, improve circulation times, protect siRNA from enzymatic degradation by providing steric protection.[16] Shorter chain PEI (<10 kDa) have been shown to not lead to significant toxicity in a range of normal and tumor cells.[17-18]

Buchman and colleagues created an siRNA delivery platform using base prepared solid silica nanoparticles (32.8 nm based on TEM images) with APTES covalently attached to the particle's surface and PEI 25 kDa attached to the amine by a *bis*-Michäel acceptor divinyl sulfone (DVS) linker (**Figure 2.9.**).[3] The aim of using DVS to attach the 25 kDa PEI is to mitigate the branched polymer's toxicity. The process of functionalization requires first functionalizing the exterior with APTES to distribute free amines on the surface. DVS was then added in a 1:1 ratio with respect to APTES.[3] After two hours of stirring, the particles were washed and various amounts of 25 kDa PEI were added. The final system had an average TEM diameter of 34.2 ± 4.2 and a zeta potential of 26.6 ± 1.0 determined by a Zetasizer Nano.[3]

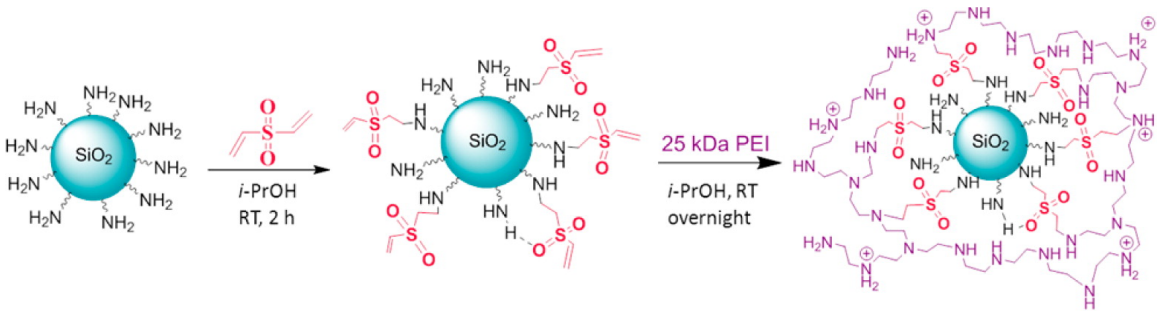

Figure 2.9. The exterior functionalization of Buchman et al.'s delivery system. The silica base is first functionalized with APTES, resulting in the amine exterior on the nanoparticle on the left. DVS is then added with *i*-PrOH and the mixture is stirred for two hours. Finally, 25 kDa PEI is attached by stirring at room temperature overnight. Image modified from reference 3.

The final particles successfully complexed with siRNA with the most effective PEI/siRNA w/w ratio being 2:1.[3] This was determined by using two luciferase proteins, *Firefly* and *Renilla*, to investigate in vitro gene silencing and toxicity (**Figure 2.10.**). Both *Firefly* (61 kDa) and *Renilla* (36 kDa) luciferases are oxidative enzymes that produce bioluminescence upon oxidizing their specific substrate.[3] Since both reporters use different substrates and produce bioluminescence at different wavelengths, the dual luciferase system allowed measurement of the specific silencing of *Firefly* luciferase due to delivered siRNA and *Renilla* luciferase due to nanoparticle induced toxicity.[3] A constant amount of siRNA targeting *Firefly* luciferase (100 nM) was used and the weight of 25 kDa PEI was varied in order to determine the optimal weight ratio for in vitro delivery while avoiding toxicity.[3] The group compared this data to free 25 kDa complexed with *Firefly* luciferase targeting siRNA to establish whether the nanoparticle improved efficacy. The nanoparticle system demonstrated a high level of *Firefly* luciferase silencing (69%) while demonstrating cellular viability.[3] Higher PEI/siRNA ratios (2:1 and 5:1) demonstrated increased silencing effects (90% and 89% respectively)

without any observed toxicity.[3] Greater weight ratios resulted in the reduction of *Renilla* luciferase's signal, indicating toxicity. The need for a greater PEI/siRNA ratio than 1:1 is likely due to the resulting charge of the polyplex.[3] The 1:1 ratio resulted in a zeta potential of -30.1 mV that likely decreased cell uptake and endosomal escape, while 2:1 PEI/siRNA had a zeta potential of 10.4 mV.[3] The 2:1 nanoparticles did display a tendency to aggregate that could be alleviated by either conjugating PEG to the PEI or increasing the zeta potential by using a weight ratio of 5:1 PEI/siRNA (26.3 mV).

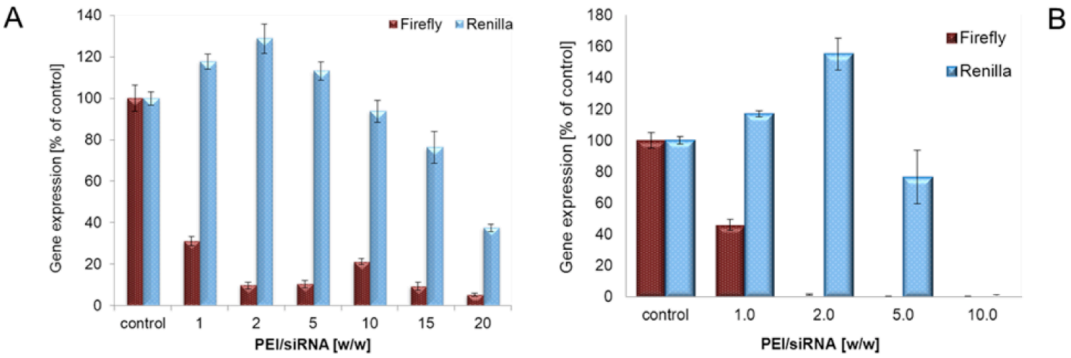

Figure 2.10. Luciferase levels 48 hours after transfection. A reduction in Firefly demonstrates successful gene silencing, while a reduction in Renilla demonstrates toxicity. A) siRNA complexed on NP and B) free 25 kDa PEI/siRNA. Image modified from reference 3.

The free PEI/siRNA complex also silenced *Firefly* luciferase but with greater toxicity at higher weight ratios. At a 10:1 PEI/siRNA ratio, the nanoparticle complex reduced *Renilla* luciferase expression much less (94%) than the free PEI/siRNA complex (0%).[3] Thus, the nanoparticle likely mitigated toxicity from PEI while still delivering the siRNA.

Other groups synthesized a larger polymer shell that would further protect the transfection agent and, due to its increased charge, load more nucleic acids. Lee et al. sought to achieve greater cell transfection and siRNA loading by using PEI, PEG, and trimethoxy(3-(oxiran-2-ylmethoxy)propyl)silane (3-GTMS).[19] Their three-step method involves synthesizing the block-copolymer from PEI (25 kDa) and PEG (5 kDa), modifying the block-copolymer with 3-GTMS to include a silane, and then conjugating the product of the second step to the silica nanoparticles (**Figure 2.11.**). The final system had a high zeta potential of 66 mV based on Zetasizer Nano analysis.[19] The high zeta potential is likely due to the thick copolymer shell (12-15 nm based on TEM) on the 28-30 nm core nanoparticle.[19] The group used a gel retardation assay to determine which weight percent resulted in the most protection for siRNA. Ratios of 1:5 to 1:15 (siRNA undefined wt%:particles wt%) were the most stable, although the optimal weight percent was found to be 1:10 to protect the siRNA from RNAse as well as allow for cellular delivery.[19] The system demonstrated low cytotoxicity in vitro when transfected in human alveolar basal epithelial cells (A549) and is being explored as a platform to develop a hybrid nanoparticle for MR imaging and siRNA transfection.[19]

Ngamcherdtrakul et al. similarly used PEI and PEG to load siRNA and attach a targeting ligand to their base prepared, mesoporous silica nanoparticle (47 nm diameter). In their method, PEI was first coated on the exterior of the MSNP. Once complete, the PEI-MSNP was crosslinked using dithiobis(succinimidyl propionate) (DSP), an amine-reactive crosslinker with an *N*-hydroxysuccimidine (NHS) ester at each end and a disulfide bond in the spacer arm. This disulfide bond is cleaved by reduced glutathione once entering the cell where the glutathione concentration is 50-1000 times higher than

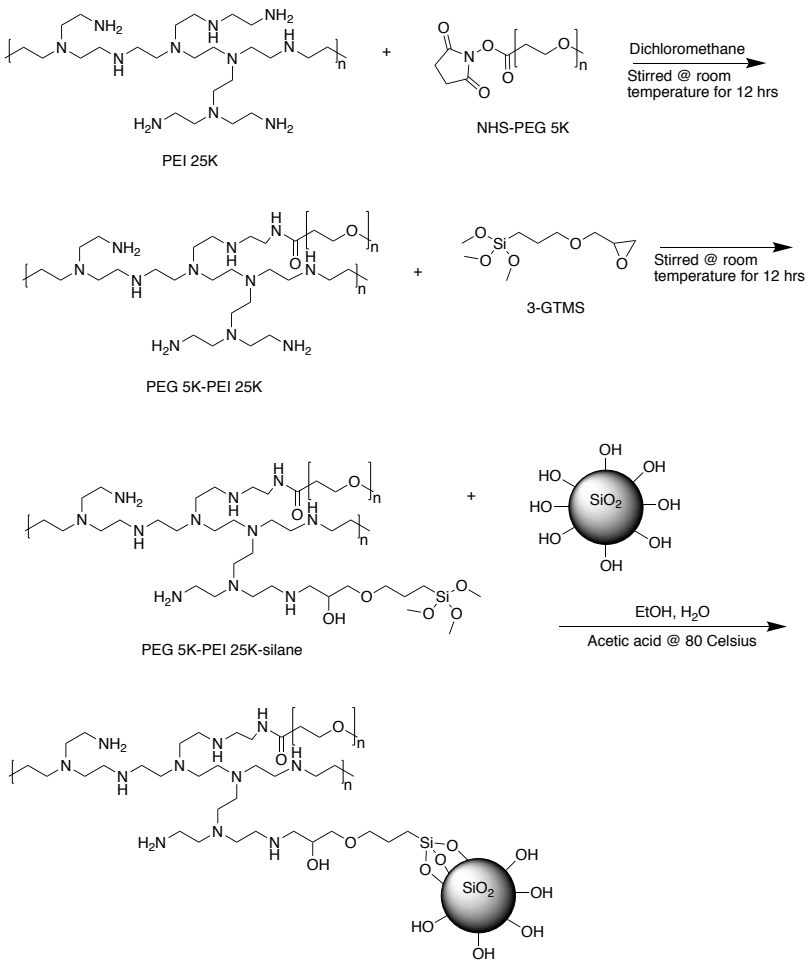

Figure 2.11. The three-step prep for the external polymer layer for siRNA loading and delivery. Image modified from reference 19.

outside the cell.[20] Thus, the siRNA cargo loaded within the PEI is released upon entering the cell. PEG was then conjugated to the primary amine of MSNP-PEI by using maleimide-PEG5kDa-NHS.[8] Finally, the HER2 antibody trastuzumab was conjugated with the thiol-maleimide reaction by thiolating the antibody with 2-iminothiolane (C_4H_7NS) and then mixing it with MSN-PEI-PEG.[8] The optimal formulation had an average hydrodynamic diameter of 117 nm determined by DLS and an average zeta potential of 25 mV.

Compared to Lee and colleague's surface modification method using a higher weight PEI, Ngamcherdtrakul's group found 10-kDa PEI to provide optimal gene silencing efficacy (76%) while minimizing the use of PEI due to toxicity concerns.[8] This is consistent with other studies' results where reducing the chain length of PEI increases the MSNs' safety profile.[18] The group measured silencing efficacy by delivering siRNA targeting HER2 to $HER2^+$ breast cancer cell lines.

The targeting moiety's ability to target $HER2^+$ expressing cancer cells was demonstrated in vitro by measuring cell uptake in two $HER2^+$ breast cancer cells, BT474 and SKBR3, and one $HER2^-$ cell line, MCF-7 (**Figure 2.12.**). Scrambled siRNA was tagged with Alexa 488, a fluorophore to quantify uptake (siSCR). The two trastuzumab groups targeting $HER2^+$ cell lines were T-siSCR-$NP^{1.8C}$ with 1.8 kDa PEI and T-siSCR-NP^{10C} with 10 kDa PEI. The negative control was two different PEI-conjugated nanoparticles conjugated with rituximab targeting CD20 (R-siSCR-$NP^{1.8C}$ with 1.8 kDa PEI and R-siSCR-NP^{10C} with 10 kDa PEI). The two different weights of PEI were used in order to test whether the efficacy of the siRNA loaded nanoparticles could be increased by increasing the particle's buffer capacity.[8] Polymers like PEI have buffering capacity in the pH range of 5-7 due to their unprotonated secondary and tertiary amines, which is believed to result in the proton sponge effect and, consequently, endosome escape.[8] For example, an estimated 15% of nitrogens are protonated on PEI in the extracellular space that increases to 45% upon entry into a lysosome.[21]

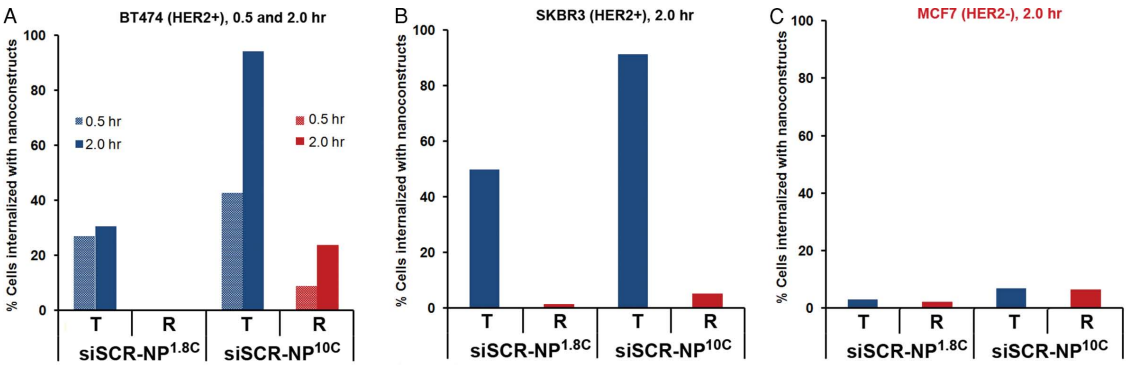

Figure 2.12. Cellular uptake of siRNA carrying nanoparticles bearing trastuzumab or rituximab targeting moieties. R-siSCR-NP1.8C is functionalized with 1.8-kDa PEI and R-siSCR-NP10C with 10-kDa PEI. A) BT474 ($HER2^+$) taken at two time points, 0.5 and 2 hours B) SKBR3 ($HER2^+$) taken at 2 hours C) MCF7 ($HER2^-$) taken at 2 hours. Image modified from reference 8.

The two systems also differed in the amount of PEG: R-siSCR-$NP^{1.8C}$ had 6.1% PEG and R-siSCR-NP^{10C} had 18.2% PEG based on TGA measurements.[8] This is likely due to the higher molecular weight of PEI between the two groups, since the 10 kDa PEI contains more reactive amine groups for PEG binding than 1.8 kDa PEI.[8] The amount of Alexa-488 tagged siRNA in the interior of each cell was measured using flow cytometry. In the two $HER2^+$ cell lines (**Figure 2.12.**) the trastuzumab and 10 kDa PEI functionalized delivery system outperformed the 1.8 kDa PEI decorated system. The trastuzumab targeting system also successfully targeted $HER2^+$ cell lines and did not transfect $HER2^-$ cell line.

In order to confirm successful siRNA delivery and HER2 suppression, Ngamcherdtrakul and colleagues delivered HER2 targeted siRNA to three HER2+ breast cancer lines: BT474, SKBR3, and HCC1954 (**Figure 2.13.**). They used quantitative immunofluorescent imaging to determine HER2 protein levels for T-siHER2-NP^{10C} and

T-siSCR-NP^{10C}. The nanoparticle system delivery HER2 targeting siRNA reduced HER2 levels by 81%-93% compared to the scrambled siRNA system.[8] This confirms successful siRNA delivery and targeted protein suppression.

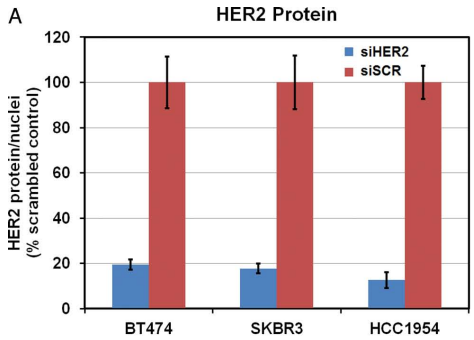

Figure 2.13. HER2 expression in three HER2+ breast cancer cell lines 72 hours post incubation with siHER2 or siSCR delivered via trastuzumab decorated nanoparticles. Image modified from reference 8.

When evaluated in vivo via intravenous tail injection of T-siHER2-NP^{10C} to treat the breast cancer xenograft HCC1954 (a tissue graft from a human donor), Ngamcherdtrakul's group found 58.6% tumor reduction compared with saline control ($p < 0.0013$) and 46.5% ($p < 0.015$) compared to the control T-siSCR-NP^{10C}, nanoparticles carrying a scrambled siRNA coupled with trastuzumab.[8] The tumor reduction caused by the control T-siSCR-NP^{10C} is likely caused by the targeting moiety trastuzumab, since it is known to cause HER2 reduction.[8] While the study demonstrates effectiveness in treating resistant tumor lines, the study did not include information concerning the in vivo fate of the particles.

2.3 Chapter Conclusion

Several methods have been pursued to synthesize silica nanoparticles for loading DNA and RNAi on the particle's exterior. The most commonly used method is the sol-gel method. Two groups, Rejeeth et. al and Ye et. al, modified the sol-gel procedure to incorporate amines during synthesis to reduce procedural and purification steps. The sol-gel synthesized solid nanoparticles had a diameter of 20-31.5 nm, whereas Rejeeth et. al's procedure produced 54 nm particles and Ye et. al's method resulted in 140-160 nm particles. Thus, a range of solid silica nanoparticles with different diameters have been produced and could be compared for in vivo and in vitro efficacy.

Ngamcherdtrakul et. al created mesoporous silica nanoparticles functionalized with PEI and PEG to externally attach siRNA. The mesoporous silica nanoparticles could be used for dual delivery of an internally loaded drug and externally attached RNAi, since drug molecules are smaller than siRNA.[8] This may be a promising strategy for externally loaded systems to treat cancer, since siRNA combined with medications like doxorubicin have been shown to overcome drug resistance in cancer cells.[22]

Both amino groups and polymers have been investigated for loading DNA and RNAi for delivery to cancer cells. While some studies demonstrated cell growth inhibition due to oligonucleotide loaded amine decorated nanoparticles, the particle systems may be aggregating to load DNA as in Xiao et. al's study.[2] They found a ratio of 30 nanoparticles to 1 DNA necessary for complexation but a transfection efficacy of 48% in vitro.[2] These aggregations would likely not remain viable during in vivo application and increase the delivery system's diameter. Future studies should investigate

the necessary ratio required to complex the desired oligonucleotide in addition to in vitro efficacy to produce a viable system for clinic.

Polymer decorated nanoparticles exhibited relatively high transfection and protein suppression rates in a number of different cell lines. Most promising is the combined use of PEI for endosomal escape and PEG to protect the loaded oligonucleotides by repelling blood proteins. While more studies are needed in order to determine the optimal PEI weight, Ngamcherdtrakul et. al demonstrated 10 kDa PEI as more effective than 1.8 kDa PEI while not increasing toxicity.[8]

In addition to improving delivery, targeting ligands can easily be conjugated to a polymer exterior. Ngamcherdtrakul et. al showed significant targeting specificity for cancerous cell lines using the targeting antibody trastuzumab.[8] Hopefully future studies will indicate the overall in vivo fate of the particles to confirm the targeting effectiveness of the system.

2.4 References

1. Huang, X.; Li, L.; Liu, T.; Hao, N.; Liu, H.; Chen, D.; Tang, F. The Shape Effect of Mesoporous Silica Nanoparticles on Biodistribution, Clearance, and Biocompatibility in Vivo. *ACS Nano* **2011,** *5*, 5390-5399.
2. Xiao, X.; He, Q.; Huang, K. Novel Amino-Modified Silica Nanoparticles as Efficient Vector for Hepatocellular Carcinoma Gene Therapy. *Med. Oncol.* **2010,** *27*, 1200-1207.
3. Buchman, Y. K.; Lellouche, E.; Zigdon, S.; Bechor, M.; Michaeli, S.; Lellouche, J.-P. Silica Nanoparticles and Polyethyleneimine (PEI)-Mediated Functionalization: A New Method of PEI Covalent Attachment for siRNA Delivery Applications. *Bioconjugate Chem.* **2013,** *24*, 2076-2087.
4. Ye, S. F.; Tian, M. M.; Wang, T. X.; Ren, L.; Wang, D.; Shen, L. H.; Shang, T. Synergistic Effects of Cell-Penetrating Peptide Tat and Fusogenic Peptide HA2-Enhanced Cellular Internalization and Gene Transduction of Organosilica Nanoparticles. *Nanomed.* **2012,** *8*, 833-841.

5. Wang, Z. Y.; Zhao, Y.; Ren, L.; Jin, L. H.; Sun, L. P.; Yin, P.; Zhang, Y. F.; Zhang, Q. Q. Novel Gelatin–Siloxane Nanoparticles Decorated by TAT Peptide as Vectors for Gene Therapy. *Nanotechnology* **2008,** *19*, 445103.
6. Rejeeth, C.; Kannan, S.; Muthuchelian, K. Development of In Vitro Gene Delivery System Using ORMOSIL Nanoparticle: Analysis of p53 Gene Expression in Cultured Breast Cancer Cell (MCF-7). *Cancer Nanotechnol.* **2012,** *3*, 55-63.
7. Roy, I.; Ohulchanskyy, T. Y.; Pudavar, H. E.; Bergey, E. J.; Oseroff, A. R.; Morgan, J.; Dougherty, T. J.; Prasad, P. N. Ceramic-Based Nanoparticles Entrapping Water-Insoluble Photosensitizing Anticancer Drugs: A Novel Drug− Carrier System for Photodynamic Therapy. *J. Am. Chem. Soc.* **2003,** *125*, 7860-7865.
8. Ngamcherdtrakul, W.; Morry, J.; Gu, S.; Castro, D. J.; Goodyear, S. M.; Sangvanich, T.; Reda, M. M.; Lee, R.; Mihelic, S. A.; Beckman, B. L. Cationic Polymer Modified Mesoporous Silica Nanoparticles for Targeted siRNA Delivery to HER2+ Breast Cancer. *Adv. Drug Delivery Rev.* **2015,** *25*, 2646-2659.
9. Owens, G. J.; Singh, R. K.; Foroutan, F.; Alqaysi, M.; Han, C.-M.; Mahapatra, C.; Kim, H. W.; Knowles, J. C. Sol–Gel Based Materials for Biomedical Applications. *Prog. Mater. Sci.* **2016,** *77*, 1-79.
10. Kobler, J.; Möller, K.; Bein, T. Colloidal Suspensions of Functionalized Mesoporous Silica Nanoparticles. *ACS Nano* **2008,** *2*, 791-799.
11. Nel, A. E.; Mädler, L.; Velegol, D.; Xia, T.; Hoek, E. M.; Somasundaran, P.; Klaessig, F.; Castranova, V.; Thompson, M. Understanding Biophysicochemical Interactions at the Nano–Bio Interface. *Nat. Mater.* **2009,** *8*, 543-557.
12. Resnier, P.; Montier, T.; Mathieu, V.; Benoit, J. P.; Passirani, C. A Review of the Current Status of siRNA Nanomedicines in the Treatment of Cancer. *Biomaterials* **2013,** *34*, 6429-6443.
13. Major, R. C.; Zhu, X. Y. Two-Step Approach to the Formation of Organic Monolayers on the Silicon Oxide Surface. *Langmuir* **2001,** *17*, 5576-5580.
14. Wadia, J. S.; Stan, R. V.; Dowdy, S. F. Transducible TAT-HA Fusogenic Peptide Enhances Escape of TAT-Fusion Proteins After Lipid Raft Macropinocytosis. *Nat. Med.* **2004,** *10*, 310-315.
15. Khalil, I. A.; Kogure, K.; Futaki, S.; Harashima, H. Octaarginine-Modified Liposomes: Enhanced Cellular Uptake and Controlled Intracellular Trafficking. *Int. J. Pharm.* **2008,** *354*, 39-48.
16. Mao, S.; Neu, M.; Germershaus, O.; Merkel, O.; Sitterberg, J.; Bakowsky, U.; Kissel, T. Influence of Polyethylene Glycol Chain Length on the Physicochemical and Biological Properties of Poly (Ethylene Imine)-Graft-Poly (Ethylene Glycol) Block Copolymer/SiRNA Polyplexes. *Bioconjugate Chem.* **2006,** *17*, 1209-1218.
17. Meng, H.; Xue, M.; Xia, T.; Ji, Z.; Tarn, D. Y.; Zink, J. I.; Nel, A. E. Use of Size and a Copolymer Design Feature to Improve the Biodistribution and the Enhanced Permeability and Retention Effect of Doxorubicin-Loaded Mesoporous Silica Nanoparticles in a Murine Xenograft Tumor Model. *ACS Nano* **2011,** *5*, 4131-4144.

18. Xia, T.; Kovochich, M.; Liong, M.; Meng, H.; Kabehie, S.; George, S.; Zink, J. I.; Nel, A. E. Polyethyleneimine Coating Enhances the Cellular Uptake of Mesoporous Silica Nanoparticles and Allows Safe Delivery of siRNA and DNA Constructs. *ACS Nano* **2009,** *3*, 3273-3286.
19. Lee, H.; Sung, D.; Veerapandian, M.; Yun, K.; Seo, S. W. PEGylated Polyethyleneimine Grafted Silica Nanoparticles: Enhanced Cellular Uptake and Efficient siRNA Delivery. *Anal. Bioanal. Chem.* **2011,** *400*, 535-545.
20. Peng, Q.; Zhong, Z.; Zhuo, R. Disulfide Cross-Linked Polyethylenimines (PEI) Prepared Via Thiolation of Low Molecular Weight PEI as Highly Efficient Gene Vectors. *Bioconjugate Chem.* **2008,** *19*, 499-506.
21. Boussif, O.; Lezoualc'h, F.; Zanta, M. A.; Mergny, M. D.; Scherman, D.; Demeneix, B.; Behr, J.-P. A Versatile Vector for Gene and Oligonucleotide Transfer Into Cells in Culture and In Vivo: Polyethylenimine. *Proc. Natl. Acad. Sci.* **1995,** *92*, 7297-7301.
22. Zhou, X.; Chen, L.; Nie, W.; Wang, W.; Qin, M.; Mo, X.; Wang, H.; He, C. Dual-Responsive Mesoporous Silica Nanoparticles Mediated Co-Delivery of Doxorubicin and Bcl-2 siRNA for Targeted Treatment of Breast Cancer. *J. Phys. Chem. C* **2016,** *120*, 22375–22387.

CHAPTER 3: PORE LOADING DELIVERY SYSTEMS

3.1 Optimizing pore size and functionalization for encapsulating oligonucleotides

The first hurdle in encapsulating oligonucleotides for delivery by mesoporous silica nanoparticles is synthesizing a particle with optimal size pores for loading and release. Mesoporous silica is generally produced using the sol-gel method where a silica precursor and surfactant self-assemble to form pores. The pores can then easily be expanded by swelling the surfactant with 1,3,5-trimethylbenzene (TMB) or etching the silica with ammonium hydroxide. TMB can penetrate the micelles forming the pores (**Figure 3.1.**) due to the hydrophobic forces between the surfactant alkyl chain and TMB.[1] This caused the micelles to expand, widening the pores. Surfactant is then removed either through solvent extraction or high temperature calcination (>500 °C) that evaporates the surfactant and condenses the silica.

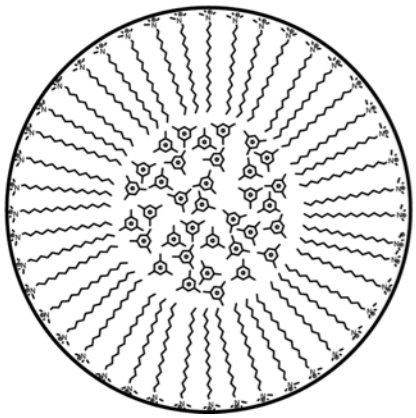

Figure 3.1. Surfactant structure with the swelling agent TMB in its center. TMB causes the micelle to increase in size. However, swelling agents can cause disorder and heterogeneity in the surrounding silica structure.[2] Image modified from reference 2.

3.1.1. Loading pDNA and DNA

Kim and colleagues synthesized MSNPs with two different pore sizes, 2 nm and 23 nm, in order to evaluate the dependence of pore diameter on gene uptake and delivery.[3] The particles were synthesized at a basic pH using CTAB and tetramethyl orthosilicate (TMOS). This produced MSNPs with 2.1 nm pores (MMSN-2). The 23 nm pore nanoparticles (MMSN-23) were prepared by soaking the as-synthesized nanoparticles in ethanol, water, and TMB at 140 °C for four days. After removing the surfactant by refluxing in an acidic ethanolic solution, the nanoparticles were functionalized with amine groups via APTES (3.6 mmol/g) (**Figure 3.2.**). The group reported both particles had a diameter of approximately 250 nm based on TEM images and the degree of amination was determined to be 3.6 mmol/g by elemental analysis.[3]

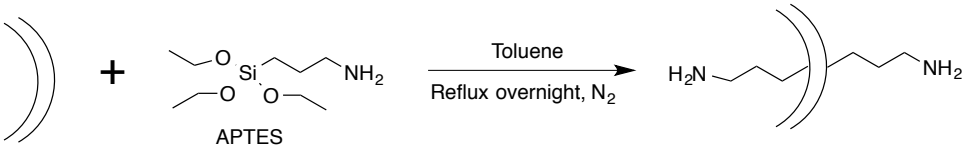

Figure 3.2. Amine functionalization of the pore interior and the MSN exterior using (3-amnopropyl)triethoxysilane (APTES).

Kim and colleagues reported the MMSN-23 could adsorb more plasmid DNA (pDNA) internally than MMSN-2 based on zeta potential readings and gel retardation assay results (**Figure 3.3.**). The group used a pDNA encoding for luciferase (pLuc, 4.8 kbp).[3] Zeta potential measurements remain positive before and after pLuc loading for MMSN-23 (17.5 and 4.53 mV respectively), whereas MMSN-2 are positive before loading (12.3 mV) and highly negative after loading (-34.5 mV). The extremely low zeta

potential of MMSN-2 is likely due to measuring the zeta potential of the pDNA (2 μg/mL) and MMSN (80 μg/mL) in PBS without removing any unabsorbed pDNA. The authors interpreted the low zeta potential of MMSN-2 as the pDNA being electrostatically bound to the surface of MMSN-2, whereas it is successfully loaded into the pores for MMSN-23.[3] However, at such a low zeta potential the negatively charged pDNA would repel one another without a countercharge on the surface of the particle, so the zeta potential reading was likely complicated by free pDNA in solution.

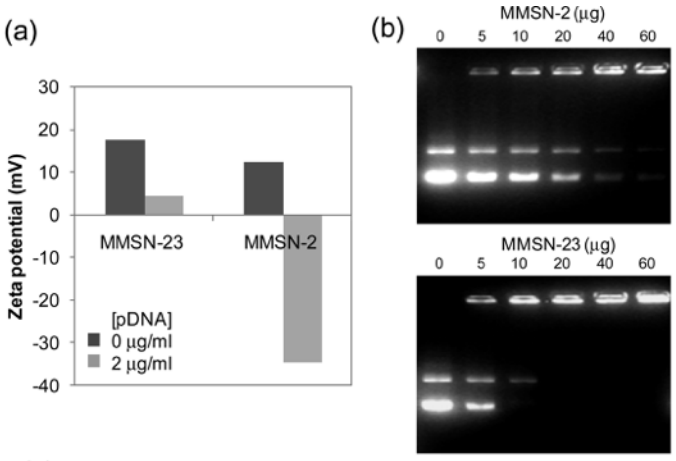

(c)

Amount of used MMSN	number of pDNA per MMSN-2	number of pDNA per MMSN-23
20 μg	15.0	36.6
40 μg	11.4	18.3
60 μg	8.8	12.2

Figure 3.3. Adsorption data for MMSN-2 and MMSN-23. A) Zeta potential of the two nanoparticle types before and after pDNA binding (80 μg/mg of MMSN). Zeta potential was measured in pH 7.4 buffer and pDNA was present at the time of measurement. B) Gel retardation assay with increasing amounts of MMSN. The amount of pDNA (pLuc) was kept constant at 0.5 μg. The MSN and pDNA were incubated for 1 hour prior to loading on the agrarose gel. C) Average amount of loaded plasmid based on gel assay fluorescence. Image modified from reference 3.

The luciferase gene (pLuc) was then loaded into both formulations to determine the loading capacity. A gel retardation assay was then employed to determine the loading

capacity of the two particle types. The assay uses a gel through which the DNA/particle or free DNA travel under an electric field that separates them by weight. The gel retardation assay revealed that MMSN-23 had almost four times higher loading capacity based on the intensities on the gel (**Figure 3.3.**) where pDNA was imaged with a UV trans-illuminator. This is demonstrated quantitatively in **Figure 3.3. (C)** where 20 μg of MMSN-2 loaded 15 pDNA, while MMSN-23 loaded 36.6.

Solberg and colleagues used an acid prepared mesoporous silica (APMS) nanoparticles to investigate the DNA loading capacity of 34 (APMS-34), 54 (APMS-54), and 100 (APMS-100) Å pores.[4] The nanoparticles were prepared via the sol-gel method under acidic conditions, and the pores were varied by suspending the particles post synthesis and surfactant removal in NH_4OH for different time periods.[4] The benefits of APMS include a spherical shape, fast preparation (under 2 hours), and easily controllable particle size and pore diameter.[4] The double-stranded calf thymus DNA (~2000 bp) was loaded via incubation and the DNA adsorption was measured at equilibrium using UV adsorption at 260 nm. Pore size comparison was made with Mg^{2+}-doped APMS and modified with APTES (~2.2 mmol/g) (**Figure 3.4.**). When APMS was doped with Mg^{2+}, APMS-54 demonstrated the highest adsorption capacity at 5.7 μg/mg. Solberg and colleagues hypothesized that the higher loading capacity of APMS-54 when compared to APMS-100 (4.3 μg/mg) was due to the amount of loaded cation, in turn correlated to the larger surface area of APMS-54.[4] When APMS was functionalized with APTES, APMS-100 had the largest adsorption capacity at 15.7 μg/mg. This is almost three times larger than APMS-54 doped with Mg^{2+}. The large adsorption difference between the two

can be explained by the more favorable direct electrostatic interaction between the cationic ammonium group covalently attached to APMS when compared with a metal cation that interacts with both the anionic silica and DNA.[4]

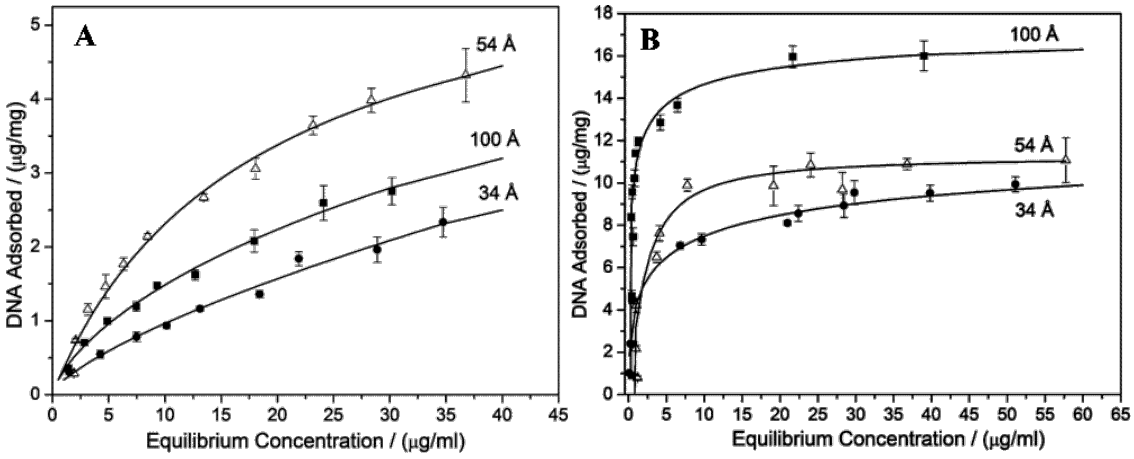

Figure 3.4. The adsorption of DNA for three pore sizes, 34, 54, 100 Å. (A) The DNA adsorption when APMS was doped with Mg^{2+}. A Langmuir fit, which assumes a monolayer on the surface of a homogenous surface, was used for the 54 and 100 Å materials. A Freundlich fit, which works well for heterogeneous surfaces and low adsorbate concentrations, was used for the 34 Å material. (B) The DNA adsorption when APMS was modified with amino linkers via APTES. A Langmuir fit was used for all three materials. Image adapted from reference 4.

3.1.2. Loading siRNA

Whereas DNA and pDNA can vary in size, siRNA is conventionally a 19 base pair duplex with a symmetric two base overhang on either strand on the end that terminates in a hydroxide group (termed the 3' end).[5] Longer RNAi duplexes (dsRNA) that are processed by enzymes in the cell into siRNA have been investigated as silencing agents and are usually 27 bp.[5]

Na and colleagues used the same preparation method as Kim and colleagues to examine siRNA adsorption and delivery of MSNs with 2 nm pores (MSN2) and MSNs

with 23 nm pores (MSN23).[6] Both were approximately 200 nm in diameter based on TEM measurements and were grafted with APTES to possess approximately 3.6 mmol/g of amines per gram of MSN.[6] PEG was conjugated to the exterior to minimize corona formation and aggregates forming the final particles P-T-MSN23 and P-T-MSN2.

Initially the study attempted to compare the two pore sized nanoparticles with the PEG exterior, but P-T-MSN2 loaded a negligible amount of siRNA based on gel electrophoresis data.[6] The authors interpreted this as evidence that siRNA was adsorbing onto the surface of the MSNs and not in the pores, which is consistent with Kim and colleagues' study with pDNA. Instead, the unPEGylated formulation (T-MSN2) was used. Zeta potential measurements before and after siRNA loading were consistent with DNA pore optimization studies; the zeta potential changed from 8.1 to -6.49 mV for T-MSN2 and 19.4 to 2.54 mV for P-T-MSN23.[6] The ability for the two formulations to protect siRNA against GFP (siGFP) was evaluated by first incubating the siRNA loaded particles in PBS with RNase for 1 and 2 hours. The siRNA was then detached from the particles by heparin, a highly polyanionic polymer that disturbs the electrostatic interactions between siRNA and the functionalized silica surface.[3] Gel electrophoresis determined how much intact siRNA remained following this procedure (**Figure 3.5.**). At 0 hours naked siGFP, T-MSN2 loaded with siGFP (siGFP+T-MSN2), and P-T-MSN23 loaded with siGFP (siGFP+P-T-MSN23) have the same amount of intact siRNA. After 1 hour both siGFP and siGFP+T-MSN2 no longer have intact siRNA, while siGFP+P-T-MSN23 still releases intact siRNA. After two hours incubation, significant siRNA degradation occurred for P-T-MSN23, which is likely due to slow diffusion of the loaded genes from the pores.[6] The additional protection by P-T-MSN23 may also be due to the

fact that it included PEG, since PEG has been shown to reduce protein adsorption and decrease oligonucleotide degradation.[7]

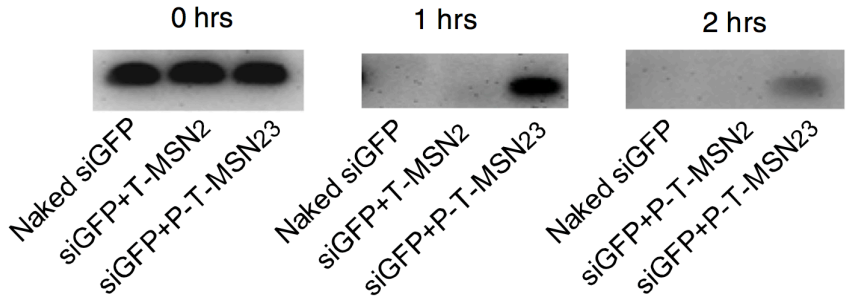

Figure 3.5. Gel electrophoresis study examining siRNA protection by T-MSN2 and P-T-MSN23 when loaded with green fluorescent protein siRNA (siGFP). At 0 hours, naked siGFP, siGFP+T-MSN2, and siGFP+P-T-MSN23 have a strong signal due to the siRNA not being degraded by the RNase. After 1 hour, the naked siRNA and loaded in the T-MSN2 has been degraded, while P-T-MSN23 continues to have a signal. After 2 hours, the signal from the P-T-MSN23 system has diminished. Image modified from reference 6.

A later study by Kim and colleagues compared 2, 4, 7, and 10, and 23 nm pore base prepared, amine decorated MSN for siRNA loading.[8] The intermediate pore sizes were synthesized using different amounts of TMB. Surfactant was removed using ethanolic hydrochloric acid solution. Based on TEM images, the MSNs were approximately 200 nm and pore expansion resulted in an increased pore volume and decreased surface size based on nitrogen adsorption isotherms.[8] The MSNs were amine functionalized by APTES (3.1-3.6 mmol/g). Zeta potentials before and after siRNA adsorption reveal a sharp decrease for MSN2 and MSN4 (**Figure 3.6. (A)**). This is consistent with external adsorption.

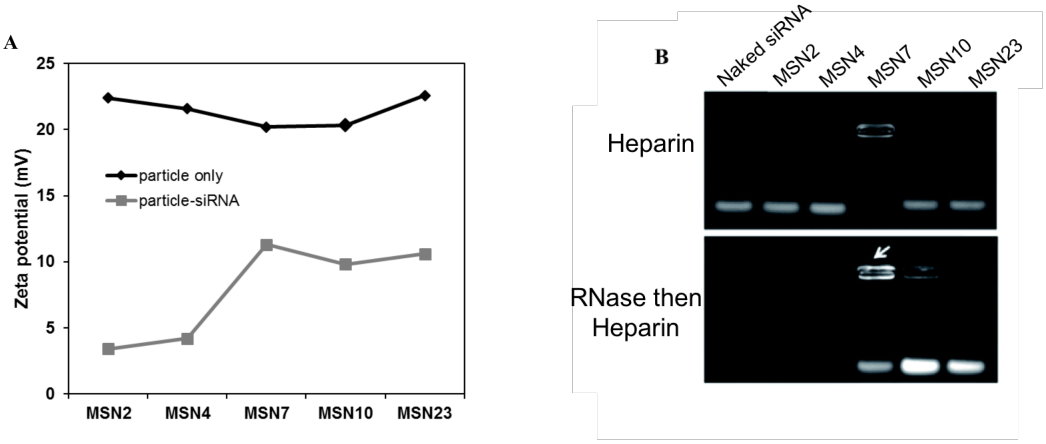

Figure 3.6. A) Comparison of zeta potential before and after siRNA loading. B) Gel retardation assay investigating siRNA release (top) and protection against RNase (bottom).[8] Image modified from reference 8.

Two gel retardation assays determined slightly better protection from RNase for MSN10 compared to MSN7 and MSN23 (**Figure 3.6. (B)**). In the first procedure without RNase, the particles were loaded and then the siRNA was released using heparin. The naked siRNA, MSN2, MSN4, MSN10, and MSN23 released intact siRNA that traveled the length of the gel. MSN7 did not release a discernable amount of siRNA, possibly because it was energetically favorable for siRNA to remain in the pores due to their size.[8] In the second study, the loaded particles were first incubated with RNase in buffer and then the remaining intact siRNA was released from the pores with heparin. Like the naked siRNA, both MSN2 and MSN4 produced no signal because of siRNA degradation, further suggesting external attachment. MSN7 protected and released some siRNA, while a portion remained in the pores like before and, consequently, does not travel on the gel. MSN10 and MSN23 both protect their loaded siRNA from RNase and successfully release it upon treatment with heparin.

The five different MSN were then loaded with siRNA targeting vascular endothelial growth factor (siVEGF) and incubated with a breast cancer cell line (MDA-MB-231). VEGF is upregulated in cancer and allow tumors to grow and metastasize. Knockdown efficiency was measured at 48 and 96 hours post transfection. Gene expression levels were evaluated by using reverse transcription polymerase chain reaction (RT-PCR) to synthesize complementary DNA (cDNA) from the messenger RNA (mRNA) of the targeted protein and amplify that gene. Then gel electrophoresis was used to detect the amount of cDNA present where the greater signal indicated more of the specified mRNA (**Figure 3.7.**). The expression of VEGF was compared to GAPDH (GDH), a housekeeping gene, as a control.[8] MSN10 demonstrated the most efficient knockdown at the two time points. MSN7 increased knockdown efficacy at 96 hours when compared to its efficiency at 48 hours, while MSN23 exhibited greater knockdown efficacy at 48 hours when compared to its results at 96 hours. These results are consistent with earlier studies indicating the importance of pore diameter upon release kinetics.

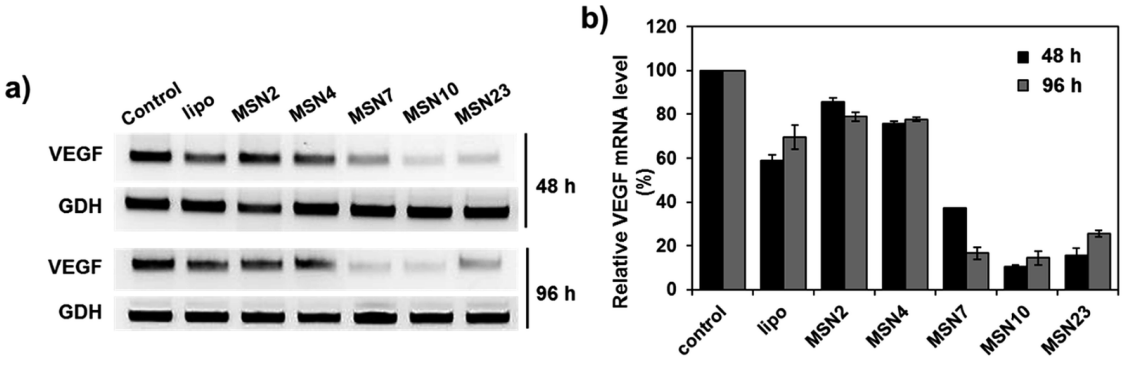

Figure 3.7. Investigation of VEGF gene knockdown dependent on pore size and incubation time. A) Gene expression levels at 48 and 96 hours measured by gel electrophoresis. B)

The band intensities from the gel electrophoresis were normalized and compared to GDH expression. Image modified from reference 8.

Steinbacher and colleagues similarly found pore sizes larger than 4 nm were optimal for siRNA loading and release. Using APMS externally functionalized with tetraethylene glycol (TEG) and internally with 1-(3-trimethoxysilylpropyl)-diethylenetriamine (DETA) (**Figure 3.8.**), Steinbacher's group compared three pore diameters (4, 8, 15 nm) and three different percent functionalizations of DETA (0.5, 2.5, 15%). The pore diameter was varied using ammonium hydroxide to etch the silica post synthesis.

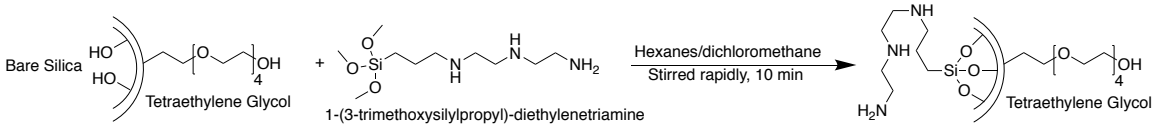

Figure 3.8. Modification of the interior of APMS. TEG is first conjugated to the exterior, followed by surfactant extraction via acid reflux. DETA is then attached to the interior by stirring rapidly for ten minutes. The particles are then filtered and then cured at 80 °C for 18 hours. Image modified from reference 9.

DETA/TEG functionalized APMS was loaded by incubating siRNA with APMS in a buffer. Release was then measured by stirring the siRNA loaded NPs in cell culture medium at 37 °C. Both loading and release were measured with UV/Vis. The amount of DETA functionalization was found to have a substantial impact on the release efficiency for 8 and 15 nm pores.[9] Release kinetics found that 8 nm pores with 15% DETA functionalization released the largest amount of siRNA per APMS, while 8 nm pores with 0.5% DETA functionalization had the largest fraction of release (**Figure 3.9.**).[9]

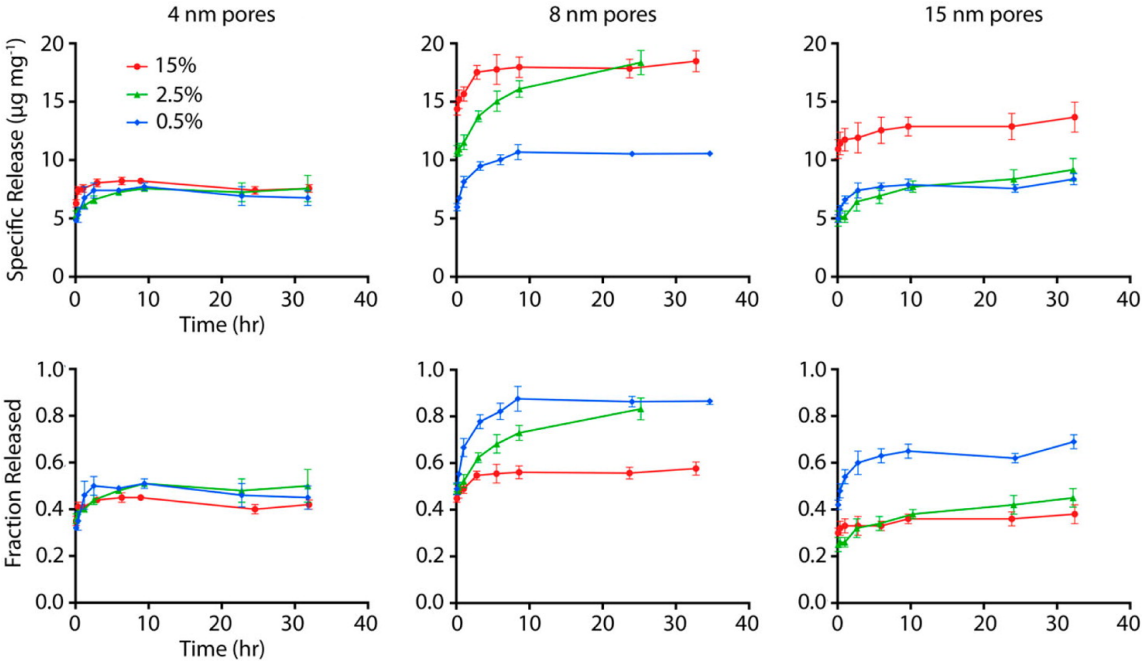

Figure 3.9. Graphs showing the specific release (top) and fraction release (bottom) of 4, 8, and 15 nm pores with either 0.5%, 2.5%, or 15% DETA functionalization. The largest amount of siRNA was released by 8 nm pores with 15% DETA, while the most efficient was 8 nm pores with 0.5% DETA Image modified from reference 9.

3.2 Additional large pore synthesis methods

While both acid and base catalyzed MSN can undergo pore enlargement with either the swelling agent TMB or acid etching with ammonium hydroxide, these methods can result in structural instability. Thus, other methods have been explored to synthesize large pore MSN.

3.2.1. Variations on sol-gel method

Wu and colleagues synthesized a small MSN with larger pores by adding a silica precursor with a hydrophobic group. They used bis[3-(triethoxysilyl)propyl]tetrasulfide (BTES) in addition to TEOS to form the silica nanoparticle.[10] BTES co-hydrolyzes and co-condenses with TEOS and produces larger pores due to its hydrophobic – $CH_2CH_2CH_2$-S-S-S-S-$CH_2CH_2CH_2$- group can penetrate into the hydrophobic micelles (**Figure 3.10.**).[10] Micelles were formed by CTAC to direct the structure and the base catalyst was triethanolamine (TEA). The final particles have a diameter of ~30 nm determined by TEM and a 50.75 nm diameter based on DLS measurements.[10] Nitrogen sorption data determined the conical pores have an average diameter of 6.2 nm (**Figure 3.11.**).[10] The surface area was determined to be 613.9 m^2 g^{-1} with a pore volume of 2.19 cm^3 g^{-1}.

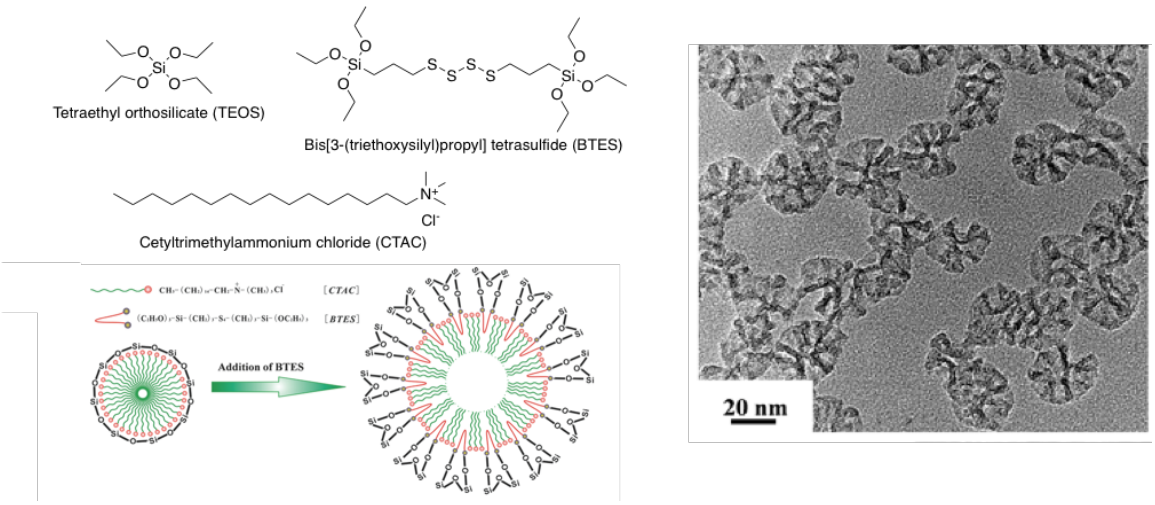

Figure 3.10. The addition of BTES is thought to cause the CTAC micelles to become enlarged due to the long hydrophobic chain between the two silica groups. The final particles are approximately 30 nm in diameter as measured by TEM (right image). Image modified from reference 10.

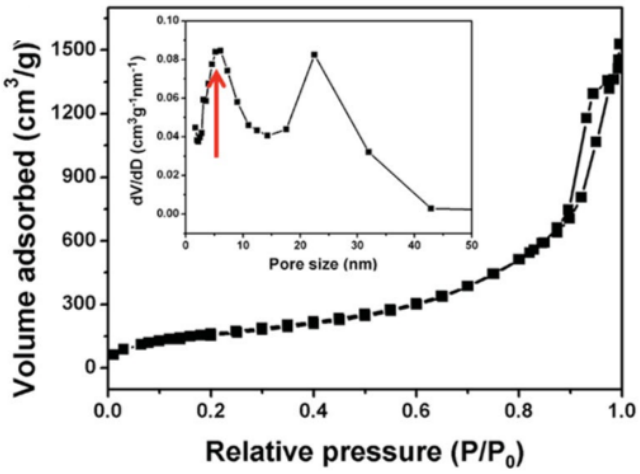

Figure 3.11. Nitrogen sorption isotherm of Wu and colleagues' small MSN is consistent with well-defined, monodispersed pores. The inset demonstrates the pore distribution (red arrow), whereas the larger pore reading is likely due to capillary action between particles. Image adapted from reference 10.

3.2.2. Microemulsion templating

Microemulsion templating was first described by Carroll and colleagues as a method to create MSNPs with both larger and smaller pores.[11] Ashley and colleagues then used this emulsion processing technique to form large pore MSNPs (3-13 nm and 23-30 nm pores determined by nitrogen physisorption) for siRNA delivery.[12] Microemulsion templating uses two surfactants, a nonionic surfactant (Abil EM 90) that forms the oil phase and a cationic surfactant (CTAB) that is only soluble in the aqueous phase.[11] TEOS is the silica precursor and is hydrolyzed in an acidic solution. By stirring the system, micrometer sized aqueous emulsion droplets (containing TEOS) form in the oil phase and are stabilized by Abil EM 90.[11] These emulsion droplets direct the microemulsion formation by CTAB around which the TEOS condenses.[13] Because CTAB is above the critical micellization concentration, the micelles form within the

aqueous phase to produce pores.[11] Once the solvent is removed, a bimodal porous network is produced. The pores are larger on the exterior of the particle (23-30 nm) due to being formed by both surfactants and smaller on the interior (3-13 nm) due to consisting mainly of CTAB (**Figure 3.12.**).[11]

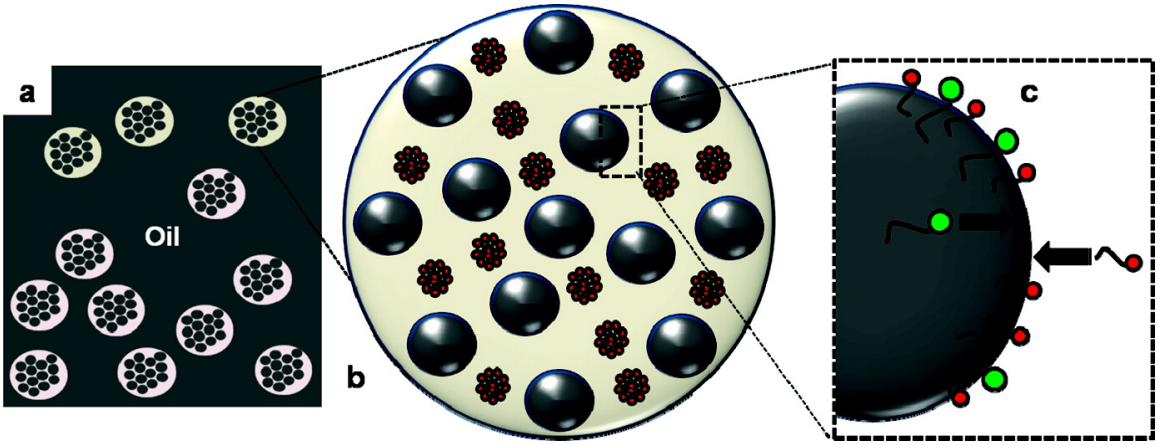

Figure 3.12. Schematic of microemulsion technique. A) Emulsion droplets form in Abil EM 90, the oil phase (dark grey). B) A single aqueous droplet containing microemulsion droplets (dark grey) and micelles (red). C) Oil/water interface that is absorbing both surfactants causing a drop in the interfacial tension. Image modified from reference 11.

After undergoing size separation, the final particles had an average particle diameter of 165 nm based on DLS (**Figure 3.13.**). Nitrogen sorption is consistent with the presence of larger and smaller pores. The BET surface area was 850 m^2 g^{-1} with a pore volume fraction of ~65%.[12]

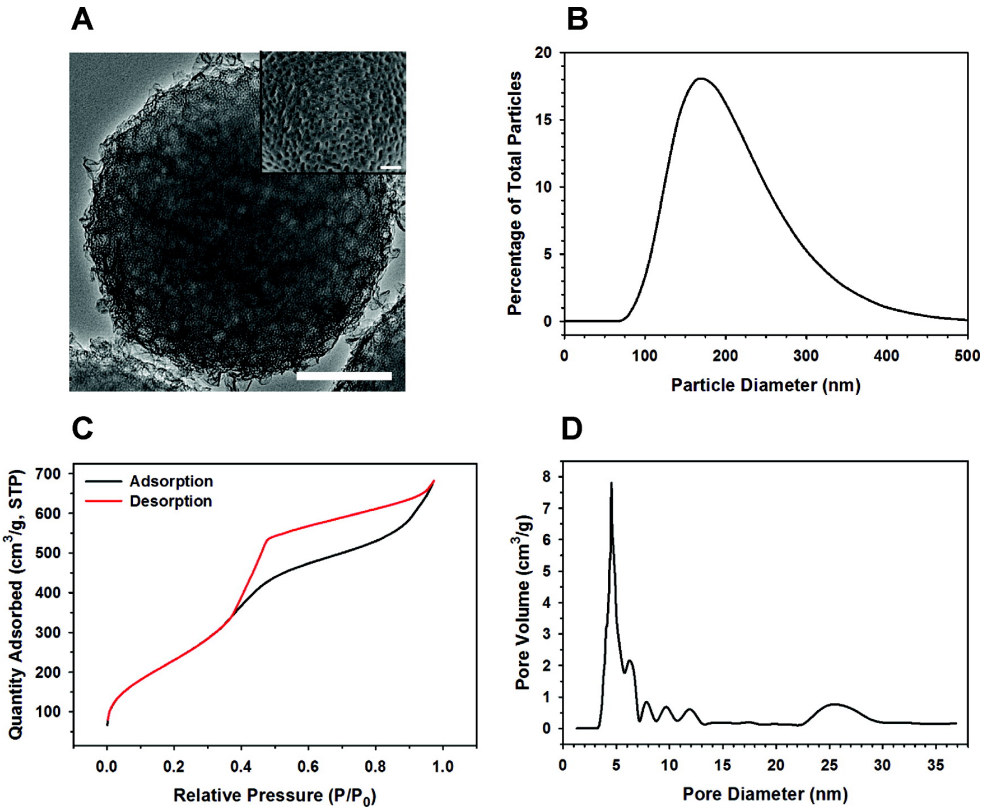

Figure 3.13. Physical characterization of unmodified microemulsion MSNPs. A) TEM image of the bare silica mesoporous nanoparticle formed by microemulsion technique. The scale bar = 100 nm. B) DLS after size based separation. Final particles had a diameter of ~165 nm. C) Nitrogen sorption isotherm of size separated MSN. The hysteresis is consistent with a network of larger pores connected by smaller pores. D) Pore volume plot calculated from the adsorption branch of the isotherm using Barrett-Joyner-Halenda model. It demonstrates the presence of 23 – 30 nm pores and 3 – 13 nm pores. Image adapted from reference 12.

3.3 Modifications for efficient delivery

Once the base silica particle is synthesized and optimized for oligonucleotide loading and delivery, the exterior must be optimized for delivery. Exterior functionalization often includes increasing biocompatibility with PEG, including a polymer such as PEI for endosomal escape, cell penetrating peptides, and/or a targeting moiety.

3.3.1. Polymer exterior

As discussed previously, PEI and PEG are used due to their ability to cause endosomal escape and increase circulation times respectively. A PEI exterior without PEG has been utilized by several groups, with varying results. Finlay and colleagues used a base catalyzed method to create an siRNA delivery system. In the group's procedure, CTAB was used as a surfactant, sodium hydroxide as the base, and TEOS as the silica precursor. Shortly after particle formation 3-(trihydroxysilyl)propyl methylphosphonate was added to prevent interparticle aggregation.[14] The final NPs were smaller than 127 nm in diameter and had an average pore diameter of 2.5 nm, both determined by TEM.[15-16] Acidic methanol was used to remove the surfactant. The PEI coating (1.8 kDa) was added to the MSNs by suspending the particles in PEI and ethanolic solution. Electrostatic attachment occurs between the weakly charged PEI and the negatively charged silica surface, since PEI may adjust its charge density in the absorbed layer to compensate for the electrostatic potential at the surface.[17]

After attaching the short chain PEI, the system was loaded with siRNA by incubation.[15-16] Because siRNA has a diameter of 2.6 nm, it is possible that siRNA adopts the necessary orientation to enter the pores. However, the authors note this is unlikely, since PEI coats both the particle's interior and exterior.[16] The nanoparticle successfully bound with siRNA and could protect it from cleavage by RNase-A after 1 hour incubation (**Figure 3.14.**).[16] The nanoparticle system was loaded with siRNA targeting TWIST1, a transcription factor whose reactivation increases cancer cell ability to self-renew, survive, and metastasis.[15] Intravenous treatment of TWIST1 siRNA demonstrated

tumor size reduction but no reduction in metastatic lesions.[15] This may be due to the lack of targeting ligand that would aid in delivery to cancer cells that have not yet developed pathological vasculature with enhanced permeability.[18]

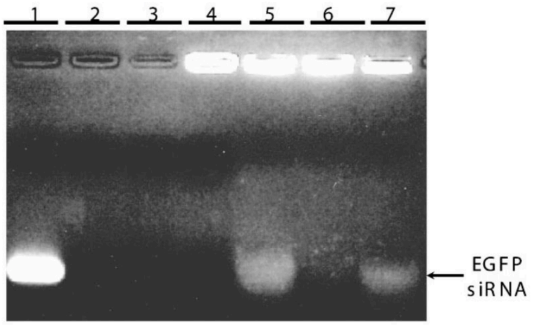

Lane 1	siRNA
Lane 2	siRNA+RNase
Lane 3	MSN+RNase
Lane 4	MSN(siRNA)+RNase
Lane 5	MSN(siRNA)+Hep
Lane 6	MSN(siRNA)+Hep+RNase
Lane 7	MSN(siRNA)+RNase+Hep

Figure 3.14. Gel electrophoresis post incubation with RNase-A demonstrates that PEI functionalized MSN can protect siRNA from RNase-A cleavage. Lane 1 shows gel migration of free siRNA. Lane 2 is the result of siRNA after RNase A treatment. Lane 4 shows that siRNA bound to MSNs remain in the gel wells and was not degraded by the RNase A. Lane 5 and 7 demonstrate some siRNA dissociation but not degradation. Image adapted from reference 16.

Na and colleagues demonstrated successful in vivo delivery of siRNA affecting vascular endothelial growth factor (siVEGF) in MDA-MB-231 xenographs with an amine (3.6 mmol g^{-1}) and PEG decorated MSN. The base prepared silica nanoparticle had 23 nm pores expanded with TMB and a diameter of 250 nm based on TEM images. The amine was then conjugated to the silica surface using APTES upon which PEG was

conjugated (siVEGF-P-T-MSN23). The siRNA loaded MSNs were intratumorally injected four times over a period of 20 days. Intratumor injection was chosen due to the aggregation tendency of the particles.[6] After thirty days the excised tumors weighed 240, 190, and 52 mg after being treated with PBS, naked siVEGF, and siVEGF-P-T-MSN23 (**Figure 3.15.**).

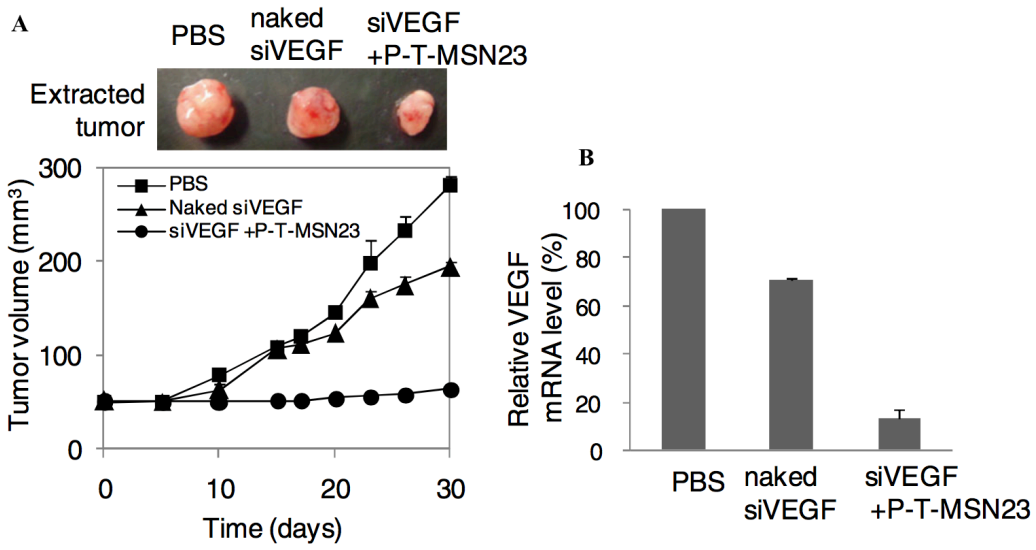

Figure 3.15. A) The three excised tumors after treatment with PBS, naked siVEGF, and siVEGF-P-T-MSN23 for twenty days. Tumors were extracted on day 30. The siRNA loaded MSNs reduced tumor volume. B) VEGF mRNA was significantly downregulated in the tumor treated with siVEGF-P-T-MSN23 compared with the other two treatment groups. Image adapted from reference 6.

3.3.2. Amino acid functionalization

As of yet, the only publication on amino acid functionalization as a biocompatible exterior for efficient oligonucleotide delivery has been poly-L-lysine (PLL). Hartono and colleagues contrasted the effectiveness of PLL with an amine exterior.[19] The silica particle was synthesized using a two surfactants, triblock copolymer (F127) and a

fluorocarbon surfactant (FC-4), TMB, and TEOS as the silica precursor in acidic conditions.[19] The final MSN had a particle diameter between 100-200 nm and an average 13.4 nm pore entrance and 27.9 nm cavity.[19] Amine attachment was performed with APTES, while PLL functionalization was achieved by first grafting an epoxy silane (3-GPS) to the interior and exterior surfaces. PLL was then attached through a nucleophilic addition to the epoxide on 3-GPS.[19] The final particles retained large pore cavities and entrances, as well as having a similar positive zeta potential (**Table 3.1.**).

Table 3.1.: Properties of the two functionalized materials developed by Hartono and colleagues.

Functional group	BET (m^2/g)	Pore volume (mL/g)	Pore cavity (nm)	Pore entrance (nm)	Zeta potential (mV)
Amine	155	0.63	24.6	11.3	3.23
PLL	171	0.64	24.1	11.8	1.90

Both modifications adsorbed similar amounts of oligo DNA (21-nucleotides long conjugated with cyanine dye Cy3), although PLL resulted in higher cellular uptake (**Figure 3.16.**). While PLL decorated MSN are taken up by cells more efficiently, cytotoxicity studies performed using the cervical cancer cell line SiHa found PLL to be more toxic than both the bare MSNP and amino functionalized nanoparticle. The authors attribute this to the primary amine surface groups that induce toxicity due to strong interactions with the cell membrane (which also leads to increased cell uptake).[19] The exact mechanism of PLL's cytotoxicity is poorly understood, however it is thought to be for the same reasons as higher weight PEI.[20] Thus, cytotoxicity may be reduced if a lower weight PLL is employed.

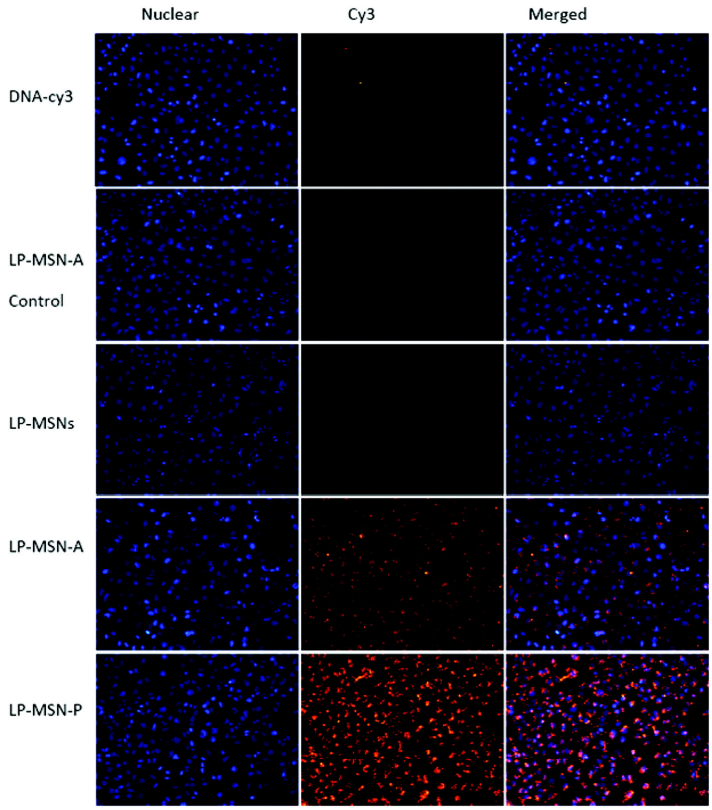

Figure 3.16. Cell uptake by HeLa cells was determined by labeling DNA with Cy3. Both the free DNA (DNA-Cy3) and bare silica MSNs (LP-MSNs) result in no Cy3 signal. The amine decorated MSN (LP-MSN-A) resulted in a positive signal. The PLL decorated MSN (LP-MSN-P) has a much higher signal and, thus, a higher transfection. Image modified from reference 19.

Delivery of siRNA was then measured based on cell viability by delivering siRNAs against polo-like kinase 1 (PLK1) and minibrain-related kinase (Mirk) to osteosarcoma cell line KHOS. Both PLK1 and Mirk are highly expressed in osteosarcoma cells and silencing them can inhibit cell growth.[19] The control was siRNA S10, an siRNA effective against the human papillomavirus (HPV) type 16 E6 gene.[19] Amine decorated MSN (LP-MSN-A) successfully delivered both PLK1 and Mirk siRNA and effected significant decrease in cell viability at high siRNA concentrations (100 nM)

(**Figure 3.17.**).[19] PLL decorated MSN (LP-MSN-P) delivering PLK1 siRNA also caused a decrease in cell viability at high siRNA concentrations (100 nM). The difference between the two modifications, amine and PLL, were 15% and 30% respectfully. Although PLL modified MSNPs resulted in a higher reduction of cellular viability, this result is complicated by the higher cellular uptake and toxicity of PLL (10%) when compared to the amino functionalization (5%).[19]

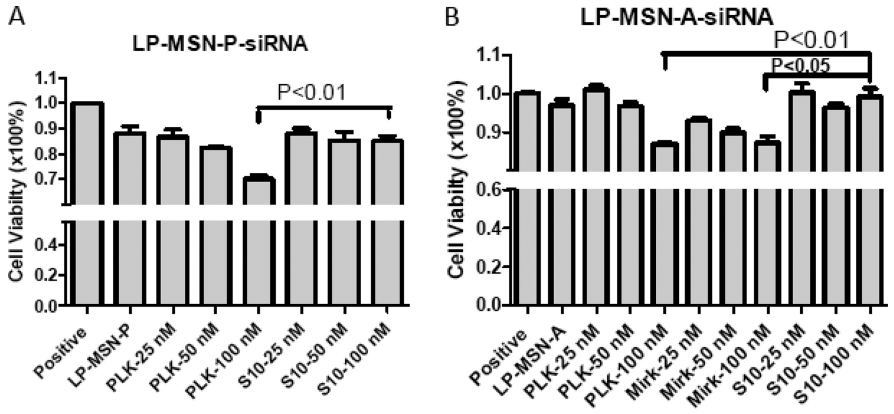

Figure 3.17. LP-MSN-P and LP-MSN-A were loaded with siRNAs targeting PLK and Mirk that were overexpressed in the osteosarcoma cell line KHOS. Three siRNA loading concentrations were tested (25, 50, 100 nM), and the positive control was the cell viability without any treatment. Another siRNA , S10, was used as a negative control. A) LP-MSN-P; B) LP-MSN-A. Image modified from reference 19.

3.3.3. Cell penetrating peptides

First discovered in 1988, cell penetrating peptides can trigger cell internalization into the cytoplasm of cell and direct its intracellular delivery.[21] Cell penetrating peptides are generally less than 30 amino acids and are derived from both natural or unnatural protein sequences.[21] They are easily attached to MSN delivery systems by conjugating the peptide to the outer covering (such as PEI).

Wu and colleagues used transcription-transactivating (Tat) protein for their nucleus targeting MSN system. Tat was first discovered on HIV-1, allowing the virus to enter cells and translocate into the nucleus.[21] The silica nanoparticles were synthesized using a modified sol-gel method as described previously where both BTES and TEOS were silica precursors.[10] The MSN had a TEM diameter of approximately 30 nm and pores with a diameter of 8-13 nm, which the group termed MONs.[10] The MONs were then functionalized first with an amine via APTES, then reacted with succinic acid to produce MONs-COOH, and finally with PEI (1.2 kDa) resulting in MONs-PEI (**Figure 3.18.**). The cell penetrating moiety TAT peptide was grafted onto the surface by an esterification reaction (MONs-PTAT), leaving free amines on the PEI to load the pDNA. The final particle had a DLS average diameter of 91.28 nm and a positive zeta potential of 40.6 mV (**Figure 3.19.**). pDNA was then loaded by vortexing.[10]

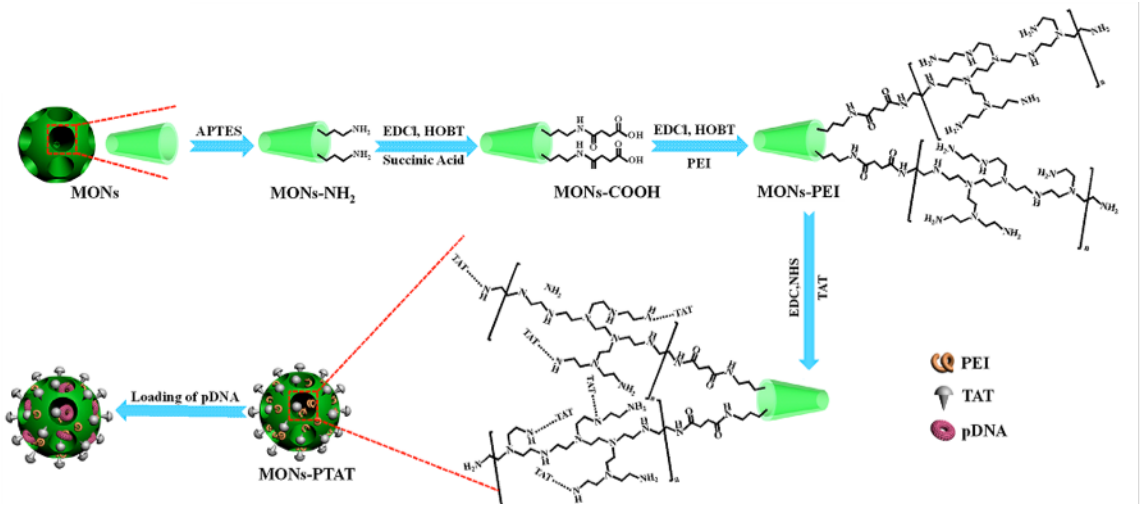

Figure 3.18. The pores and exterior of the small MSN were first functionalized with APTES. Succinic acid was then used to attach a carboxylic acid. PEI was conjugated to this exterior, followed by TAT. Finally, pDNA was loaded into the pores. Image modified from reference 10.

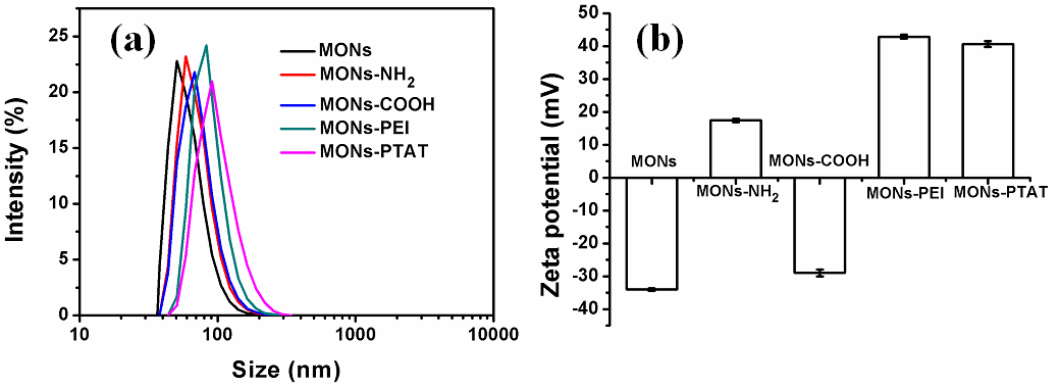

Figure 3.19. A) DLS particle size distribution after each modification step. B) The zeta potential measurement after each modification step. Image modified from reference 10.

The final delivery vehicle MON-TAT demonstrated successful internuclear accumulation and high transfection efficiency in vitro when compared to MON-PEI in HeLa cells (**Figure 3.20.**). The group used confocal fluorescence laser scanning microscopy (CLSM) to track MONs-PTAT with green fluorescence (FITC) to determine the uptake and particle location. The CLSM studies demonstrated that TAT decorated MSN had a higher cellular uptake and accumulation in the nucleoplasm.

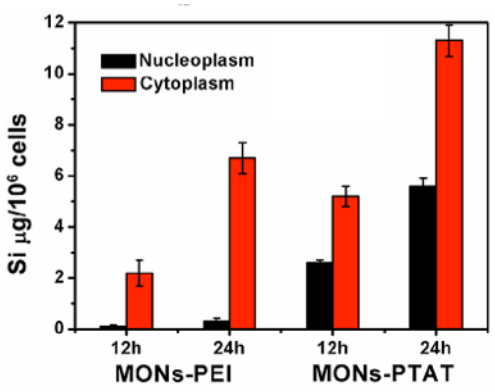

Figure 3.20. Cellular and nuclear uptake amounts of MONs-PEI and MONs-TAT by HeLa cells after 12 and 24 hours. Image modified from reference 13.

Transfection efficiencies were evaluated by loading MON-PEI and MON-PTAT with pEGFP, pDNA encoding for enhanced green fluorescent protein, and incubating with HeLa cells. Both fluorescent intensity and the proportion of cells exhibiting EGFP expression were calculated (**Figure 3.21.**). The significantly higher transfection efficacy of MON-PTAT is likely due to the cell uptake moiety that facilitates translocation to the cell's nucleus.

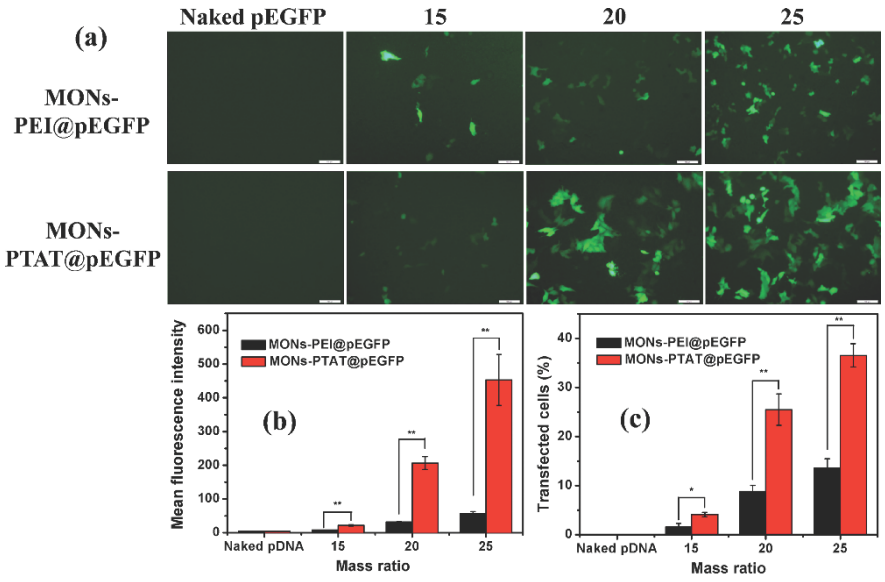

Figure 3.21. Tranfection efficacy of MON-PEI and MON-PTAT when loaded with pEGFP. A) Fluorescent images of EGFP expression. B) Fluorescence intensity and C) percentage of cells exhibiting EGFP expression (n = 3, *p < 0.05 and **p < 0.01). The mass ratio is nanoparticles to pDNA. Image modified from reference 10.

3.3.4. Ligand mediated targeting

To direct in vivo delivery of an MSN system, affinity ligands can be used to specify uptake and retention by particular cells. Ligands are usually an antibody or

peptide in cancer delivery and are selected that bind to molecules or receptors overexpressed on a cancer cell line. Affinity is only increased once the delivery system is in close enough proximity to the targeted tissue.[22] This strategy of active targeting can also selectively deliver therapies for other applications where the intended cell type has unique receptors not found on other cells.[23]

Ashley and colleagues developed a system with the targeting peptide SP94 that binds specifically to hepatocellular carcinoma cells, as well as the membrane fusion peptide H5WYG. The silica nanoparticle was prepared via the microemulsion templating described in section 3.2.2. The final MSN had an average diameter of 165 nm with 23-30 nm pores and 3-13 nm pores. After removing the surfactant via calcination, the silica was modified with 3-[2-(2-aminoethylamino)ethylamino]propyltrimethoxysilane (AEPTMS) to decorate the silica surface with amines. Cationic liposomes composed of 1,2-dioleoyl-3-trimethylammoniumpropane (DOTAP), 1,2-dioleoyl-*sn*-glycero-3-phosphocholine (DOPC), and cholesterol were synthesized with a Mini Extruder set.[12] They were then attached to the particles' surfaces by incubating the MSNs with 2- to 4-fold volumetric excess of liposomes.[12] The liposome fusion to the MSN's exterior is electrostatic and occurs when the MSN diameter is greater than 30 nm.[24] The final system, termed DOPC protocells, were separated from the excess lipid via centrifugation (**Figure 3.22.**).[12] Peptides SP94 and H5WYG were conjugated to primary amines present in the head groups using the heterobifunctional crosslinker SM $(PEG)_{24}$ (**Figure 3.23.**).[12]

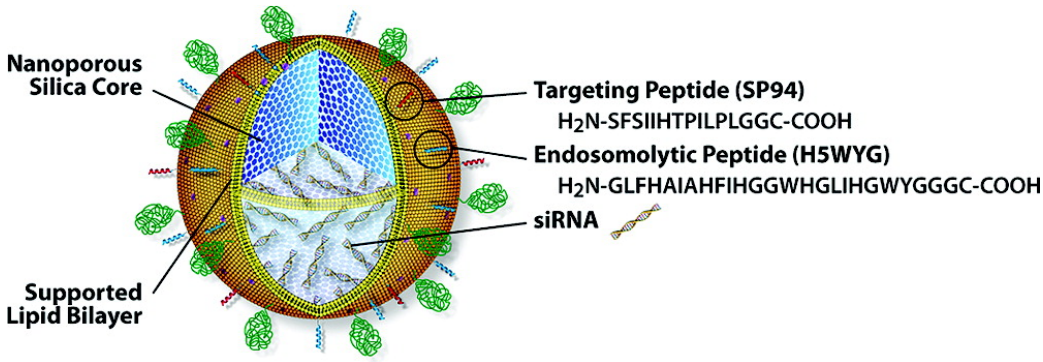

Figure 3.22. Schematic of the final protocell where the silica core loads siRNA and supports an external lipid bilayer. The exterior of the lipid is functionalized with the targeting peptide SP94 and endosomolytic peptide H5WYG. Image modified from reference 12.

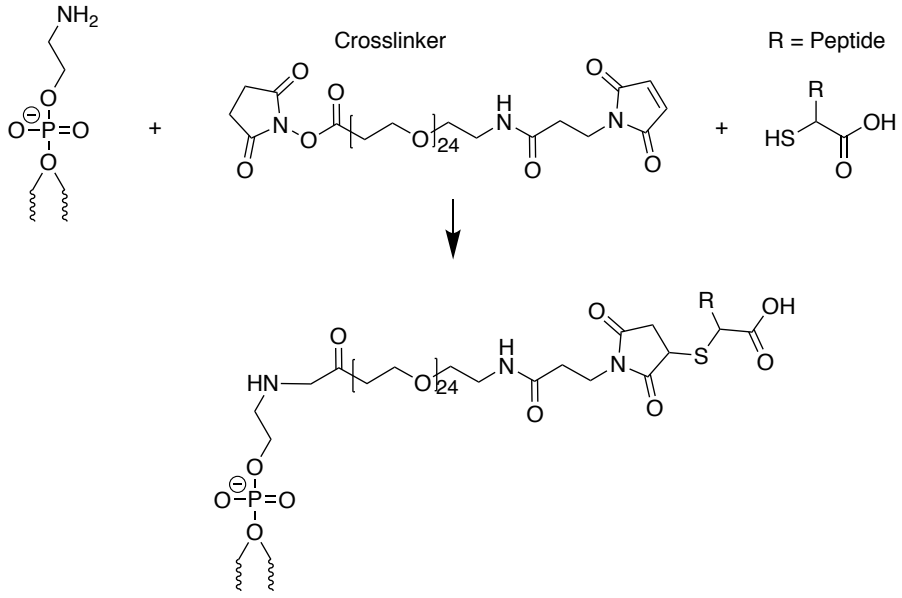

Figure 3.23. Peptides SP94 and H5WYG were conjugated to the primary amines in lipid head groups by using the crosslinker SM $(PEG)_{24}$.

Protocells protect and retain their cargo until reaching an acidic pH that triggers release (**Figure 3.24.**). This ability was determined by examining the rate at which DOPC protocells released their siRNA cargo at pH 7.4 to simulate body fluid and pH 5.0 as the

acidic conditions present in tumor cells.[12] Both DOPC and DOTAP lipid nanoparticles (LNPs) were tested in order to determine the improved protection and delivery of DOPC protocells. Under pH 7.4 DOPC protocells released very little of their cargo over 72 hours, while DOTAP LNPs lost approximately 50% and DOPC LNPs lost 100%. At pH 5 DOPC protocells released their cargo over 24 hours. DOPC and DOTAP LNPs released the loaded siRNA faster at pH 5 than the DOPC protocells but did not retain the cargo at pH 7.4.

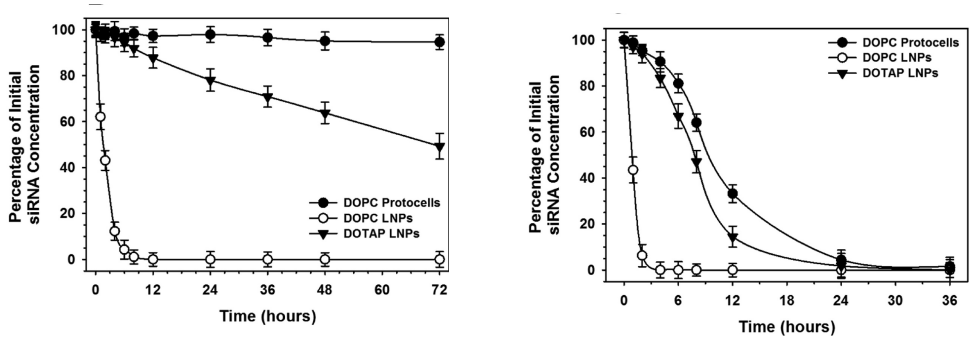

Figure 3.24. The rates at which DOPC protocells, DOPC LNPs, and DOTAP LNPs release their siRNA cargo under pH 7 (left) and pH 5 (right). Figure modified from reference 12.

In order to confirm targeted delivery of siRNA in vitro, protocells were loaded with an equimolar mixture of siRNAs targeting proteins involved in the regulation of the cell cycle regulating cell growth and viability: cyclin A2, cyclin B1, cyclin D1, and cyclin E.[12] Protein expression in treated cells were measured by Alexa Fluor 488 antibody labeling and then flow cytometry analysis that counts the labeled proteins.[12] The group found that by increasing the concentration of protocells there was a dose-dependent decrease in the protein levels of each of the targeted genes (**Figure 3.25. (A)**). When 125

pM of siRNA loaded in protocells was incubated with a type of hepatocellular carcinoma cells (Hep3B), the targeted proteins were repressed by nearly 90% after 72 hours (**Figure 3.25. (B)**).[12] Protocells demonstrated superior efficiency when compared with SP94 targeted DOTAP lipid nanoparticles (**Figure 3.25. (C)**). While DOTAP lipid nanoparticles loaded with the same amount of siRNA (125 pM) caused ~60% repression in cyclin A2 expression in Hep3B, 300-fold fewer protocells were needed to reduce cyclin A2 expression by 90%.

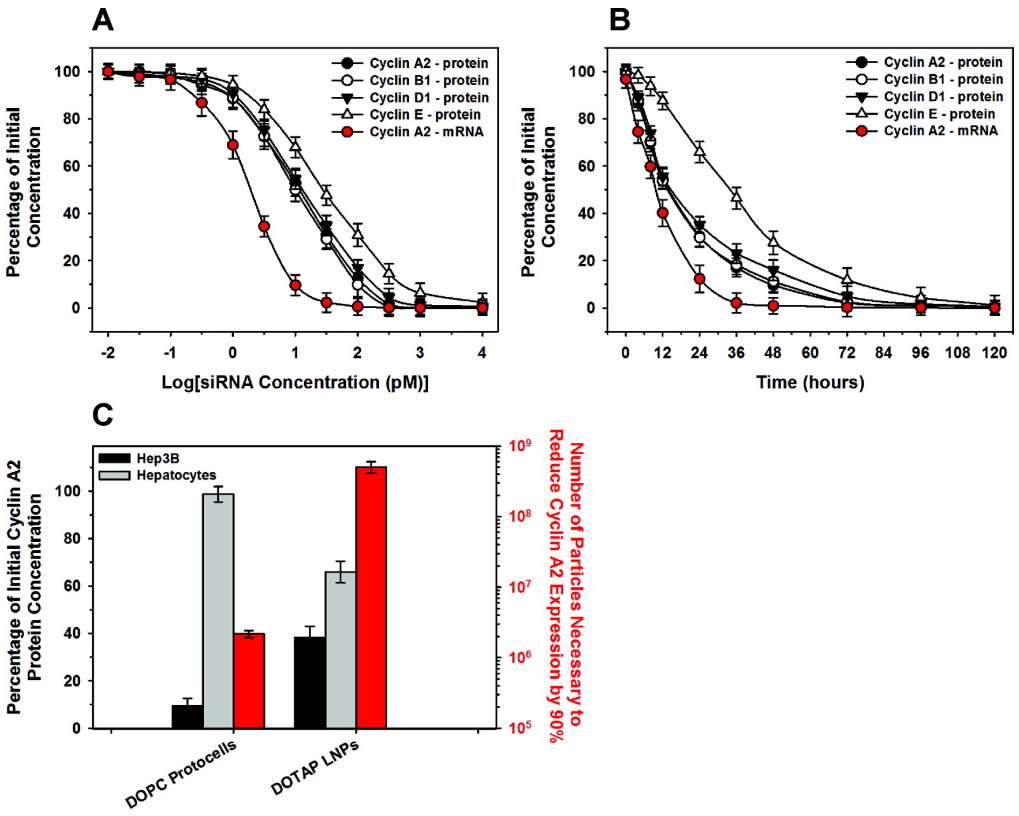

Figure 3.25. A) Dose dependent decrease in the expression of cyclin A2, B1, D1, and E protein as well as cyclin A2 mRNA in Hep3B cells after exposure with siRNA loaded, SP94 targeted procells. Cells were incubated for 48 hours. B) Time dependent decrease in the expression cyclin A2, B1, D1, and E protein as well as cyclin A2 mRNA in Hep3B cells after exposure with 125 pM siRNA for various periods of time. C) The left axis shows the percentages of initial cyclin A2 protein after exposure with protocells (DOPC protocells) and DOTAP lipid nanoparticles. The right axis illustrates the number of

particles required to reduce cyclin A2 expression by 90%. Image modified from reference 12.

3.3.5. Triggered release

Triggered release systems exploit either the lower pH or larger number of reducing agents in cancer cells when compared to normal tissue. Thiol based redox triggered mechanisms use the large difference in GSH concentration found in normal tissue (1-10 mM) and blood (2 μM) compared to tumor cells where GSH concentration is 7 to 10 times higher.[1] Human tumors also are more acidic than normal tissue and have exhibited pH states ranging from 5.7 to 7.8.[25] This is partly due to rapid growth and lactic acid accumulation, termed Warburg's effect, as well as insufficient blood supply and poor lymphatic drainage.[25] Harnessing pH-triggered delivery is challenged by the rapid pH drop following endocytosis to pH < 6.0, because the system may release the cargo in the endosome rather than the cytosol.[25] Consequently, techniques to escape the endosome via the proton sponge effect as well as triggered release are necessary.

Lin and colleagues created a redox triggered delivery system using a base prepared MSN with TMB widened pores.[26] The final MSN had a diameter of 100-150 nm based on TEM, and a pore diameter of 10 nm based on Nitrogen sorption data.[26]

The polymer was attached to the silica walls by adsorption of vinyl monomers, cross-linkers, and radical initiators via wet-impregnation method (**Figure 3.26.**).[27] The monomer, dimethylaminoethyl methacrylate (DMAEMA), N,N'-(dithiodi-2,1-ethanediyl)bis(acrylamide) (BAC) cross-linker, and α,α-azoisobutyronitrile (AIBN) radical initiator were dissolved in ethanol and incorporated into the walls of the MSN via the wet-impregnation method. Reduced pressure is then used to ensure uniform

distribution, followed by polymerization via heating to form a uniform polymer coating.[27] The final MSN (ssCP-MSN) still had a pore diameter of 10 nm with a reduced pore volume (0.63 cm^3 g^{-1}) and BET surface area (159 m^2 g^{-1}) (**Figure 3.27.**).[26] The final average hydrodynamic diameter was 141.8 nm, and the cationic polymer modification produced a positively charged nanoparticle with a 27.1 mV zeta potential.[26] The ssCP-MSN/siRNA complex (30 ssCP-MSN:1 siRNA ratio) continued to have a positive zeta potential of 24.6 mV.[26]

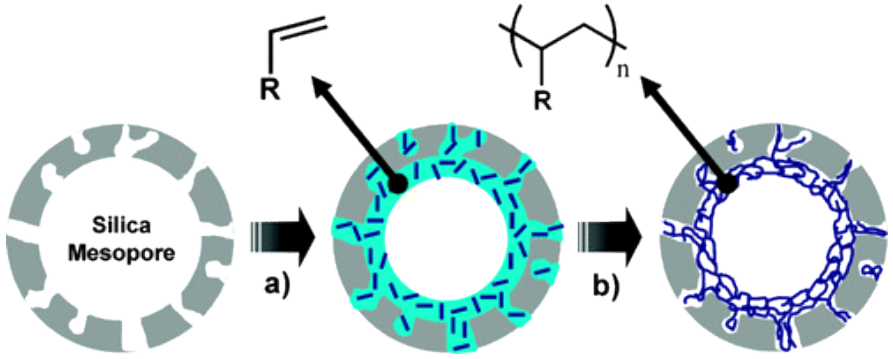

Figure 3.26. (A) First the DMAEMA monomer, BAC cross-linker, and AIBN radical initiator mixture is adsorbed onto the surface of the MSN. (B) After drying to remove the ethanol, polymerization was performed to result in thermal polymerization.[26-27] Image modified from reference 27.

Protection and release studies demonstrated siRNA was protected against exchange with low concentrations of negatively charged heparin. This could be due to the high weight ratio between the positively charged particles and siRNA (30 ssCP-MSN: 1 siRNA). The heparin may be interacting with the free positively charged particle surface before displacing the siRNA. Dithiothreitol (DTT), a reducing agent used to create an in vitro model for the reducing environment of the cytoplasm, successfully

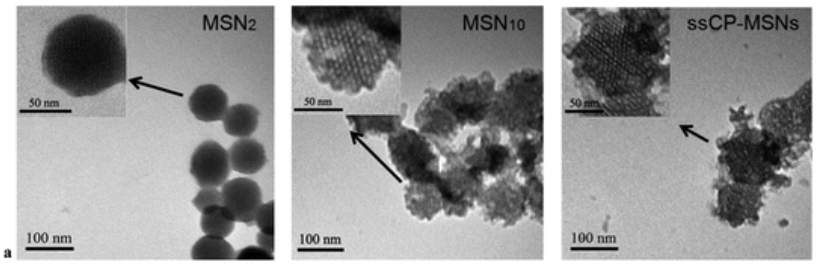

a

b

	BET surface area(m^2/g)	Pore volume(cm^3/g)	Pore size(nm)
MSN_2	1249	1.01	2.7
MSN_{10}	432	1.08	10.0
ssCP-MSN	159	0.63	10.0

Figure 3.27. A) TEM images of the 2 nm pore base prepared MSN (MSN_2), the 10 nm pore enlarged MSN (MSN_{10}), and the modified MSN (ssCP-MSNs). B) BET surface area, pore volume, and pore size for the three particle types. Image modified from reference 26.

caused siRNA release when examined with gel electrophoresis (**Figure 3.28.**). While DTT is a strong reducing agent, cancer cells have 7 to 10 times higher the GSH concentration than normal cells (1-10 mM).[1] Thus, this concentration of DTT likely mimics the increased reduction potential in cancer cells. However, other studies employ GSH to more closely mimic the reduction potential in cancer cells.[28]

The loaded ssCP-MSNs successfully silenced luciferase in vitro (**Figure 3.29.**), but were unable to reduce tumor growth in vivo. In vitro gene silencing was also less than transfection by siRNA loaded Lipofectamine 2000. Upon tail vein injection, ssCP-MSNs/siRNA accumulated in the liver, lung, spleen, and kidney as determined by confocal microscopy of tissue samples, indicating the MSNs were mainly taken up by the RES.[26] This indicates PDMAEMA does not offer increased circulation time and RES

escape found with PEG. The ssCP-MSN/siRNA complexes were also found in the adrenal gland, heart, and thymus.[26]

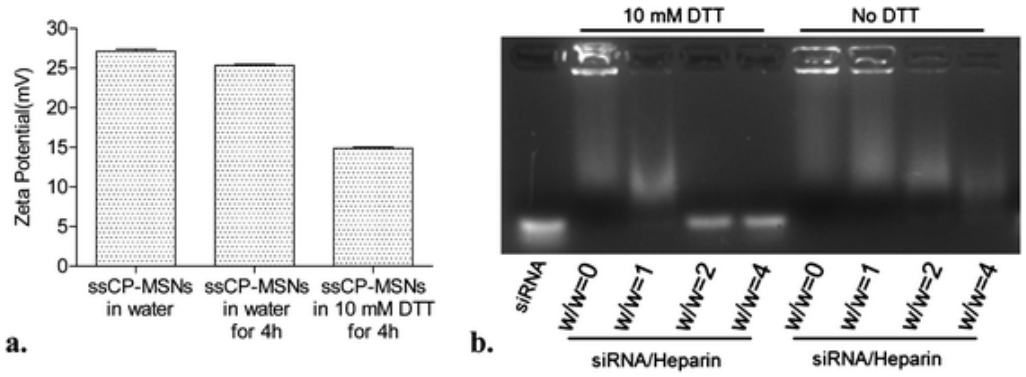

Figure 3.28. A) Zeta potential for ssCP-MSNs after being stored in water with and without 10 mM DTT. After four hours in water the zeta potential dropped from 27.1 mV to 25.3 mV. In water with DTT the zeta potential dropped to 14.9 mV. This is attributed to the PDMAEMA separating from the surface of the ssCP-MSNs after cleavage of the disulfide linkages. B) Gel electrophoresis of ssCP-MSN/siRNA complexes (30:1 w/w) treated with heparin with/without DTT. DTT treatment at higher concentrations resulted in is migration similar to free siRNA. Image modified from reference 26.

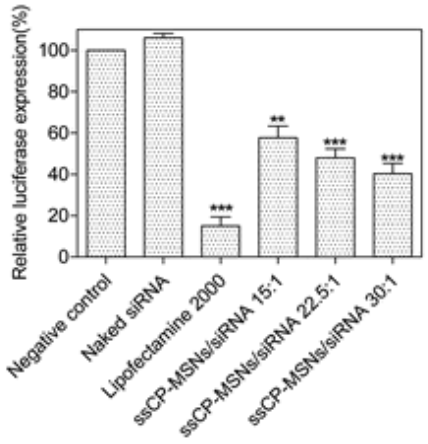

Figure 3.29. Luciferase expression silencing in HeLa-Luc cells after treatment with either Lipofectamine 2000/siRNA complex or ssCP-MSN/siRNA complexes at different w/w. The negative control is untreated HeLa Luc cells. *P < 0.05, **P < 0.01, ***P < 0.001 vs. naked siRNA. Figure modified from reference 26.

Sun and colleagues similarly used a base preparation method that was followed by enlarging the pores with TMB to build a redox responsive system.[1] The synthesized MSNs had an average diameter ~160 nm based on TEM measurements and the nitrogen sorption isotherm found a BET surface area of 771.65 m^2 g^{-1}, a pore diameter of 5.7 nm, and pore volume of 1.67 cm^3 g^{-1}.[1] After the surfactant was removed via acidic ethanolic solution, siRNA was loaded under dehydrated conditions with a salt solution (guanidine hydrochlorine) that disrupts the hydrogen between water molecules (i.e. chaotropic). The high concentration of ions enable loading by decreasing the debye length and shield silica and DNA's negative charges, which weakens the repulsive electrostatic force between DNA and the silica surface.[29] The loaded particles were then suspended in PEI (2kDa) ethanol solution to cap the particles with PEI (MSN-siRNA/PEI). PEI was then crosslinked by disulfide bonds by using dithiobis(succinimidyl propionate) (DSP) to create the triggered release system (**Figure 3.30.**). The final MSN-siRNA/PEI complex had a 210 nm diameter based on TEM images and a positive zeta potential of 16.9 mV (**Figure 3.31.**).[1]

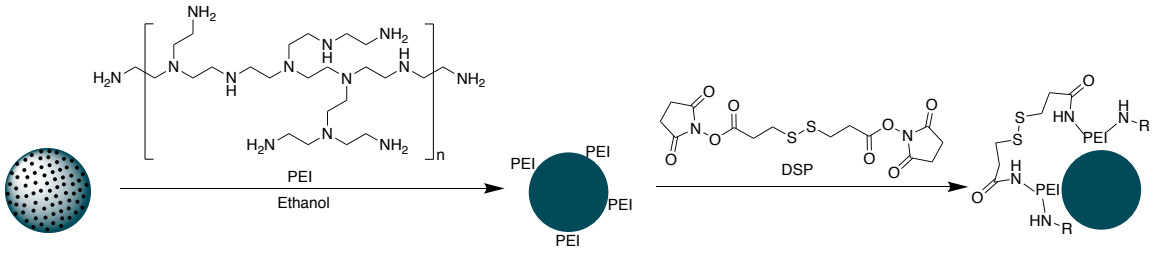

Figure 3.30. PEI is first adsorbed onto the MSN surface and then crosslinked with DSP.

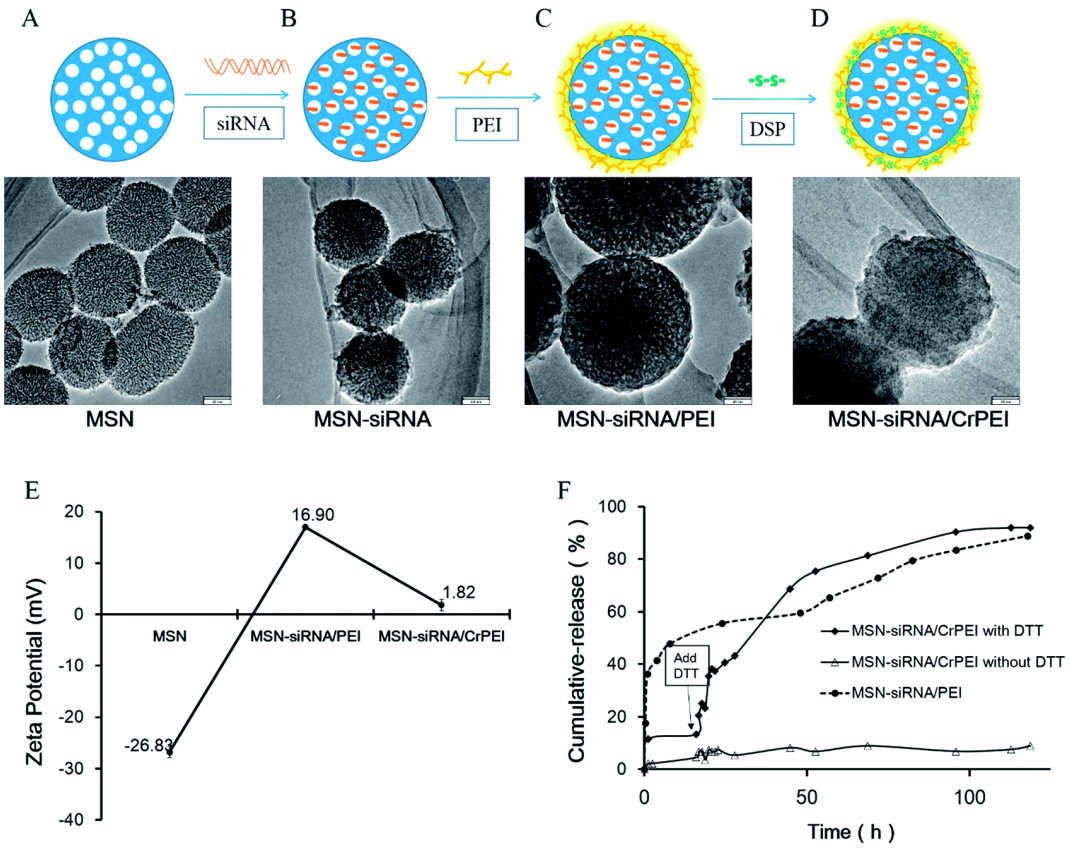

Figure 3.31. A) Bare particles with the surfactant removed. B) siRNA is loaded into the pores in a chaotropic salt solution. C) PEI is attached to the surface to cap the pores, facilitated delivery, and protect the siRNA. D) The disulfide linker DSP is conjugated to PEI to create a redox triggered delivery system. E) The zeta potential of the bare MSN, MSN-siRNA/PEI, and with the DSP linker (MSN-siRNA/CrPEI. F) siRNA release study of MSN-siRNA/CrPEI and MSN-siRNA/PEI in phosphate buffer solution (PBS) at pH 7.4. Image modified from reference 1.

MSN-siRNA/CrPEI successfully released its cargo under redox conditions while otherwise retaining it under neutral conditions (**Figure 3.31.**). DTT is a redox agent that simulates exposure to GSH.[1] Without the disulfide linker, siRNA is not contained in the MSN and leaves through diffusion. Compared to other systems where PEI is conjugated in the pores, MSN-siRNA/PEI diffusion is more rapid, since PEI is attached following siRNA loading. Capping with DSP significantly reduces siRNA release compared to

MSN-siRNA/PEI. Upon the addition of DTT a burst release is seen and the overall release exceeds MSN-siRNA/PEI.

Both in vitro and in vivo delivery significantly downregulated the targeted protein VEGF when compared with the control group, cells treated with serum free medium, and MSN-siRNA/PEI (**Figure 3.32.**). Two types of siRNA were used to treat KB cancer cells, a subline of the keratin-forming tumor cell line HeLa: siRNA targeting VEGF (siRNA) and scrambled siRNA (siNC). The KB cells exhibited a 40% decrease ($P < 0.05$) in VEGF protein expression after treatment with MSN-siRNA/PEI and a 75% decrease ($P < 0.01$) after MSN-siRNA/CrPEI treatment.[1] Protein expression was determined with a BCA Protein Assay Kit. The mRNA expression was measured with an ELISA and quantitative real time PCR to confirm VEGF expression was reduced by VEGF siRNA.[1] The mRNA levels were consistant with the protein expression levels in that MSN-siRNA/CrPEI caused a greater downregulation of mRNA than MSN-siRNA/PEI, naked VEGF siRNA, and MSN-siNC/CrPEI.[1]

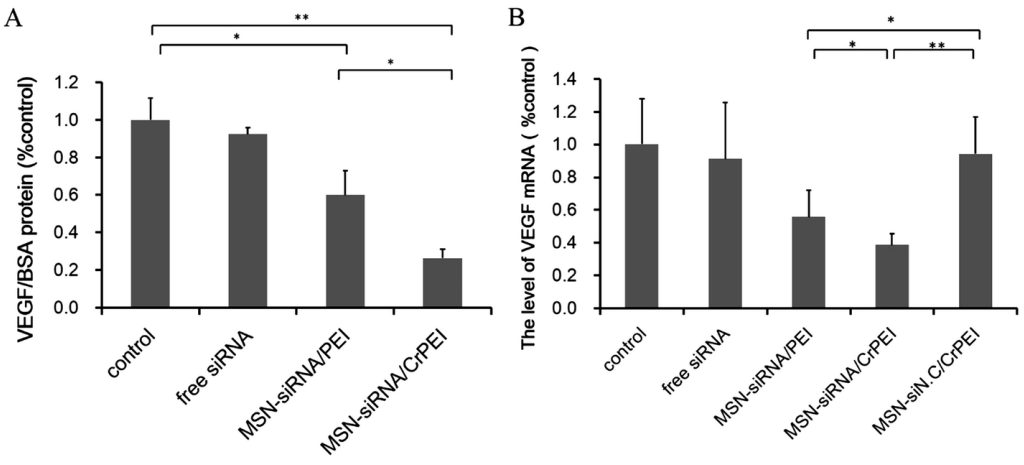

Figure 3.32. A) The VEGF/BSA protein level for KB cells treated with free siRNA, MSN-siRNA/PEI, and MSN-siRNA/CrPEI. The control is serum free medium. B) The VEGF

mRNA for KB cells treated with free siRNA, MSN-siRNA/PEI, MSN-siRNA/CrPEI, and MSN-siNC/CrPEI. Image modified from reference 1.

The in vivo tumor growth inhibition study on nude mice bearing a KB xenograft tumor similarly found a significant inhibition of the VEGF protein of 46% ($P < 0.05$) when treated with MSN-siRNA/CrPEI compared with the control, injections with 5% glucose (**Figure 3.33.**).[1] Injections were performed peritumorally.[1] The intratumoral VEGF mRNA level was also significantly reduced between the two groups.[1] In addition, the treated group demonstrated a significant reduction in CD31-positive tumor vessels and increased blood flow when investigated by immunofluorescent staining.[1]

Li and colleagues combined these triggering strategies to create a pH and redox triggered system. The silica MSN were synthesized by means of a soft-templating method using triethanolamine ($TEAH_3$), cetyl-trimethylammonium tosylate (CTATos), and tetraethyl orthosilicate (TEOS).[30] The benefit of this synthesis method is a small, monodisperse diameter (80-110 nm) and large pores (15-23 nm) as determined by TEM

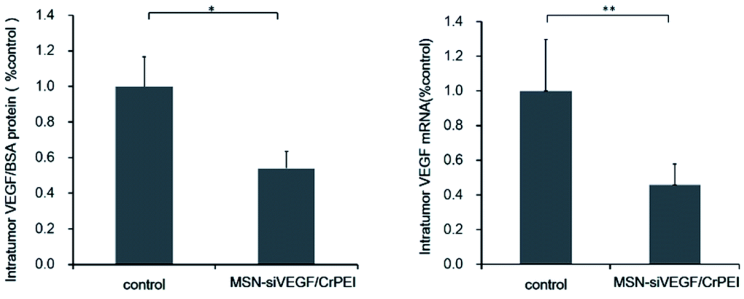

Figure 3.33. Left- The level of VGSF/BSA protein in KB tumors after treatment with 5% glucose (control) and MSN-siVEGF/CrPEI (dose of siRNA 1.00 mg kg^{-1}). Right- The level of intratumoral VEGF mRNA for the two in vivo treatment groups. Images modified from reference 1.

measurements.[30-31] After removing the surfactant via acid reflux, APTES was then attached. Mercaptopropionic acid was then attached to the amine groups (**Figure 3.34.**). Finally, 2-(2-Pyridinyldithio)-ethanamine hydrochloride was attached to produce a highly positive charged surface for loading and a redox and pH sensitive coating to trigger release.[30] Nitrogen sorption measurements revealed the final system (CMSN-A) had a BET surface area of 481 $m^2 g^{-1}$, 21 nm pore diameter, and 1.42 $cm^3 g^{-1}$ pore volume.

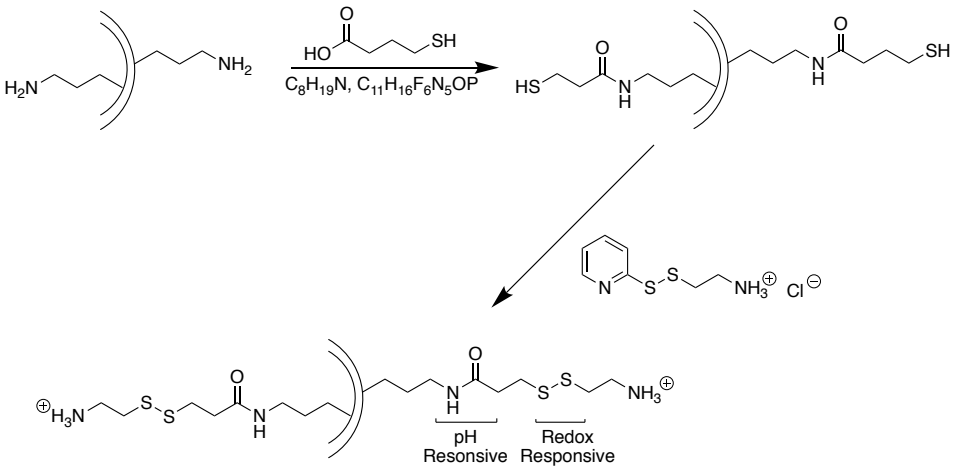

Figure 3.34. Functionalization of Li et al.'s MSN. The amine functionalized particles (both within the pores and exterior) are reacted with Mercaptopropionic acid. 2-(2-Pyridinyldithio)-ethanamine hydrochloride is then attached to the free sulfide group to produce a pH and redox responsive section. Due to the lower pH in cancer cells (pH 6.5 compared to pH 7.4 in normal tissue) and acidic endosome (pH 5-6) and lysosome (pH 4.5-5) in tumor cells, the positive moiety electrostatically bound to the loaded gene are released and the cargo is delivered. Image modified from reference 30.

Agarose gel electrophoresis demonstrated that CMSN-A could load and protect pDNA from DNase1 degradation (**Figure 3.35.**). DNA was visualized on UV trans-illuminator.[30] DNase degradation is confirmed by comparing lane 1 (pDNA) and lane 2 (pDNA and DNase1). The pDNA loaded CMSN-A remain in the gel wells (lane 3) even after being treated with DNase1 (lane 4). When the loaded CMSN-A were treated with

the reducing agent DTT that is used to simulate the effects of GSH in vivo[1] (lane 5), the pDNA was released, confirming the efficacy of the redox release mechanism.[30] Subsequent treatment by DNase1 of the DTT treated system resulted in pDNA degradation (lane 6) that confirms the previous protection in lane 4.[30]

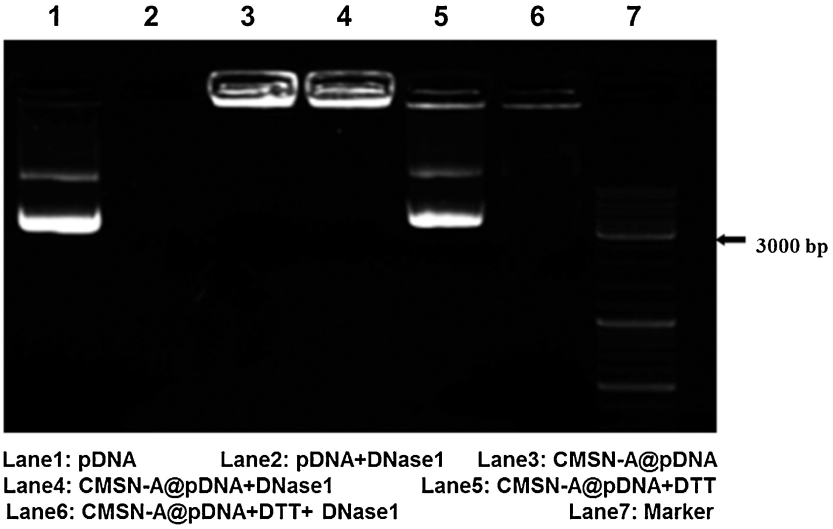

Figure 3.35. Agarose gel electrophoresis demonstrating the pDNA protection provided by CMSN-A. The amount of pDNA (1 μg) and CMSN-A (40 μg) were constant. Figure modified from reference 30.

Gene transfection experiments confirmed the ability for CMSN-A loaded with pDNA to enter cells and deliver its genetic cargo. The gene pGFP was delivered to HeLa and 293-T cell lines (**Figure 3.36.**). Compared to the negative control (free pGFP), the CMSN-A delivery system successfully delivered its cargo, evidenced by the expression of the green fluorescent protein coded by pGFP. However, the positive control, Lipofectamine 2000 loaded with pGFP, exhibited a higher transfection efficacy thank CMSN-A.[30]

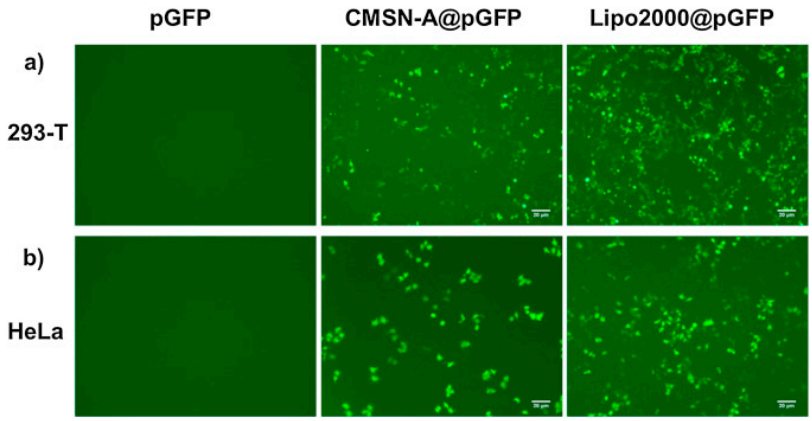

Figure 3.36. Gene transfection study demonstrating the successful delivery of pGFP by CMSN-A. Image modified from reference 30.

3.4 Chapter conclusions

MSN based delivery systems are a promising platform for oligonucleotide delivery due to their high surface area and ability to internalize cargo in their pores when compared to solid silica nanoparticle systems. The first obstacle for MSN is optimizing the pores for DNA or RNAi loading. Current studies comparing pore sizes for DNA and pDNA indicate large pores are necessary (10 nm for ~2 kbp DNA and 23 nm for 4.8 kbp pDNA).[3-4] Intermediate size pores (8-10 nm) were found by two groups to be optimal for siRNA loading and release.[8-9] Only one group, Steinbacher and colleagues, investigated how the percent of pore functionalization influenced siRNA loading and release. They discovered the percent of pore functionalization could be optimized, indicating an important parameter that should be analyzed in future studies.

Aside from pore expansion with TMB or etching with ammonium hydroxide, two main techniques have been explored to produce MSN with large pores and variable particle diameter. Wu and colleagues synthesized a small MSN (50.75 nm based on DLS)

with ~6.2 nm pores by adding another silica precursor, BTES, to co-condense with TEOS.[10] Ashley and colleagues used microemulsion templating to produce 165 nm particles based on DLS with smaller and larger pores (approximately 3-13 nm and 23-30 nm).[12]

Several modification techniques have been investigated, although the lack of comparison within many of the studies to a benchmark result in difficulty comparing efficacy.[32] Amine and PEG modified MSN with large 23 nm pores demonstrated in vivo tumor size reduction, but the particles had to be injected intratumorally due to their aggregation tendency.[6] Poly-L-lysine modification demonstrated high cellular uptake but also cellular toxicity.[19] The cellular toxicity may be mitigated by using lower weight poly-l-lysine that would reduce its' cationic charge density. This would also reduce cellular uptake. Cell penetrating peptides such as TAT have exhibited increased cellular uptake of MSN, however this increased uptake is unspecific and would affect both normal and cancerous cells.

Ligand mediated targeting is a promising solution to reducing off-target effects and deliver the particle to its intended target. While only one group has studied targeting ligands in the context of MSN for oligonucleotide delivery, many studies have employed this strategy for cancer therapy that are outside the scope of this review.[18, 33-34] Ashley and colleagues demonstrated this potential with the targeting peptide SP94 that preferentially targeted liver cancer cells (Hep3B) while avoiding uptake by healthy hepatocytes.[12]

Triggered release systems are another strategy purposed to limit loss of cargo caused by diffusion and a burst release upon entering the cancerous cell. The two main

strategies take advantage of the increased acidity and reducing agents in cancer cells because of their rapid growth. Sun and colleagues developed a redox triggered capping system by covering their loaded particles with PEI cross-linked with DSP.[1] This system demonstrated redox triggered release and resulted in significantly reduced expression of the targeted protein in both in vitro and in vivo studies. Li and colleagues combined these strategies to create a pH and redox triggered system that would release the positively charged amine group electrostatically attaching the pDNA to the particle.[30] The system successfully protected the loaded pDNA from degradation by DNase1 and exhibited release upon reduction by DTT.

3.5 References

1. Sun, L.; Liu, Y. J.; Yang, Z. Z.; Qi, X. R. Tumor Specific Delivery with Redox-Triggered Mesoporous Silica Nanoparticles Inducing Neovascularization Suppression and Vascular Normalization. *RSC Adv.* **2015,** *5*, 55566-55578.
2. Kruk, M. Access to Ultralarge-Pore Ordered Mesoporous Materials through Selection of Surfactant/Swelling-Agent Micellar Templates. *Acc. Chem. Res.* **2012,** *45*, 1678-1687.
3. Kim, M. H.; Na, H. K.; Kim, Y. K.; Ryoo, S. R.; Cho, H. S.; Lee, K. E.; Jeon, H.; Ryoo, R.; Min, D. H. Facile Synthesis of Monodispersed Mesoporous Silica Nanoparticles with Ultralarge Pores and Their Application in Gene Delivery. *ACS Nano* **2011,** *5*, 3568-3576.
4. Solberg, S. M.; Landry, C. C. Adsorption of DNA into Mesoporous Silica. *J. Phys. Chem. B* **2006,** *110*, 15261-15268.
5. Kim, D. H.; Behlke, M. A.; Rose, S. D.; Chang, M. S.; Choi, S.; Rossi, J. J. Synthetic dsRNA Dicer Substrates Enhance RNAi Potency and Efficacy. *Nat. Biotechnol.* **2005,** *23*, 222-226.
6. Na, H. K.; Kim, M. H.; Park, K.; Ryoo, S. R.; Lee, K. E.; Jeon, H.; Ryoo, R.; Hyeon, C.; Min, D. H. Efficient Functional Delivery of siRNA Using Mesoporous Silica Nanoparticles with Ultralarge Pores. *Small* **2012,** *8*, 1752-1761.
7. Mao, S.; Neu, M.; Germershaus, O.; Merkel, O.; Sitterberg, J.; Bakowsky, U.; Kissel, T. Influence of Polyethylene Glycol Chain Length on the Physicochemical and Biological Properties of Poly (Ethylene Imine)-Graft-Poly (Ethylene Glycol) Block Copolymer/SiRNA Polyplexes. *Bioconjugate Chem.* **2006,** *17*, 1209-1218.

8. Kim, S.; Na, H. K.; Won, C.; Min, D. H. In-Depth Study on the Gene Silencing Capability of Silica Nanoparticles with Different Pore Sizes: Degree and Duration of RNA Interference. *RSC Adv.* **2016,** *6*, 27143-27150.
9. Steinbacher, J. L.; Landry, C. C. Adsorption and Release of siRNA from Porous Silica. *Langmuir* **2014,** *30*, 4396-4405.
10. Wu, M.; Meng, Q.; Chen, Y.; Du, Y.; Zhang, L.; Li, Y.; Zhang, L.; Shi, J. Large-Pore Ultrasmall Mesoporous Organosilica Nanoparticles: Micelle/Precursor Co-templating Assembly and Nuclear-Targeted Gene Delivery. *Adv. Mater.* **2015,** *27*, 215-222.
11. Carroll, N. J.; Pylypenko, S.; Atanassov, P. B.; Petsev, D. N. Microparticles with Bimodal Nanoporosity Derived by Microemulsion Templating. *Langmuir* **2009,** *25*, 13540-13544.
12. Ashley, C. E.; Carnes, E. C.; Epler, K. E.; Padilla, D. P.; Phillips, G. K.; Castillo, R. E.; Wilkinson, D. C.; Wilkinson, B. S.; Burgard, C. A.; Kalinich, R. M. Delivery of Small Interfering RNA by Peptide-Targeted Mesoporous Silica Nanoparticle-Supported Lipid Bilayers. *ACS Nano* **2012,** *6*, 2174-2188.
13. Ashley, C. E.; Carnes, E. C.; Phillips, G. K.; Padilla, D.; Durfee, P. N.; Brown, P. A.; Hanna, T. N.; Liu, J.; Phillips, B.; Carter, M. B.; Carroll, N. J.; Jiang, X.; Dunphy, D. R.; Willman, C. L.; Petsev, D. N.; Evans, D. G.; Parikh, A. N.; Chackerian, B.; Wharton, W.; Peabody, D. S.; Brinker, C. J. The Targeted Delivery of Multicomponent Cargos to Cancer Cells by Nanoporous Particle-Supported Lipid Bilayers. *Nat. Mater.* **2011,** *10*, 389-397.
14. Liong, M.; Lu, J.; Kovochich, M.; Xia, T.; Ruehm, S. G.; Nel, A. E.; Tamanoi, F.; Zink, J. I. Multifunctional Inorganic Nanoparticles for Imaging, Targeting, and Drug Delivery. *ACS Nano* **2008,** *2*, 889-896.
15. Finlay, J.; Roberts, C. M.; Dong, J.; Zink, J. I.; Tamanoi, F.; Glackin, C. A. Mesoporous Silica Nanoparticle Delivery of Chemically Modified siRNA Against TWIST1 Leads to Reduced Tumor Burden. *Nanomed.* **2015,** *11*, 1657-1666.
16. Hom, C.; Lu, J.; Liong, M.; Luo, H.; Li, Z.; Zink, J. I.; Tamanoi, F. Mesoporous Silica Nanoparticles Facilitate Delivery of siRNA to Shutdown Signaling Pathways in Mammalian Cells. *Small* **2010,** *6*, 1185-1190.
17. Angelescu, D. G.; Nylander, T.; Piculell, L.; Linse, P.; Lindman, B.; Tropsch, J.; Detering, J. Adsorption of Branched-Linear Polyethyleneimine–Ethylene Oxide Conjugate on Hydrophilic Silica Investigated by Ellipsometry and Monte Carlo Simulations. *Langmuir* **2011,** *27*, 9961-9971.
18. Howard, M.; Zern, B. J.; Anselmo, A. C.; Shuvaev, V. V.; Mitragotri, S.; Muzykantov, V. Vascular Targeting of Nanocarriers: Perplexing Aspects of the Seemingly Straightforward Paradigm. *ACS Nano* **2014,** *8*, 4100-4132.
19. Hartono, S. B.; Gu, W.; Kleitz, F.; Liu, J.; He, L.; Middelberg, A. P.; Yu, C.; Lu, G. Q.; Qiao, S. Z. Poly-L-lysine Functionalized Large Pore Cubic Mesostructured Silica Nanoparticles as Biocompatible Carriers for Gene Delivery. *ACS Nano* **2012,** *6*, 2104-2117.

20. Putnam, D.; Gentry, C. A.; Pack, D. W.; Langer, R. Polymer-Based Gene Delivery with Low Cytotoxicity by a Unique Balance of Side-Chain Termini. *Proc. Natl. Acad. Sci.* **2001,** *98*, 1200-1205.
21. Heitz, F.; Morris, M. C.; Divita, G. Twenty Years of Cell-Penetrating Peptides: From Molecular Mechanisms to Therapeutics. *Br. J. Pharmacol.* **2009,** *157*, 195-206.
22. Bertrand, N.; Wu, J.; Xu, X.; Kamaly, N.; Farokhzad, O. C. Cancer Nanotechnology: The Impact of Passive and Active Targeting in the Era of Modern Cancer Biology. *Adv. Drug Delivery Rev.* **2014,** *66*, 2-25.
23. Petros, R. A.; DeSimone, J. M. Strategies in the Design of Nanoparticles for Therapeutic Applications. *Nat. Rev. Drug Discovery* **2010,** *9*, 615-627.
24. Liu, J.; Stace-Naughton, A.; Brinker, C. J. Silica Nanoparticle Supported Lipid Bilayers for Gene Delivery. *Chem. Commun.* **2009**, 5100-5102.
25. Gao, W.; Chan, J. M.; Farokhzad, O. C. pH-Responsive Nanoparticles for Drug Delivery. *Mol. Pharmaceutics* **2010,** *7*, 1913-1920.
26. Lin, D. S.; Cheng, Q.; Jiang, Q.; Huang, Y. Y.; Yang, Z.; Han, S. C.; Zhao, Y. N.; Guo, S. T.; Liang, Z. C.; Dong, A. J. Intracellular Cleavable Poly(2-Dimethylaminoethyl Methacrylate) Functionalized Mesoporous Silica Nanoparticles for Efficient siRNA Delivery In Vitro and In Vivo. *Nanoscale* **2013,** *5*, 4291-4301.
27. Choi, M.; Kleitz, F.; Liu, D.; Lee, H. Y.; Ahn, W.-S.; Ryoo, R. Controlled Polymerization in Mesoporous Silica Toward the Design of Organic− Inorganic Composite Nanoporous Materials. *J. Am. Chem. Soc.* **2005,** *127*, 1924-1932.
28. Wen, H. Y.; Dong, H. Q.; Xie, W. J.; Li, Y. Y.; Wang, K.; Pauletti, G. M.; Shi, D. L. Rapidly Disassembling Nanomicelles with Disulfide-Linked PEG Shells for Glutathione-Mediated Intracellular Drug Delivery. *Chem. Commun.* **2011,** *47*, 3550-3552.
29. Li, X.; Xie, Q. R.; Zhang, J.; Xia, W.; Gu, H. The Packaging of siRNA Within the Mesoporous Structure of Silica Nanoparticles. *Biomaterials* **2011,** *32*, 9546-9556.
30. Li, Y.; Hei, M.; Xu, Y.; Qian, X.; Zhu, W. Ammonium Salt Modified Mesoporous Silica Nanoparticles for Dual Intracellular-Responsive Gene Delivery. *Int. J. Pharm.* **2016,** *511*, 689-702.
31. Zhang, K.; Xu, L. L.; Jiang, J. G.; Calin, N.; Lam, K. F.; Zhang, S. J.; Wu, H. H.; Wu, G. D.; Albela, B. l.; Bonneviot, L. Facile Large-Scale Synthesis of Monodisperse Mesoporous Silica Nanospheres with Tunable Pore Structure. *J. Am. Chem. Soc.* **2013,** *135*, 2427-2430.
32. Bligaard, T.; Bullock, R. M.; Campbell, C. T.; Chen, J. G.; Gates, B. C.; Gorte, R. J.; Jones, C. W.; Jones, W. D.; Kitchin, J. R.; Scott, S. L. Toward Benchmarking in Catalysis Science: Best Practices, Challenges, and Opportunities. *ACS Catal.* **2016,** *6*, 2590-2602.
33. Gandhi, N. S.; Tekade, R. K.; Chougule, M. B. Nanocarrier Mediated Delivery of siRNA/miRNA in Combination with Chemotherapeutic Agents for Cancer Therapy: Current Progress and Advances. *J. Controlled Release* **2014,** *0*, 238-256.

34. Kim, E. M.; Jeong, H. J. Current Status and Future Direction of Nanomedicine: Focus on Advanced Biological and Medical Applications. *Nucl. Med. Mol. Imaging* **2016**, 1-12.

CHAPTER 4: CONCLUSION

4.1 Optimizing external loading delivery systems

Externally loaded delivery systems tend to use a small core silica nanoparticle and have a final diameter after exterior modifications between 20-230 nm. Unfortunately, few comparative conclusions concerning the optimal diameter can be reached due to the variety of exterior modifications between the studies (amine, PEI, PEI and PEG, etc.) and silica synthesis methods. Only Ngamcherdtrakul and colleagues compared different silica core sizes, although that group used a mesoporous silica nanoparticle core rather than solid silica. Future studies comparing efficacy of various diameter systems and previously explored external modifications such as PEI and PEG would greatly enhance the field.

Systems externally loading oligonucleotides must both electrostatically hold and protect their cargo while also being biocompatible and targeting cell uptake. Amino decorated nanoparticles (NPs) are able to load and deliver DNA with similar success to Lipofectin when investigated in vitro in some studies,[1] while other studies compared 7.5 times as much of their amino decorated silica NP to Lipofectin.[2] While tumor uptake and gene expression was enhanced when Tat/HA2 NP were administered intratumorally, intravenous injection resulted in uptake by the RES system and the majority of gene expression in the spleen and liver.[3] A solution to avoiding immune system uptake is decorating the exterior with PEG. Ngamcherdtrakul's group had greater success intravenously injecting their PEI and PEG decorate NP (58.6% tumor reduction)[4] likely due to PEG's ability to increase circulation time.

Although the toxicity of PEI remains a concern,[5] several groups reduced PEI's toxicity by conjugating it with PEG and/or using a lower weight PEI. Lee and colleagues found between 90-100% cell viability when incubated with 25 kDa PEI and PEG decorated NPs. Another group, Ngamcherdtrakul and colleagues, determined their nanoparticles were non-toxic when functionalized with crosslinked 1.8 or 10 kDa PEI and decorated with PEG.[4]

While Ngamcherdtrakul's group compared their findings to FDA approved Abraxane (Paclitaxel-albumin conjugates), Lee's group did not make an outside comparison. This hinders cross comparison between studies and reinforces the need for a benchmark. For exterior loading nanoparticles, an FDA approved formulation like Abraxane is ideal. Abraxane has a particle size of ~130 nm[6] that would likely be similar to a silica based formula. Furthermore, both an exterior loading silica nanoparticle formula and Abraxane load and deliver a hydrophobic molecule. The benchmark comparison would then change once a nanoparticle formula with external loading is approved by the FDA.

4.2 Optimizing internal loading delivery systems

Much like externally loaded systems, internal loading systems can vary in synthesis methods, functionalization, size, etc. Because of this, comparisons between studies is sometimes tenuous. However, several useful lessons can be discerned from the aforementioned studies. Furthermore, many studies are beginning to compare their systems to FDA approved liposome formulations. Liposomes are a natural benchmark,

since they also encapsulate their cargo, can be decorated with PEG, targeting moieties, and cell penetrating peptides.

4.2.1. Pore size

While there is still much work to be done in understanding the optimal pore size for DNA and siRNA loading and release, it is clear that larger pore sizes tend to optimize DNA and pDNA loading, while an intermediate pore size allow for the highest siRNA adsorption and release. For example, larger, amine functionalized pores (10 or 23 nm) adsorbed more DNA and pDNA respectively than smaller, amine functionalized pores (2, 3.4, and 5.4 nm).[7-8] For siRNA larger pores adsorb more oligonucleotides but create an energetically favorable environment that hinders release. Thus, studies found intermediate sized pores (8 or 10 nm) were optimal compared to smaller and larger pores (2, 4, 7, 15, 23 nm).[9-10] The ideal pore size for the MSN will change depending on whether a bulky functionalization is used that reduces the functional pore diameter.

As pore size is fine-tuned, synthesis techniques for large pore MSN are also being perfected. The most commonly used method is expanding the synthesized pores with the swelling agent TMB. However, this method can result in structural instability for larger final pore sizes. Other avenues explored by studies loading and delivering oligonucleotides include additional silica precursors (BTES)[11] and microemulsion templating.[12] Compared to base prepared mesoporous silica, microemulsion templating results in a wider variation in particle diameter (100 – 200 nm and ~100 – 400 nm after size exclusion respectively). This wide range may hinder in vivo development depending

on whether the size range results in different delivery outcomes. The addition of BTES in the sol-gel method results in smaller, monodisperse MSN (50.75 nm).

4.2.2. External functionalizations for delivery

The most common base functionalization is PEI, while the second common is a combination of PEI and PEG. This is likely due to PEI's ability to be endocytosed by cells, escape the endosome, and enter the cell's nucleus even when unconjugated.[13] Furthermore, shorter chain PEI (<10 KDa) have been demonstrated as not causing significant toxicity in normal and tumor cells.[14-15] PEG is usually added to reduce protein adsorption in vivo and reduce aggregation.[16]

Upon this PEI and/or PEG base, a variety of peptides or antibodies can be attached. Cell penetrating peptides can increase cell uptake and direct intercellular fate (such as Tat).[11] This can be combined with a targeting ligand to specify delivery to a certain cancer cell type. Both cell fusion peptides and targeting moieties have demonstrated efficacy when studied in vitro. Clearly the next step is to evaluate in vivo effectiveness. Since both targeting and cell uptake ligands require proximity to function, other methods to ensure this proximity is achieved will need to be employed.

Two techniques to increase the probability that the MSN formulation will reach a close enough proximity to the targeted cancer cell that are usually employed are increasing circulation time[17] (often with PEGylation) and triggered release systems to ensure the payload is not diminished during circulation time. Both strategies aim to reduce off-target effects and delivering the maximum amount of cargo to the cancer cell's cytosol. The most pursued system exploits the large difference in reducing agents in

tumor cells compared to normal tissue. The capped pores reduce oligonucleotide loss via diffusion and result in higher gene delivery. For example, Sun and colleagues reported in vitro treatment of KB cells by siRNA loaded MSN decorated with either just PEI (MSN/PEI) or crosslinked PEI (MSN/CrPEI) that released its cargo upon reducing conditions. When compared with the control group, the MSN/PEI downregulated the targeted gene 40% ($P < 0.05$), while MSN/CrPEI downregulated it 75% ($P < 0.01$).[18] Unfortunately the only group that performed in vivo testing injected the triggered release system peritumorally.[18] Thus, more studies investigating the effectiveness of reducing triggered systems in vivo are needed.

4.3 Final thoughts

Silica based oligonucleotide delivery systems are a promising alternative to medication currently on the market due to their ability to reduce cargo leakage, off-target effects, and target the intended cells for treatment. While much progress has been made in the last ten years, many obstacles still lie ahead before a delivery system will make the transition from bench to bedside. One strategy that would further the field as a whole would be to compare solid and mesoporous silica nanoparticle formulations to an FDA approved formulation across studies. This would allow for more accurate comparisons between studies.

4.4 References

1. Rejeeth, C.; Kannan, S.; Muthuchelian, K. Development of In Vitro Gene Delivery System Using ORMOSIL Nanoparticle: Analysis of p53 Gene Expression in Cultured Breast Cancer Cell (MCF-7). *Cancer Nanotechnol.* **2012,** *3*, 55-63.
2. Xiao, X.; He, Q.; Huang, K. Novel Amino-Modified Silica Nanoparticles as Efficient Vector for Hepatocellular Carcinoma Gene Therapy. *Med. Oncol.* **2010,** *27*, 1200-1207.
3. Ye, S. F.; Tian, M. M.; Wang, T. X.; Ren, L.; Wang, D.; Shen, L. H.; Shang, T. Synergistic Effects of Cell-Penetrating Peptide Tat and Fusogenic Peptide HA2-Enhanced Cellular Internalization and Gene Transduction of Organosilica Nanoparticles. *Nanomed.* **2012,** *8*, 833-841.
4. Ngamcherdtrakul, W.; Morry, J.; Gu, S.; Castro, D. J.; Goodyear, S. M.; Sangvanich, T.; Reda, M. M.; Lee, R.; Mihelic, S. A.; Beckman, B. L. Cationic Polymer Modified Mesoporous Silica Nanoparticles for Targeted siRNA Delivery to HER2+ Breast Cancer. *Adv. Drug Delivery Rev.* **2015,** *25*, 2646-2659.
5. Lv, H.; Zhang, S.; Wang, B.; Cui, S.; Yan, J. Toxicity of Cationic Lipids and Cationic Polymers in Gene Delivery. *J. Controlled Release* **2006,** *114*, 100-109.
6. Ma, P.; Mumper, R. J. Paclitaxel Nano-Delivery Systems: A Comprehensive Review. *J. Nanomed. Nanotechnol.* **2013,** *4*, 1000164.
7. Solberg, S. M.; Landry, C. C. Adsorption of DNA into Mesoporous Silica. *J. Phys. Chem. B* **2006,** *110*, 15261-15268.
8. Kim, M. H.; Na, H. K.; Kim, Y. K.; Ryoo, S. R.; Cho, H. S.; Lee, K. E.; Jeon, H.; Ryoo, R.; Min, D. H. Facile Synthesis of Monodispersed Mesoporous Silica Nanoparticles with Ultralarge Pores and Their Application in Gene Delivery. *ACS Nano* **2011,** *5*, 3568-3576.
9. Kim, S.; Na, H. K.; Won, C.; Min, D. H. In-Depth Study on the Gene Silencing Capability of Silica Nanoparticles with Different Pore Sizes: Degree and Duration of RNA Interference. *RSC Adv.* **2016,** *6*, 27143-27150.
10. Steinbacher, J. L.; Landry, C. C. Adsorption and Release of siRNA from Porous Silica. *Langmuir* **2014,** *30*, 4396-4405.
11. Wu, M.; Meng, Q.; Chen, Y.; Du, Y.; Zhang, L.; Li, Y.; Zhang, L.; Shi, J. Large-Pore Ultrasmall Mesoporous Organosilica Nanoparticles: Micelle/Precursor Co-templating Assembly and Nuclear-Targeted Gene Delivery. *Adv. Mater.* **2015,** *27*, 215-222.
12. Ashley, C. E.; Carnes, E. C.; Epler, K. E.; Padilla, D. P.; Phillips, G. K.; Castillo, R. E.; Wilkinson, D. C.; Wilkinson, B. S.; Burgard, C. A.; Kalinich, R. M. Delivery of Small Interfering RNA by Peptide-Targeted Mesoporous Silica Nanoparticle-Supported Lipid Bilayers. *ACS Nano* **2012,** *6*, 2174-2188.
13. Godbey, W.; Wu, K. K.; Mikos, A. G. Tracking the Intracellular Path of Poly (Ethylenimine)/DNA Complexes for Gene Delivery. *Proc. Natl. Acad. Sci.* **1999,** *96*, 5177-5181.

14. Meng, H.; Xue, M.; Xia, T.; Ji, Z.; Tarn, D. Y.; Zink, J. I.; Nel, A. E. Use of Size and a Copolymer Design Feature to Improve the Biodistribution and the Enhanced Permeability and Retention Effect of Doxorubicin-Loaded Mesoporous Silica Nanoparticles in a Murine Xenograft Tumor Model. *ACS Nano* **2011,** *5*, 4131-4144.
15. Xia, T.; Kovochich, M.; Liong, M.; Meng, H.; Kabehie, S.; George, S.; Zink, J. I.; Nel, A. E. Polyethyleneimine Coating Enhances the Cellular Uptake of Mesoporous Silica Nanoparticles and Allows Safe Delivery of siRNA and DNA Constructs. *ACS Nano* **2009,** *3*, 3273-3286.
16. Mao, S.; Neu, M.; Germershaus, O.; Merkel, O.; Sitterberg, J.; Bakowsky, U.; Kissel, T. Influence of Polyethylene Glycol Chain Length on the Physicochemical and Biological Properties of Poly (Ethylene Imine)-Graft-Poly (Ethylene Glycol) Block Copolymer/SiRNA Polyplexes. *Bioconjugate Chem.* **2006,** *17*, 1209-1218.
17. Nichols, J. W.; Bae, Y. H. Odyssey of a Cancer Nanoparticle: From Injection Site to Site of Action. *Nano Today* **2012,** *7*, 606-618.
18. Sun, L.; Liu, Y. J.; Yang, Z. Z.; Qi, X. R. Tumor Specific Delivery with Redox-Triggered Mesoporous Silica Nanoparticles Inducing Neovascularization Suppression and Vascular Normalization. *RSC Adv.* **2015,** *5*, 55566-55578.

CHAPTER 5: COMPREHENSIVE BIBLIOGRAPHY

Adolphi, N. L.; Butler, K. S.; Lovato, D. M.; Tessier, T. E.; Trujillo, J. E.; Hathaway, H. J.; Fegan, D. L.; Monson, T. C.; Stevens, T. E.; Huber, D. L.; Ramu, J.; Milne, M. L.; Altobelli, S. A.; Bryant, H. C.; Larson, R. S.; Flynn, E. R. Imaging of Her2-Targeted Magnetic Nanoparticles for Breast Cancer Detection: Comparison of SQUID-Detected Magnetic Relaxometry and MRI. *Contrast Media Mol. Imaging* **2012,** *7*.

Altin, J.; Atmosukarto, I.; De Wildt, R. M.; Parish, C.; Price, J. Composition for Targeting Dendritic Cells. US8779107 B2: July 15, 2014.

Angelescu, D. G.; Nylander, T.; Piculell, L.; Linse, P.; Lindman, B.; Tropsch, J.; Detering, J. Adsorption of Branched-Linear Polyethyleneimine–Ethylene Oxide Conjugate on Hydrophilic Silica Investigated by Ellipsometry and Monte Carlo Simulations. *Langmuir* **2011,** *27*, 9961-9971.

Anselmo, A. C.; Mitragotri, S. Nanoparticles in the Clinic. *Bioengineering & Translational Medicine* **2016**.

Ashley, C. E.; Carnes, E. C.; Epler, K. E.; Padilla, D. P.; Phillips, G. K.; Castillo, R. E.; Wilkinson, D. C.; Wilkinson, B. S.; Burgard, C. A.; Kalinich, R. M. Delivery of Small Interfering RNA by Peptide-Targeted Mesoporous Silica Nanoparticle-Supported Lipid Bilayers. *ACS Nano* **2012,** *6*, 2174-2188.

Ashley, C. E.; Carnes, E. C.; Phillips, G. K.; Padilla, D.; Durfee, P. N.; Brown, P. A.; Hanna, T. N.; Liu, J.; Phillips, B.; Carter, M. B.; Carroll, N. J.; Jiang, X.; Dunphy, D. R.; Willman, C. L.; Petsev, D. N.; Evans, D. G.; Parikh, A. N.; Chackerian, B.; Wharton, W.; Peabody, D. S.; Brinker, C. J. The Targeted Delivery of Multicomponent Cargos to Cancer Cells by Nanoporous Particle-Supported Lipid Bilayers. *Nat. Mater.* **2011,** *10*, 389-397.

Babu, A.; Templeton, A. K.; Munshi, A.; Ramesh, R. Nanoparticle-Based Drug Delivery for Therapy of Lung Cancer: Progress and Challenges. *J. Nanomater.* **2013,** *2013*, 14.

Barnaby, S. N.; Sita, T. L.; Petrosko, S. H.; Stegh, A. H.; Mirkin, C. A., Therapeutic Applications of Spherical Nucleic Acids. In *Nanotechnology-Based Precision Tools for the Detection and Treatment of Cancer*, Springer: New York, 2015; pp 23-50.

Bertrand, N.; Wu, J.; Xu, X.; Kamaly, N.; Farokhzad, O. C. Cancer Nanotechnology: The Impact of Passive and Active Targeting in the Era of Modern Cancer Biology. *Adv. Drug Delivery Rev.* **2014,** *66*, 2-25.

Bligaard, T.; Bullock, R. M.; Campbell, C. T.; Chen, J. G.; Gates, B. C.; Gorte, R. J.; Jones, C. W.; Jones, W. D.; Kitchin, J. R.; Scott, S. L. Toward Benchmarking in Catalysis Science: Best Practices, Challenges, and Opportunities. *ACS Catal.* **2016,** *6*, 2590-2602.

Blumen, S. R.; Cheng, K.; Ramos-Nino, M. E.; Taatjes, D. J.; Weiss, D. J.; Landry, C. C.; Mossman, B. T. Unique Uptake of Acid-Prepared Mesoporous Spheres by Lung Epithelial and Mesothelioma Cells. *Am. J. Respir. Cell Mol. Biol.* **2007,** *36*, 333-342.

Boussif, O.; Lezoualc'h, F.; Zanta, M. A.; Mergny, M. D.; Scherman, D.; Demeneix, B.; Behr, J.-P. A Versatile Vector for Gene and Oligonucleotide Transfer Into Cells in Culture and In Vivo: Polyethylenimine. *Proc. Natl. Acad. Sci.* **1995,** *92*, 7297-7301.

Bradbury, M. S.; Phillips, E.; Montero, P. H.; Cheal, S. M.; Stambuk, H.; Durack, J. C.; Sofocleous, C. T.; Meester, R. J.; Wiesner, U.; Patel, S. Clinically-Translated Silica Nanoparticles as Dual-Modality Cancer-Targeted Probes for Image-Guided Surgery and Interventions. *Integr. Biol.* **2013,** *5*, 74-86.

Braeckmans, K.; Buyens, K.; Bouquet, W.; Vervaet, C.; Joye, P.; Vos, F. D.; Plawinski, L.; Doeuvre, L.; Angles-Cano, E.; Sanders, N. N. Sizing Nanomatter in Biological Fluids by Fluorescence Single Particle Tracking. *Nano Lett.* **2010,** *10*, 4435-4442.

Branton, P. J.; Hall, P. G.; Sing, K. S.; Reichert, H.; Schüth, F.; Unger, K. K. Physisorption of Argon, Nitrogen and Oxygen by MCM-41, a Model Mesoporous Adsorbent. *J. Chem. Soc., Faraday Trans.* **1994,** *90*, 2965-2967.

Buchman, Y. K.; Lellouche, E.; Zigdon, S.; Bechor, M.; Michaeli, S.; Lellouche, J.-P. Silica Nanoparticles and Polyethyleneimine (PEI)-Mediated Functionalization: A New Method of PEI Covalent Attachment for siRNA Delivery Applications. *Bioconjugate Chem.* **2013,** *24*, 2076-2087.

Carroll, N. J.; Pylypenko, S.; Atanassov, P. B.; Petsev, D. N. Microparticles with Bimodal Nanoporosity Derived by Microemulsion Templating. *Langmuir* **2009,** *25*, 13540-13544.

Chaudhry, A. T.; Akhtar, D. Gene Therapy and Modification as a Therapeutic Strategy for Cancer. *University of Ottawa Journal of Medicine* **2016,** *6*, 44-48.

Chen, Y.; Wu, J. J.; Huang, L. Nanoparticles Targeted with NGR Motif Deliver C-MYC siRNA and Doxorubicin for Anticancer Therapy. *Mol. Ther.* **2010,** *18*, 828-834.

Cheng, K.; Blumen, S. R.; MacPherson, M. B.; Steinbacher, J. L.; Mossman, B. T.; Landry, C. C., Enhanced Uptake of Porous Silica Microparticles by Bifunctional Surface

Modification with a Targeting Antibody and a Biocompatible Polymer. *ACS Appl. Mater. Interfaces* **2010,** *2* (9), 2489-2495.

Cheok, C. F.; Verma, C. S.; Baselga, J.; Lane, D. P. Translating p53 Into the Clinic. *Nat. Rev. Clin. Oncol.* **2011,** *8*, 25-37.

Choi, M.; Kleitz, F.; Liu, D.; Lee, H. Y.; Ahn, W.-S.; Ryoo, R. Controlled Polymerization in Mesoporous Silica Toward the Design of Organic− Inorganic Composite Nanoporous Materials. *J. Am. Chem. Soc.* **2005,** *127*, 1924-1932.

Cross, D.; Burmester, J. K. Gene Therapy for Cancer Treatment: Past, Present and Future. *Clin. Med. Res.* **2006,** *4*, 218-227

Davis, M. E. The First Targeted Delivery of siRNA in Humans Via a Self-Assembling, Cyclodextrin Polymer-Based Nanoparticle: From Concept to Clinic. *Mol. Pharmaceutics* **2009,** *6*, 659-668.

Davis, M. E.; Zuckerman, J. E.; Choi, C. H. J.; Seligson, D.; Tolcher, A.; Alabi, C. A.; Yen, Y.; Heidel, J. D.; Ribas, A. Evidence of RNAi in Humans from Systemically Administered siRNA Via Targeted Nanoparticles. *Nature* **2010,** *464*, 1067-1070.

DeSantis, C. E.; Lin, C. C.; Mariotto, A. B.; Siegel, R. L.; Stein, K. D.; Kramer, J. L.; Alteri, R.; Robbins, A. S.; Jemal, A. Cancer Treatment and Survivorship Statistics, 2014. *CA. Cancer J. Clin.* **2014,** *64*, 252-271.

Eriguchi, M.; Yanagie, H.; Maruyama, K.; Fujisawa, T., Liposome Preparations Containing Oxaliplatin. US20040022842 A1: Feb 5, 2004.

Espelin, C. W.; Leonard, S. C.; Geretti, E.; Wickham, T. J.; Hendriks, B. S. Dual HER2 Targeting with Trastuzumab and Liposomal-Encapsulated Doxorubicin (MM-302) Demonstrates Synergistic Antitumor Activity in Breast and Gastric Cancer. *Cancer Res.* **2016,** *76*, 1517-1527.

Finlay, J.; Roberts, C. M.; Dong, J.; Zink, J. I.; Tamanoi, F.; Glackin, C. A. Mesoporous Silica Nanoparticle Delivery of Chemically Modified siRNA Against TWIST1 Leads to Reduced Tumor Burden. *Nanomed.* **2015,** *11*, 1657-1666.

Gabizon, A.; Shmeeda, H.; Barenholz, Y. Pharmacokinetics of PEGylated Liposomal Doxorubicin. *Clin. Pharmacokinet.* **2003,** *42*, 419-436.

Gandhi, N. S.; Tekade, R. K.; Chougule, M. B. Nanocarrier Mediated Delivery of siRNA/miRNA in Combination with Chemotherapeutic Agents for Cancer Therapy: Current Progress and Advances. *J. Controlled Release* **2014,** *0*, 238-256.

Gao, W.; Chan, J. M.; Farokhzad, O. C. pH-Responsive Nanoparticles for Drug Delivery. *Mol. Pharmaceutics* **2010,** *7*, 1913-1920.

Godbey, W.; Wu, K. K.; Mikos, A. G. Tracking the Intracellular Path of Poly (Ethylenimine)/DNA Complexes for Gene Delivery. *Proc. Natl. Acad. Sci.* **1999,** *96*, 5177-5181.

Goldburg, W. Dynamic Light Scattering. *Am. J. Phys.* **1999,** *67*, 1152-1160.

Grant, B. D.; Donaldson, J. G. Pathways and Mechanisms of Endocytic Recycling. *Nat. Rev. Mol. Cell Biol.* **2009,** *10*, 597-608.

Han, Y.; Ying, J. Y., Generalized Fluorocarbon-Surfactant-Mediated Synthesis of Nanoparticles with Various Mesoporous Structures. *Angew. Chem.* **2005,** *117* (2), 292-296.

Hartono, S. B.; Gu, W.; Kleitz, F.; Liu, J.; He, L.; Middelberg, A. P.; Yu, C.; Lu, G. Q.; Qiao, S. Z. Poly-L-lysine Functionalized Large Pore Cubic Mesostructured Silica Nanoparticles as Biocompatible Carriers for Gene Delivery. *ACS Nano* **2012,** *6*, 2104-2117.

He, Q.; Zhang, Z.; Gao, F.; Li, Y.; Shi, J. In vivo biodistribution and urinary excretion of mesoporous silica nanoparticles: effects of particle size and PEGylation. *Small* **2011,** *7*, 271-280.

Heitz, F.; Morris, M. C.; Divita, G. Twenty Years of Cell-Penetrating Peptides: From Molecular Mechanisms to Therapeutics. *Br. J. Pharmacol.* **2009,** *157*, 195-206.

Hom, C.; Lu, J.; Liong, M.; Luo, H.; Li, Z.; Zink, J. I.; Tamanoi, F. Mesoporous Silica Nanoparticles Facilitate Delivery of siRNA to Shutdown Signaling Pathways in Mammalian Cells. *Small* **2010,** *6*, 1185-1190.

Howard, M.; Zern, B. J.; Anselmo, A. C.; Shuvaev, V. V.; Mitragotri, S.; Muzykantov, V. Vascular Targeting of Nanocarriers: Perplexing Aspects of the Seemingly Straightforward Paradigm. *ACS Nano* **2014,** *8*, 4100-4132.

Hrkach, J.; Von Hoff, D.; Ali, M. M.; Andrianova, E.; Auer, J.; Campbell, T.; De Witt, D.; Figa, M.; Figueiredo, M.; Horhota, A. Preclinical Development and Clinical Translation of a PSMA-Targeted Docetaxel Nanoparticle with a Differentiated Pharmacological Profile. *Sci. Transl. Med.* **2012,** *4*, 128ra39.

Hu, L.; Mao, Z.; Gao, C. Colloidal Particles for Cellular Uptake and Delivery. *J. Mater. Chem.* **2009,** *19*, 3108-3115.

Huang, X.; Li, L.; Liu, T.; Hao, N.; Liu, H.; Chen, D.; Tang, F., The Shape Effect of Mesoporous Silica Nanoparticles on Biodistribution, Clearance, and Biocompatibility in Vivo. *ACS Nano* **2011,** *5* (7), 5390-5399.

Jaetao, J. E.; Butler, K. S.; Adolphi, N. L.; Lovato, D. M.; Bryant, H. C.; Rabinowitz, I.; Winter, S. S.; Tessier, T. E.; Hathaway, H. J.; Bergemann, C.; Flynn, E. R.; Larson, R. S. Enhanced Leukemia Cell Detection Using a Novel Magnetic Needle and Nanoparticles. *Cancer Res.* **2009,** *69*, 8310-8316.

Kamaly, N.; Yameen, B.; Wu, J.; Farokhzad, O. C. Degradable Controlled-Release Polymers and Polymeric Nanoparticles: Mechanisms of Controlling Drug Release. *Chem. Rev.* **2016,** *116*, 2602-2663.

Kanasty, R.; Dorkin, J. R.; Vegas, A.; Anderson, D. Delivery Materials for siRNA Therapeutics. *Nat. Mater.* **2013,** *12*, 967-977.

Khalil, I. A.; Kogure, K.; Futaki, S.; Harashima, H. Octaarginine-Modified Liposomes: Enhanced Cellular Uptake and Controlled Intracellular Trafficking. *Int. J. Pharm.* **2008,** *354*, 39-48.

Kim, D. H.; Behlke, M. A.; Rose, S. D.; Chang, M. S.; Choi, S.; Rossi, J. J. Synthetic dsRNA Dicer Substrates Enhance RNAi Potency and Efficacy. *Nat. Biotechnol.* **2005,** *23*, 222-226.

Kim, E. M.; Jeong, H. J. Current Status and Future Direction of Nanomedicine: Focus on Advanced Biological and Medical Applications. *Nucl. Med. Mol. Imaging* **2016**, 1-12.

Kim, M. H.; Na, H. K.; Kim, Y. K.; Ryoo, S.-R.; Cho, H. S.; Lee, K. E.; Jeon, H.; Ryoo, R.; Min, D.-H. Facile Synthesis of Monodispersed Mesoporous Silica Nanoparticles with Ultralarge Pores and Their Application in Gene Delivery. *ACS Nano* **2011,** *5*, 3568-3576.

Kim, S.; Na, H. K.; Won, C.; Min, D.-H. In-Depth Study on the Gene Silencing Capability of Silica Nanoparticles with Different Pore Sizes: Degree and Duration of RNA Interference. *RSC Adv.* **2016,** *6*, 27143-27150.

Knežević, N. Ž.; Durand, J. O. Targeted Treatment of Cancer with Nanotherapeutics Based on Mesoporous Silica Nanoparticles. *ChemPlusChem* **2015,** *80*, 26-36.

Kobler, J.; Möller, K.; Bein, T. Colloidal Suspensions of Functionalized Mesoporous Silica Nanoparticles. *ACS Nano* **2008,** *2*, 791-799.

Kohl, H.; Reimer, L., *Transmission Electron Microscopy*. Springer: New York, 2008.

Kruk, M. Access to Ultralarge-Pore Ordered Mesoporous Materials through Selection of Surfactant/Swelling-Agent Micellar Templates. *Acc. Chem. Res.* **2012,** *45*, 1678-1687.

Lee, B. Y.; Li, Z.; Clemens, D. L.; Dillon, B. J.; Hwang, A. A.; Zink, J. I.; Horwitz, M. A. Redox-Triggered Release of Moxifloxacin from Mesoporous Silica Nanoparticles Functionalized with Disulfide Snap-Tops Enhances Efficacy Against Pneumonic Tularemia in Mice. *Small* **2016,** *12*, 3690–3702.

Lee, H.; Sung, D.; Veerapandian, M.; Yun, K.; Seo, S.-W. PEGylated Polyethyleneimine Grafted Silica Nanoparticles: Enhanced Cellular Uptake and Efficient siRNA Delivery. *Anal. Bioanal. Chem.* **2011,** *400*, 535-545.

Li, X.; Xie, Q. R.; Zhang, J.; Xia, W.; Gu, H. The Packaging of siRNA Within the Mesoporous Structure of Silica Nanoparticles. *Biomaterials* **2011,** *32*, 9546-9556.

Li, Y.; He, W.; Wang, R.; Yang, L.; Zhou, C.; Zhang, B. Antitumor Effects of Recombinant Human Adenovirus‐p53 Against Human Cutaneous Squamous Cell Carcinoma in Mice. *Exp. Ther. Med.* **2016,** *12*, 4159-4167.

Li, Y.; Hei, M.; Xu, Y.; Qian, X.; Zhu, W. Ammonium Salt Modified Mesoporous Silica Nanoparticles for Dual Intracellular-Responsive Gene Delivery. *Int. J. Pharm.* **2016,** *511*, 689-702.

Li, Z.; Barnes, J. C.; Bosoy, A.; Stoddart, J. F.; Zink, J. I. Mesoporous Silica Nanoparticles in Biomedical Applications. *Chem. Soc. Rev.* **2012,** *41*, 2590-2605.

Liberman, A.; Mendez, N.; Trogler, W. C.; Kummel, A. C. Synthesis and Surface Functionalization of Silica Nanoparticles for Nanomedicine. *Surf. Sci. Rep.* **2014,** *69*, 132-158.

Lin, D. S.; Cheng, Q.; Jiang, Q.; Huang, Y. Y.; Yang, Z.; Han, S. C.; Zhao, Y. N.; Guo, S. T.; Liang, Z. C.; Dong, A. J. Intracellular Cleavable Poly(2-Dimethylaminoethyl Methacrylate) Functionalized Mesoporous Silica Nanoparticles for Efficient siRNA Delivery In Vitro and In Vivo. *Nanoscale* **2013,** *5*, 4291-4301.

Liong, M.; Lu, J.; Kovochich, M.; Xia, T.; Ruehm, S. G.; Nel, A. E.; Tamanoi, F.; Zink, J. I. Multifunctional Inorganic Nanoparticles for Imaging, Targeting, and Drug Delivery. *ACS Nano* **2008,** *2*, 889-896.

Liu, J.; Stace-Naughton, A.; Brinker, C. J. Silica Nanoparticle Supported Lipid Bilayers for Gene Delivery. *Chem. Commun.* **2009**, 5100-5102.

LoRusso, P.; Krop, I.; Miller, K.; Ma, C.; Siegel, B. A.; Shields, A. F.; Molnar, I.; Wickham, T.; Reynolds, J.; Campbell, K. Abstract CT234: A phase I Study of MM-

302, a HER2-targeted PEGylated Liposomal Doxorubicin, in Patients with HER2+ Metastatic Breast Cancer. *Cancer Res.* **2015,** *75*.

Lu, J.; Li, Z.; Zink, J. I.; Tamanoi, F. In Vivo Tumor Suppression Efficacy of Mesoporous Silica Nanoparticles-Based Drug-Delivery System: Enhanced Efficacy by Folate Modification. *Nanomed.* **2012,** *8*, 212-220.

Lundqvist, M.; Stigler, J.; Elia, G.; Lynch, I.; Cedervall, T.; Dawson, K. A. Nanoparticle Size and Surface Properties Determine the Protein Corona with Possible Implications for Biological Impacts. *Proc. Natl. Acad. Sci.* **2008,** *105*, 14265-14270.

Lv, H.; Zhang, S.; Wang, B.; Cui, S.; Yan, J., Toxicity of cationic lipids and cationic polymers in gene delivery. *J. Control. Release* **2006,** *114* (1), 100-109.

Ma, P.; Mumper, R. J., Paclitaxel nano-delivery systems: a comprehensive review. *Journal of nanomedicine & nanotechnology* **2013,** *4* (2), 1000164.

Major, R. C.; Zhu, X.-Y. Two-Step Approach to the Formation of Organic Monolayers on the Silicon Oxide Surface. *Langmuir* **2001,** *17*, 5576-5580.

Mamaeva, V.; Rosenholm, J. M.; Bate-Eya, L. T.; Bergman, L.; Peuhu, E.; Duchanoy, A.; Fortelius, L. E.; Landor, S.; Toivola, D. M.; Lindén, M. Mesoporous Silica Nanoparticles as Drug Delivery Systems for Targeted Inhibition of Notch Signaling in Cancer. *Mol. Ther.* **2011,** *19*, 1538-1546.

Mamaeva, V.; Sahlgren, C.; Lindén, M. Mesoporous Silica Nanoparticles in Medicine—Recent Advances. *Adv. Drug Delivery Rev.* **2013,** *65*, 689-702.

Mamot, C.; Drummond, D. C.; Noble, C. O.; Kallab, V.; Guo, Z.; Hong, K.; Kirpotin, D. B.; Park, J. W. Epidermal Growth Factor Receptor–Targeted Immunoliposomes Significantly Enhance the Efficacy of Multiple Anticancer Drugs In Vivo. *Cancer Res.* **2005,** *65*, 11631-11638.

Mao, S.; Neu, M.; Germershaus, O.; Merkel, O.; Sitterberg, J.; Bakowsky, U.; Kissel, T. Influence of Polyethylene Glycol Chain Length on the Physicochemical and Biological Properties of Poly (Ethylene Imine)-Graft-Poly (Ethylene Glycol) Block Copolymer/SiRNA Polyplexes. *Bioconjugate Chem.* **2006,** *17*, 1209-1218.

Mekaru, H.; Lu, J.; Tamanoi, F. Development of Mesoporous Silica-Based Nanoparticles with Controlled Release Capability for Cancer Therapy. *Adv. Drug Delivery Rev.* **2015,** *95*, 40-49.

Meng, H.; Xue, M.; Xia, T.; Ji, Z.; Tarn, D. Y.; Zink, J. I.; Nel, A. E. Use of Size and a Copolymer Design Feature to Improve the Biodistribution and the Enhanced

Permeability and Retention Effect of Doxorubicin-Loaded Mesoporous Silica Nanoparticles in a Murine Xenograft Tumor Model. *ACS Nano* **2011,** *5*, 4131-4144.

Miller, K. D.; Siegel, R. L.; Lin, C. C.; Mariotto, A. B.; Kramer, J. L.; Rowland, J. H.; Stein, K. D.; Alteri, R.; Jemal, A. Cancer Treatment and Survivorship Statistics, 2016. *CA. Cancer J. Clin.* **2016,** *66*, 271-289.

Na, H. K.; Kim, M. H.; Park, K.; Ryoo, S. R.; Lee, K. E.; Jeon, H.; Ryoo, R.; Hyeon, C.; Min, D. H. Efficient Functional Delivery of siRNA Using Mesoporous Silica Nanoparticles with Ultralarge Pores. *Small* **2012,** *8*, 1752-1761.

Naldini, L. Gene Therapy Returns to Centre Stage. *Nature* **2015,** *526*, 351-360.

Nel, A. E.; Mädler, L.; Velegol, D.; Xia, T.; Hoek, E. M.; Somasundaran, P.; Klaessig, F.; Castranova, V.; Thompson, M. Understanding Biophysicochemical Interactions at the Nano–Bio Interface. *Nat. Mater.* **2009,** *8*, 543-557.

Ngamcherdtrakul, W.; Morry, J.; Gu, S.; Castro, D. J.; Goodyear, S. M.; Sangvanich, T.; Reda, M. M.; Lee, R.; Mihelic, S. A.; Beckman, B. L. Cationic Polymer Modified Mesoporous Silica Nanoparticles for Targeted siRNA Delivery to HER2+ Breast Cancer. *Adv. Drug Delivery Rev.* **2015,** *25*, 2646-2659.

Nichols, J. W.; Bae, Y. H., Odyssey of a cancer nanoparticle: from injection site to site of action. *Nano Today* **2012,** *7* (6), 606-618.

Northfelt, D. W.; Hamburg, S. I.; Borad, M. J.; Seetharam, M.; Curtis, K. K.; Lee, P.; Crowell, B.; Vocila, L.; Fredlund, P.; Gilbert, M. J. In *A Phase I Dose-Escalation Study of TKM-080301, a RNAi Therapeutic Directed Against Polo-Like Kinase 1 (PLK1), in Patients with Advanced Solid Tumors: Expansion Cohort Evaluation of Biopsy Samples for Evidence of Pharmacodynamic Effects of PLK1 Inhibition*, ASCO Annual Meeting Proceedings, 2013.

Owens, G. J.; Singh, R. K.; Foroutan, F.; Alqaysi, M.; Han, C.-M.; Mahapatra, C.; Kim, H.-W.; Knowles, J. C. Sol–Gel Based Materials for Biomedical Applications. *Prog. Mater. Sci.* **2016,** *77*, 1-79.

Pecot, C. V.; Calin, G. A.; Coleman, R. L.; Lopez-Berestein, G.; Sood, A. K. RNA Interference in the Clinic: Challenges and Future Directions. *Nat. Rev. Cancer* **2011,** *11*, 59-67.

Peng, Q.; Zhong, Z.; Zhuo, R. Disulfide Cross-Linked Polyethylenimines (PEI) Prepared Via Thiolation of Low Molecular Weight PEI as Highly Efficient Gene Vectors. *Bioconjugate Chem.* **2008,** *19*, 499-506.

Petros, R. A.; DeSimone, J. M. Strategies in the Design of Nanoparticles for Therapeutic Applications. *Nat. Rev. Drug Discovery* **2010,** *9*, 615-627.

Pirollo, K. F.; Rait, A.; Zhou, Q.; Zhang, X.-q.; Zhou, J.; Kim, C.-S.; Benedict, W. F.; Chang, E. H. Tumor-Targeting Nanocomplex Delivery of Tumor Suppressor RB94 Chemosensitizes Bladder Carcinoma Cells In Vitro and In Vivo. *Clin. Cancer Res.* **2008,** *14*, 2190-2198.

Popovtzer, R.; Agrawal, A.; Kotov, N. A.; Popovtzer, A.; Balter, J.; Carey, T. E.; Kopelman, R. Targeted Gold Nanoparticles Enable Molecular CT Imaging of Cancer. *Nano Lett.* **2008,** *8*, 4593-4596.

Putnam, D.; Gentry, C. A.; Pack, D. W.; Langer, R. Polymer-Based Gene Delivery with Low Cytotoxicity by a Unique Balance of Side-Chain Termini. *Proc. Natl. Acad. Sci.* **2001,** *98*, 1200-1205.

Reimer, L., *Transmission Electron Microscopy: Physics of Image Formation and Microanalysis*. Springer: New York, 2013; Vol. 36.

Rejeeth, C.; Kannan, S.; Muthuchelian, K. Development of In Vitro Gene Delivery System Using ORMOSIL Nanoparticle: Analysis of p53 Gene Expression in Cultured Breast Cancer Cell (MCF-7). *Cancer Nanotechnol.* **2012,** *3*, 55-63.

Resnier, P.; Montier, T.; Mathieu, V.; Benoit, J. P.; Passirani, C. A Review of the Current Status of siRNA Nanomedicines in the Treatment of Cancer. *Biomaterials* **2013,** *34*, 6429-6443.

Rosenholm, J. M.; Mamaeva, V.; Sahlgren, C.; Lindén, M. Nanoparticles in targeted cancer therapy: mesoporous silica nanoparticles entering preclinical development stage. *Nanomedicine* **2012,** *7*, 111-120.

Roy, I.; Ohulchanskyy, T. Y.; Pudavar, H. E.; Bergey, E. J.; Oseroff, A. R.; Morgan, J.; Dougherty, T. J.; Prasad, P. N. Ceramic-Based Nanoparticles Entrapping Water-Insoluble Photosensitizing Anticancer Drugs: A Novel Drug− Carrier System for Photodynamic Therapy. *J. Am. Chem. Soc.* **2003,** *125*, 7860-7865.

Sartor, M. Dynamic Light Scattering. *University of California, San Diego* **2003**, 2-21

Senzer, N.; Nemunaitis, J.; Nemunaitis, D.; Bedell, C.; Edelman, G.; Barve, M.; Nunan, R.; Pirollo, K. F.; Rait, A.; Chang, E. H. Phase I Study of a Systemically Delivered p53 Nanoparticle in Advanced Solid Tumors. *Mol. Ther.* **2013,** *21*, 1096-1103.

Shi, J.; Kantoff, P. W.; Wooster, R.; Farokhzad, O. C. Cancer Nanomedicine: Progress, Challenges and Opportunities. *Nat. Rev. Cancerr* **2017,** *17*, 20-37.

Side Effects - National Cancer Institute. https://www.cancer.gov/about-cancer/treatment/side-effects (accessed 3/10/2017).

Siegel, R. L.; Miller, K. D.; Jemal, A. Cancer Statistics, 2015. *CA. Cancer J. Clin.* **2015,** *65*, 5-29.

Sing, K. S. W.; Everett, D. H.; Haul, R. A. W.; Moscou, L.; Pierotti, R. A.; Rouquerol, J.; Siemieniewska, T., Reporting Physisorption Data for Gas/Solid Systems. In *Handbook of Heterogeneous Catalysis*, Wiley-VCH: Weinheim, 2008.

Sing, K. The Use of Nitrogen Adsorption for the Characterisation of Porous Materials. *Colloids Surf., A* **2001,** *187*, 3-9.

Solberg, S. M.; Landry, C. C. Adsorption of DNA into Mesoporous Silica. *J. Phys. Chem. B* **2006,** *110*, 15261-15268.

Souris, J. S.; Lee, C.-H.; Cheng, S.-H.; Chen, C.-T.; Yang, C.-S.; Ho, J.-a. A.; Mou, C.-Y.; Lo, L.-W., Surface charge-mediated rapid hepatobiliary excretion of mesoporous silica nanoparticles. *Biomaterials* **2010,** *31* (21), 5564-5574.

Steinbacher, J. L.; Landry, C. C. Adsorption and Release of siRNA from Porous Silica. *Langmuir* **2014,** *30*, 4396-4405.

Steinbacher, J. L.; Lathrop, S. A.; Cheng, K.; Hillegass, J. M.; Butnor, K. J.; Kauppinen, R. A.; Mossman, B. T.; Landry, C. C. Gd-Labeled Microparticles in MRI: In vivo Imaging of Microparticles After Intraperitoneal Injection. *Small* **2010,** *6*, 2678-2682.

Sun, L.; Liu, Y. J.; Yang, Z. Z.; Qi, X. R. Tumor Specific Delivery with Redox-Triggered Mesoporous Silica Nanoparticles Inducing Neovascularization Suppression and Vascular Normalization. *RSC Adv.* **2015,** *5*, 55566-55578.

Talelli, M.; Oliveira, S.; Rijcken, C. J.; Pieters, E. H.; Etrych, T.; Ulbrich, K.; van Nostrum, R. C.; Storm, G.; Hennink, W. E.; Lammers, T. Intrinsically Active Nanobody-Modified Polymeric Micelles for Tumor-Targeted Combination Therapy. *Biomaterials* **2013,** *34*, 1255-1260.

Thommes, M.; Kaneko, K.; Neimark, A. V.; Olivier, J. P.; Rodriguez-Reinoso, F.; Rouquerol, J.; Sing, K. S. Physisorption of Gases, with Special Reference to the Evaluation of Surface Area and Pore Size Distribution (IUPAC Technical Report). *Pure Appl. Chem.* **2015,** *87*, 1051-1069

van der Meel, R.; Vehmeijer, L. J. C.; Kok, R. J.; Storm, G.; van Gaal, E. V. B. Ligand-Targeted Particulate Nanomedicines Undergoing Clinical Evaluation: Current Status. *Adv. Drug Delivery Rev.* **2013,** *65*, 1284-1298.

Vauthier, C.; Ponchel, G., *Polymer Nanoparticles for Nanomedicines: A Guide for their Design, Preparation and Development*. Springer: New York, 2017.

Von Hoff, D. D.; Mita, M. M.; Ramanathan, R. K.; Weiss, G. J.; Mita, A. C.; LoRusso, P. M.; Burris, H. A.; Hart, L. L.; Low, S. C.; Parsons, D. M.; Zale, S. E.; Summa, J. M.; Youssoufian, H.; Sachdev, J. C. Phase I Study of PSMA-Targeted Docetaxel-Containing Nanoparticle BIND-014 in Patients with Advanced Solid Tumors. *Clin. Cancer Res.* **2016,** *22*, 3157-3163.

Wadia, J. S.; Stan, R. V.; Dowdy, S. F. Transducible TAT-HA Fusogenic Peptide Enhances Escape of TAT-Fusion Proteins After Lipid Raft Macropinocytosis. *Nat. Med.* **2004,** *10*, 310-315.

Wang, M.; Thanou, M. Targeting Nanoparticles to Cancer. *Pharmacol. Res.* **2010,** *62*, 90-99.

Wang, Z. Y.; Zhao, Y.; Ren, L.; Jin, L. H.; Sun, L. P.; Yin, P.; Zhang, Y.-f.; Zhang, Q.-Q. Novel Gelatin–Siloxane Nanoparticles Decorated by TAT Peptide as Vectors for Gene Therapy. *Nanotechnology* **2008,** *19*, 445103.

Wen, H. Y.; Dong, H. Q.; Xie, W. J.; Li, Y. Y.; Wang, K.; Pauletti, G. M.; Shi, D.-L. Rapidly Disassembling Nanomicelles with Disulfide-Linked PEG Shells for Glutathione-Mediated Intracellular Drug Delivery. *Chem. Commun.* **2011,** *47*, 3550-3552.

Wicki, A.; Ritschard, R.; Loesch, U.; Deuster, S.; Rochlitz, C.; Mamot, C. Large-Scale Manufacturing of GMP-Compliant Anti-EGFR Targeted Nanocarriers: Production of Doxorubicin-Loaded Anti-EGFR-Immunoliposomes for a First-In-Man Clinical Trial. *Int. J. Pharm.* **2015,** *484*, 8-15.

Witasp, E.; Kupferschmidt, N.; Bengtsson, L.; Hultenby, K.; Smedman, C.; Paulie, S.; Garcia-Bennett, A. E.; Fadeel, B. Efficient Internalization of Mesoporous Silica Particles of Different Sizes by Primary Human Macrophages Without Impairment of Macrophage Clearance of Apoptotic or Antibody-Opsonized Target Cells. *Toxicol. Appl. Pharmacol.* **2009,** *239*, 306-319.

Wu, M.; Meng, Q.; Chen, Y.; Du, Y.; Zhang, L.; Li, Y.; Zhang, L.; Shi, J. Large-Pore Ultrasmall Mesoporous Organosilica Nanoparticles: Micelle/Precursor Co-templating Assembly and Nuclear-Targeted Gene Delivery. *Adv. Mater.* **2015,** *27*, 215-222.

Xia, T.; Kovochich, M.; Liong, M.; Meng, H.; Kabehie, S.; George, S.; Zink, J. I.; Nel, A. E. Polyethyleneimine Coating Enhances the Cellular Uptake of Mesoporous Silica Nanoparticles and Allows Safe Delivery of siRNA and DNA Constructs. *ACS Nano* **2009,** *3*, 3273-3286.

Xiao, X.; He, Q.; Huang, K. Novel Amino-Modified Silica Nanoparticles as Efficient Vector for Hepatocellular Carcinoma Gene Therapy. *Med. Oncol.* **2010,** *27*, 1200-1207.

Yang, Y.; Yu, C. Advances in Silica Based Nanoparticles for Targeted Cancer Therapy. *Nanomed.* **2016,** *12*, 317-332.

Ye, S. F.; Tian, M.-m.; Wang, T. X.; Ren, L.; Wang, D.; Shen, L. H.; Shang, T. Synergistic Effects of Cell-Penetrating Peptide Tat and Fusogenic Peptide HA2-Enhanced Cellular Internalization and Gene Transduction of Organosilica Nanoparticles. *Nanomed.* **2012,** *8*, 833-841.

Zhang, K.; Xu, L. L.; Jiang, J.-G.; Calin, N.; Lam, K. F.; Zhang, S. J.; Wu, H. H.; Wu, G.-D.; Albela, B. l.; Bonneviot, L. Facile Large-Scale Synthesis of Monodisperse Mesoporous Silica Nanospheres with Tunable Pore Structure. *J. Am. Chem. Soc.* **2013,** *135*, 2427-2430.

Zhou, X.; Chen, L.; Nie, W.; Wang, W.; Qin, M.; Mo, X.; Wang, H.; He, C. Dual-Responsive Mesoporous Silica Nanoparticles Mediated Co-Delivery of Doxorubicin and Bcl-2 siRNA for Targeted Treatment of Breast Cancer. *J. Phys. Chem. C* **2016,** *120*, 22375–22387.

Zuckerman, J. E.; Gritli, I.; Tolcher, A.; Heidel, J. D.; Lim, D.; Morgan, R.; Chmielowski, B.; Ribas, A.; Davis, M. E.; Yen, Y. Correlating Animal and Human Phase Ia/Ib Clinical Data with CALAA-01, a Targeted, Polymer-Based Nanoparticle Containing siRNA. *Proc. Natl. Acad. Sci.* **2014,** *111*, 11449-11454.